PNL-3428
UC-12

Dry/Wet Performance of a Plate-Fin Air-Cooled Heat Exchanger with Continuous Corrugated Fins

S. G. Hauser
D. K. Kreid
B. M. Johnson

January 1981

Prepared for the U.S. Department of Energy
under Contract DE-AC06-76RLO 1830

Pacific Northwest Laboratory
Operated for the U.S. Department of Energy
by Battelle Memorial Institute

Battelle

PNL-3428

PACIFIC NORTHWEST LABORATORY
operated by
BATTELLE
for the
UNITED STATES DEPARTMENT OF ENERGY
Under Contract DE-AC06-76RLO 1830

Printed in the United States of America
Available from
National Technical Information Service
United States Department of Commerce
5285 Port Royal Road
Springfield, Virginia 22151

Price: Printed Copy $_____*; Microfiche $3.00

*Pages	NTIS Selling Price
001-025	$4.00
026-050	$4.50
051-075	$5.25
076-100	$6.00
101-125	$6.50
126-150	$7.25
151-175	$8.00
176-200	$9.00
201-225	$9.25
226-250	$9.50
251-275	$10.75
276-300	$11.00

PNL-3428
UC-12

DRY/WET PERFORMANCE OF A PLATE-FIN AIR-COOLED HEAT EXCHANGER WITH CONTINUOUS CORRUGATED FINS

S. G. Hauser
D. K. Kreid
B. M. Johnson

January 1981

Prepared for
the U.S. Department of Energy
under Contract DE-AC06-76RLO 1830
in cooperation with
the U.S. Environment Protection Agency
under DOE-EPA Interagency Agreement 79-DX-0676

EPA Project Officer
T. G. Brna
Utilities and Industrial Power Division
Industrial Environment Research Laboratory - RTP
Research Triangle Park, North Carolina 27709

Pacific Northwest Laboratory
Richland, Washington 99352

NOTICE

This document will also be released by U.S. Environmental Protection Agency as document number EPA 600/7-82-014.

FOREWORD

The Dry Cooling Enhancement Program at Pacific Northwest Laboratory (PNL) was initiated with a program scope that included the following near-term and ultimate emphasis.

Near-term Objectives:

Develop economic and performance models for cost optimization of total heat rejection systems using dry and dry/wet cooling.

Analyze and disseminate operating experience on existing dry-cooled plant performance.

Demonstrate certain features of existing technology equipment to provide confidence for specification by utilities.

Ultimate Objective:

Promote water conservation through industry use of dry cooling by developing and demonstrating the reliability of lower cost systems. The development of advanced dry/wet systems is also considered to be within this scope.

The following documents have been issued, reporting the results of the work toward these objectives.

Cost optimization of dry-cooled heat rejection systems:

A REVIEW AND ASSESSMENT OF ENGINEERING ECONOMIC STUDIES OF DRY-COOLED ELECTRICAL GENERATING PLANTS. B. C. Fryer, BNWL-1976, March 1976.

HEAT TRANSFER AND PRESSURE DROP CHARACTERISTICS OF DRY TOWER EXTENDED SURFACES. PART I: HEAT TRANSFER AND PRESSURE DROP DATA. PFR Engineering Systems, Inc., PFR 7-100, March 1976.

HEAT TRANSFER AND PRESSURE DROP CHARACTERISTICS OF DRY TOWER EXTENDED SURFACES. PART II: DATA ANALYSIS AND CORRELATION. PFR Engineering Systems, Inc., PFR 7-102, June 1976.

Analysis of performance of existing dry-cooled plants:

DRY COOLING TOWER PROGRAM: RESULTS OF INDUSTRIAL CONTACTS THROUGH AUGUST 1974. BNWL-1878, November 1, 1974.

A SURVEY OF MATERIALS AND CORROSION PERFORMANCE IN DRY COOLING APPLICATIONS. A. B. Johnson, Jr., D. R. Pratt and G. E. Zima, BNWL-1958, March 1976.

EUROPEAN DRY COOLING TOWER OPERATING EXPERIENCE. J. G. DeSteese and K. Simhan, BNWL-1955, March 1976.

MATHEMATICAL AND EXPERIMENTAL INVESTIGATIONS ON DISPERSION AND RECIRCULATION OF PLUMES FROM DRY COOLING TOWERS AT WYODAK POWER PLANT IN WYOMING. Y. Onishi and D. S. Trent, BNWL-1982, February 1976.

ALUMINUM ALLOY PERFORMANCE UNDER DRY COOLING TOWER CONDITIONS. A. B. Johnson, Jr., S. Begaj, M. W. Martini, and R. P. May, PNL-2392, December 1977.

Advanced dry (dry/wet)-cooled systems:

PRELIMINARY EVALUATION OF WET-DRY COOLING CONCEPTS FOR POWER PLANTS. W. B. Loscutoff, BNWL-1969.

COMPATIBILITY OF AMMONIA WITH CANDIDATE DRY COOLING SYSTEM MATERIALS. D. R. Pratt, BNWL-1991, April 1976.

SCALE FORMATION IN DELUGED DRY COOLING SYSTEMS. D. R. Pratt, BNWL-2060, March 1976.

AMMONIA AS AN INTERMEDIATE HEAT EXCHANGE FLUID DRY FOR DRY-COOLED TOWERS. R. T. Allemann, B. M. Johnson, and G. C. Smith, BNWL-SA-5997, September 1976.

AUGMENTED DRY COOLING SURFACE TEST PROGRAM: ANALYSIS AND EXPERIMENTAL RESULTS. H. L. Parry et al. PNL-2746, September 1979.

A group of reports (including this report) has been issued that serves the dual purpose of: 1) developing cost optimization models for dry cooling systems based on available technology and 2) comparing the results of analyzing the cost of these systems with the projected cost of several advanced dry and dry/wet systems. Included in this group are:

AN ENGINEERING AND COST COMPARISON OF THREE DIFFERENT ALL-DRY COOLING SYSTEMS. B. C. Fryer, D. W. Faletti, Daniel J. Braun, David J. Braun and L. E. Wiles, BNWL-2121, September 1976.

A STUDY OF THE COMPARATIVE COSTS OF FIVE WET/DRY COOLING TOWER CONCEPTS. F. R. Zaloudek, R. T. Allemann, D. W. Faletti, B. M. Johnson, H. L. Parry, G. C. Smith, R. D. Tokarz, and R. A. Walter, BNWL-2122, September 1976.

DRY COOLING OF POWER GENERATING STATIONS: A SUMMARY OF THE ECONOMIC EVALUATION OF SEVERAL ADVANCED CONCEPTS VIA A DESIGN OPTIMIZATION STUDY AND A CONCEPTUAL DESIGN AND COST ESTIMATE. B. M. Johnson, R. T. Allemann, D. W. Faletti, B. C. Fryer and F. R. Zaloudek, BNWL-2120, September 1976.

COSTS AND COST ALGORITHMS FOR DRY COOLING TOWER SYSTEMS. P. A. Ard, C. H. Henager, D. R. Pratt and L. E. Wiles, BNWL-2123, September 1976.

A USER'S MANUAL FOR THE BNW-I OPTIMIZATION CODE FOR DRY-COOLED POWER PLANTS. David J. Braun, Daniel J. Braun, Warren V. DeMier, D. W. Faletti and L. E. Wiles, BNWL-2180, January 1977.

COMPARATIVE COST STUDY OF FOUR WET/DRY COOLING CONCEPTS THAT USE AMMONIA AS THE INTERMEDIATE HEAT EXCHANGE FLUID. R. D. Tokarz, Daniel J. Braun, B. M. Johnson, R. T. Allemann, David J. Braun, H. L. Parry, G. C. Smith and F. R. Zaloudek, PNL-2661, September 1978.

AN ENGINEERING AND COST ANALYSIS OF A DRY COOLING SYSTEM AUGMENTED WITH A THERMAL STORAGE POND. M. K. Dorst and R. T. Allemann, PNL-2745, September 1978.

A USER'S MANUAL FOR THE BNW-II OPTIMIZATION CODE FOR DRY/WET-COOLED POWER PLANTS. Daniel J. Braun, Judith A. Bamberger, David J. Braun, Duane W. Faletti, Lawrence E. Wiles, PNL-2674, Vol. I, May 1978.

A DESCRIPTION AND COST ANALYSIS OF A DELUGE DRY/WET COOLING SYSTEM. L. E. Wiles et al. PNL-2498, June 1978.

Four reports have been issued which consider the future need for any cooling and the potential benefit/cost ratio of a large-scale demonstration.

AN OVERVIEW OF ECONOMIC, LEGAL, AND WATER AVAILABILITY FACTORS AFFECTING THE DEMAND FOR DRY AND WET/DRY COOLING OF THERMAL POWER PLANTS. P. L. Hendrickson, BNWL-2268, June 1977.

AN OVERVIEW OF ECONOMIC, LEGAL, AND WATER AVAILABILITY FACTORS AFFECTING THE DEMAND FOR DRY AND WET/DRY COOLING OF THERMAL POWER PLANTS. P. L. Hendrickson, BNWL-2268, September 1978.

ESTIMATION OF BENEFITS FROM DEMONSTRATING ADVANCED DRY COOLING TECHNOLOGY: A FRAMEWORK AND PARTIAL ANALYSIS. J. W. Currie and T. J. Foley, BNWL-2182, April 1977.

POTENTIAL USE OF DRY COOLING IN SUPPORT OF ADVANCED ENERGY GENERATION SYSTEMS. D. W. Mayer, E. M. Arnold, and R. T. Allemann, PNL-3149, September 1979.

SUMMARY

The ultimate goal of work performed in this project was to contribute to the development of improved cooling facilities for power plants that would help to conserve increasingly scarce fresh water supplies in an environmentally compatible and economically viable manner. The specific objectives of this work were to

- experimentally determine the performance and operating characteristics of a plate-fin heat exchanger in dry/wet or "deluge" operations and to
- continue development of the deluge heat/mass transfer model.

The experiments were conducted in a specially-designed wind tunnel at the Pacific Northwest Laboratory, which is operated for the Department of Energy by Battelle Memorial Institute. In the tests, air that was first heated and humidified to specified conditions was circulated at a controlled rate through a 2 ft x 6 ft heat exchanger module. The heat exchanger used in the tests was a wavy surface, plate fin on tube configuration. Hot water was circulated through the tubes at high flow rates to maintain an essentially isothermal condition on the tube side. Deionized water sprayed on the top of the vertically oriented plate fins was collected at the bottom of the core and recirculated. Instrumentation was provided for measurement of flow rates and thermodynamic conditions in the air, in the core circulation water, and in the deluge water.

Measurements of the air side pressure drop and heat rejection rate were made as a function of air flow rate, air inlet temperature and humidity, deluge water flow rate, and the core inclination from the vertical. The data were reduced to determine an overall heat transfer coefficient and an effective deluge film convective coefficient.

The "deluge" model is an approximate theory for predicting heat transfer from a wet finned heat exchanger that was developed in preceding work. The model was further developed and refined in this study, and a major extension of the model was formulated that permits simultaneous calculation of both the heat transfer and evaporation rates from the wetted surface. The model was

used for reduction and correlation of the data and for evaluation of the results. In general, the analytical predictons were in excellent agreement with the experiments.

The experiments showed an increase in the heat rejection rate due to wetting, accompanied by a proportional increase in the air side pressure drop. For operation at the same air side pressure drop, the enhancement ratio Q_w/Q_d varied between 2 and 5 for the conditions tested. Thus, the potential enhancement of heat transfer due to wetting can be substantial.

CONTENTS

FIGURES

TABLES

NOMENCLATURE

A_c -- minimum free flow area
A_{cf} -- frontal area
A_p -- primary (tube) side surface area
A_t -- average tube surface area
A_s -- total air side surface area
A_{sf} -- airside fin surface area
A_{st} -- airside tube surface area
a,b,c,d -- constants in equation for saturation pressure
a_m^* -- relative surface area (wet - mass transfer)
a_p -- primary side relative area
a_s^* -- relative surface area (wet - heat transfer)
a_t -- tube relative area
Bi_f -- Biot number of fin, dry
Bi_f^* -- Biot number of fin, wet
$C_{1,2,3}$ -- constants
C_a -- moist air specific heat
C_p -- primary fluid specific heat
D_h -- hydraulic diameter
E -- constant in equation for friction factor
F_T -- crossflow correction factor
FPI -- fins per inch of core length
f -- fanning friction factor
f_o -- effective friction factor including inlet and exit losses
f_r -- f_o evaluated at Re = 1000
G_o -- mass flux of free stream air
g_c -- gravitational constant 32.17
H_p' -- humidity ratio of saturated air at T_p

H'_r -- humidity ratio of saturated air at T_r

H'_s -- humidity ratio of saturated air at T_s

H_∞ -- humidity ratio of free-stream air

h -- heat transfer coefficient

h_d -- deluge heat transfer coefficient

h_d^* -- effective deluge heat transfer coefficient = $h_d a_s^*$

h_o -- surface heat transfer coefficient including fin effectiveness

h_p -- primary side heat transfer coefficient

h_s -- surface heat transfer coefficient

ITD -- inlet temperature difference, $T_p - T_\infty$

i'_p -- enthalpy of saturated air at T_p

i'_r -- enthalpy of saturated air at T_r

i'_∞ -- enthalpy of saturated air at T_∞

i_∞ -- enthalpy of moist air at T_∞

Δi_m -- log mean enthalpy difference

j' -- Colburn factor using h_s

j_o -- Colburn factor using h_o

j_u -- Colburn factor using U.

K -- a parameter in equation for ξ/ξ_m

k_p -- thermal conductivity of primary flow

k_t -- thermal conductivity of tube wall

k_w -- thermal conductivity of water

L -- fin length in flow direction

l_f -- effective circular fin length

m -- an exponent

$\dot{m}_a$ -- mass flow rate of air (dry)

$\dot{m}_a^*$ -- mass flow rate of air (wet)

$\dot{m}_h$ -- water flow rate in the heater

$\dot{m}_p$ -- mass flow rate of circulation water

m_p -- total mass of circulation water

$\dot{m}_d$ -- mass flow rate of deluge water

$\dot{m}_w$ -- mass flow rate of evaporated water

N' -- number of tube coils

N^* -- NTU rating for wet heat transfer

N_m^* -- NTU rating for wet mass transfer

NTU -- NTU rating for dry heat transfer

n -- an exponent

P -- barometric pressure

P_{ws} -- partial pressure of water in moist air

Pr -- Prandtl number

Pr_p -- primary side prandtl number

ΔP_{core} -- total pressure drop across core

ΔP_{ann} -- pressure drop across annubar

Q_{deluge} -- heat gain in deluge water

Q_{dry} -- total heat transferred under dry operation

Q_{losses} -- heat lost from system to surroundings

Q_o -- net rate of heat flux in deluge operation

$Q_{peripheral}$ -- $Q_{pump} - Q_{losses}$

Q_{pump} -- heat gain by system from pump

Q_{rej} -- total heat transferred from primary side to air side

Q_v -- heat flux attributable only to evaporation

Q_{wet} -- total heat transfer from primary side to air side during wet operation

R -- an experimental result, also capacity ratio in n_f

R_e -- reynolds number airside

Re_p -- reynolds number primary side

r_b -- outer tube radius

r_e -- equivalent circular fin radius

S -- surface area per unit volume

T_d -- deluge water temperature

T_p -- primary fluid temperature

T_r -- fin root temperature

T_s -- surface (air-water interface) temperature

T_∞ -- free stream air temperature

ΔT -- temperature difference

ΔT_h -- water temperature rise in the heater

ΔT_i -- inlet temperature difference, $T_p - T_\infty$

ΔT_ρ -- temperature difference in circulation water

ΔT_{lm} — log mean temperature difference
t_t — tube wall thickness
t_f — fin thickness
Δt — time interval
U_o — overall dry heat transfer coefficient
U_o^* — overall wet heat transfer coefficient
U_{pr} — overall primary side heat transfer coefficient
U_m^* — equivalent coefficient for mass transfer = $C_a \Sigma_o^*$
V_{amin} — maximum air velocity at minimum flow area
V_o — frontal velocity
$\dot{V}$ — volume flow rate
V — velocity
X_i — a general parameter in uncertainty analysis
y_b — half fin thickness
x,y,z — coordinate directions

GREEK LETTERS

α — a parameter in equation for $(T_p - T_r)$
β — a parameter in equation for saturation presence
β_w — ratio of water temperature range to ITD
β_a — ratio of air temperature range to ITD
μ — kinetic viscosity
Σ_m — overall coefficient for mass transfer
Γ — ratio of inlet driving potentials for heat transfer
Γ_m — ratio of inlet driving potentials for mass transfer
δ — product of $(\xi_m \phi_m / \xi \phi)$, also boundary layer thickness
η_f — dry fin efficiency
η_f^* — wet fin efficiency
η_m — fin efficiency for mass transfer
θ_c — core angle from vertical
ν — viscosity
ξ — transformation parameter for heat transfer
ξ_m — transformation parameter for mass transfer

ρ_∞ -- air density

ρ_m -- mean air density

ρ_w -- water density

χ -- dimensionless x coordinate

Σ_m^* -- overall mass transfer coefficient

σ -- free area/frontal area

σ_f -- constant in equation for f

σ_s -- surface mass transfer coefficient

Φ -- relative humidity

ϕ -- dry exchanger effectiveness

ϕ^* -- wet exchanger effectiveness for heat transfer

ϕ_m^* -- wet exchanger effectiveness for mass transfer

ENGLISH TO METRIC CONVERSION TABLE

To Convert from	To	Multiply by
atm	Pa	1.013 E+05
Btu/hr	W	0.2929
Btu/(lbm-^{o}F)	J/(kg•K)	4184.0
Btu/(hr-ft-^{o}F)	W/(m•K)	0.0120
Btu/(hr-ft^2-^{o}F)	W/(m^2•K)	5.6745
Btu/lbm	J/kg	2324.4
ft	m	0.3048
ft^2	m^2	9.290 E-02
ft^3	m^3	2.832 E-02
ft/s	m/s	0.3048
ft^2/s	m^2/s	9.290 E-02
ft^3/lb	m^3/kg	6.243 E-02
^{o}F	K	$T_K = (T_F + 459.67)/1.8$
gal/min.	m^3/s	6.3090 E-05
in.	m	2.540 E-02
in. H_2O	Pa	249.15
in. Hg	Pa	3386.4
lb/hr	kg/s	1.260 E-04
lb/ft^3	kg/m^3	16.018
lb/(hr-ft^2)	kg/(s•m^2)	1.356 E-03

ACKNOWLEDGEMENTS

This report contains an account of the work sponsored by the Division of Advanced Systems and Materials Production of the U.S. Department of Energy (DOE) under the Dry Cooling Enhancement Program at the Pacific Northwest Laboratory (PNL). This work was completed under the direction of I. Helms and W. F. Savage, project Officer and Manager, respectively, Advanced Concepts Evaluation Section of the Advanced Nuclear Systems and Projects Division; and B. M. Johnson, Manager of the Dry Cooling Enhancement Program at PNL.

SECTION 1

INTRODUCTION

This report provides the experimental data and the supporting theoretical relationships to substantiate a key portion of the design of an advanced concept for dry/wet cooling of thermal power generating plants.

The work has been jointly supported by the Environmental Protection Agency and the Department of Energy because of the dual incentive that exists for developing improved cooling systems. Dry cooling has been the subject of extensive studies by both agencies, as well as by the Electric Power Research Institute, because of the growing realization that the use of fresh inland water to provide a heat sink for thermal generation of power cannot continue to increase indefinitely. Thus the EPA has been in the forefront of early studies to identify the feasibility and cost of supplementing the use of freshwater for cooling and thus reduce the environmental impact of either consuming large quantities of freshwater by evaporative cooling or returning an even larger quantity of water to its original source after being heated by 8 to 12 degrees centigrade. The Department of Energy, in its concern for the cost of power and the difficulties of siting power plants, has also been interested in developing lower cost dry cooling systems so as to provide for improved siting flexibility with a minimum of extra cost.

Except in special situations, it is likely that the supplementing of the use of freshwater for cooling will occur through the use of combination wet and dry systems. This is because using a small amount of cooling water reduces the cost of a dry cooling system far more than a proportionate difference in its cost and that of an evaporative system. Nevertheless, the cost of present dry/wet cooling systems are so high that utilities generally agree they will be used only in isolated situations unless significantly lower cost systems can be developed. However, because of the uncertain market for dry cooling, it is difficult for manufacturers to expend a great amount of private capital to develop and demonstrate radically new approaches. Public agencies such as the DOE and EPA and the utility-industry-supported research organization, EPRI, have consequently taken the lead in developing advanced technology for dry/wet cooling.

The Pacific Northwest Laboratory (PNL), operated for the Department of Energy by Battelle Memorial Institute, has a major program, portions of which are funded by these organizations. The multifaceted work includes: (1) identifying the need for dry/wet cooling, (2) assessing the state of the art and potentials for improvement, (3) identifying promising advanced concepts, (4) developing technology in support of selected advanced concepts,

(5) assessing new concepts as they are proposed, and (6) carrying out a large-scale test of the most promising advanced concept.

Of the many novel concepts that have been proposed by investigators around the world, a process has been selected for large-scale testing which uses ammonia to transport the reject heat from the last stage of the turbine to the air-cooled heat exchanger. The design features of such a system and the rationale for its selection have been covered in previous documents[1,2] from the Dry Cooling Enhancement Program at PNL. The chosen system also includes the use of evaporative cooling to augment the dry cooling in either of two ways:

(1) Deluge cooling in which water is allowed to flow in excess over the dry cooling surface, and

(2) Parallel condensing of the ammonia in an evaporative condenser (one in which the bare ammonia condenser tubes are cooled by water and air flowing simultaneously over the outside surface).

Deluge cooling, in which the dry heat exchanger surface is covered with a thin film of water so that evaporative cooling and sensible heat transfer occur simultaneously, appears to be a relatively simple and inexpensive way of achieving augmented cooling (i.e., dry/wet cooling). It has been used to some extent in air conditioning applications in this country. However, for large-scale power plant use, several uncertainties must first be overcome in performance prediction and proper design of the extended surface to permit good dry performance, together with proper water distribution to avoid scaling and corrosion. The concept has been under study at PNL.

An initial report[3] of the performance of the "Forgo" plate-fin heat exchanger surface, developed by and manufactured for the HOTERV Institute of Hungary (hereafter identified as the "HOTERV" exchanger) has been issued. It covered both the dry and the dry/wet performance of this exchanger, as well as the dry performance of two configurations of a chipped fin (or skived) heat exchanger surface manufactured under license from the Curtiss-Wright Company.

The present report provides the data and theoretical basis for predicting the performance of another plate-fin heat exchanger, manufactured by the Trane Company for air conditioning service. This was selected for testing in the ACT facility because it was more readily adaptable to ammonia condensation and procurement was more convenient and less expensive, due in part to Trane Company's manufacturing capability in this country.

The objective of the work carried on in the Water Augmentation Test Apparatus (WATA) is as follows:

(1) To determine all-dry nonaugmented performance for comparison with other air-cooled heat exchanger surfaces such as the HOTERV and Curtiss-Wright surface.

(2) To establish the magnitude of the potential benefit due to augmentation.

(3) To measure dry/wet heat transfer performance and air-side pressure drop as they are affected by weather conditions (air temperature and humidity), air-flow rate and deluge flow rate.

(4) To compare measured performance to performance predicted by analytical models developed at PNL to verify and help define those models.

(5) To determine the physical operating limits of the deluged surface, particularly the limits of air flow and deluge flow such that a wetted surface is maintained.

SECTION 2

CONCLUSIONS

The conclusions that may be drawn from the results of this project relate to three principal areas:

- operating characteristics and potential benefits of the deluge concept for cooling electric power plants
- comparisons of the dry/wet performance of the two types of plate fin heat exchangers that have been tested
- the applicability and accuracy of the deluge heat/mass transfer model.

2.1 CHARACTERISTICS AND BENEFITS OF DELUGE COOLING

The notable operating characteristics observed in the experimental study of deluge cooling, as compared to dry cooling, may be summarized as follows:

- The primary parameter used in this study to characterize the performance of a dry/wet cooling system was the ratio of wet to dry heat transfer at the same operating conditions and the same air-side pressure drop. This parameter was determined to vary between 2 and 5 for conditions tested in this study.
- The size of a dry cooled system needed to meet heat rejection requirements at peak ambient temperatures could thus be reduced by a factor of 1/2 to 1/5 by the use of deluge cooling enhancement. The actual reduction in size would depend on the system design and operating conditions. In particular it would depend on the amount of water available for evaporative cooling.
- Since water would be used only during periods of peak cooling demand, the water consumption of the deluged system could be substantially less than in a wet tower of similar capacity.
- The increase in heat transfer due to deluge must be compared to dry heat transfer at the same pressure drop. At a fixed air flow rate, deluging was accompanied by a substantial increase in the air-side pressure drop. Both the heat transfer and pressure drop were observed to increase, with increases in either the air velocity or deluge water flow rate.

- In the anticipated dry/wet operation, a variable number of heat exchanger modules will be deluged operating in parallel with the remainder of the modules dry. Therefore, all modules will operate at the same air-side pressure drop which, for a given deluge flow rate, will determine the air flow rate in both wet and dry sections.

- At superficial air velocities greater than about 6-8 ft/sec, appreciable quantities of water droplets were blown from the back side of the heat exchanger. Droplet drift may thus impose an upper bound on the air flow rate when the system is being deluged.

- The heat rejection rate during deluge operation was found to be dramatically dependent on the ambient air conditions. The enhancement was greatest for low ITD and low humidity (i.e., $Q_w/Q_d \lesssim 5$ at ITD $\sim 20^oF$, 25% RH) and lowest at high ITD and high humidity (i.e., $Q_w/Q_d \lesssim 2$ at ITD $\sim 50^oF$, 75% RH).

- Therefore, heat transfer enhancement using deluge is most effective and thus most attractive where the need is greatest: in hot, dry regions where water is scarce as, for example, in most of the western U.S.

- In addition, however, deluge cooling is also likely to be attractive in humid regions where the availability of fresh water for cooling is limited. In all cases, a system design optimization will have to be performed that will be highly site-specific.

2.2 DRY/WET PERFORMANCE COMPARISONS

In the course of the present and preceding tests, dry performance data were obtained for several heat exchanger configurations that may be compared to the present dry performance results. In adition, deluge tests were performed on a plate-fin heat exchanger of substantially different design. The results of comparing these performance data may be summarized as follows.

- For dry performance, the principal basis of comparison was the heat transfer per unit ITD, per unit volume as a function of fan power. On this basis, the chipped fin Curtis-Wright design selected for the ACT facility performed best at all fan powers.

- The Trane wavy fin design selected for ACT and a design based on a five-tube bundle of wrapped helical fin tubes were next in performance at about 10% lower overall rating than the top C-W system. The performances of the Trane and helical fin designs were essentially the same.

- Comparisons were also made with two other C-W chipped fin assemblies and with a HOTERV perforated plate fin assembly. All three of these performed below the preceding three at all fan powers. The HOTERV

performed better than the two C-W assemblies at low fan power but substantially lower than all of the other assemblies at high fan power.

- For wet operation, the primary performance comparison was based on the ratio of wet to dry heat transfer rates at equal air-side pressure drop and equal air inlet superficial velocities as a function of inlet conditions. On this basis, the Trane core consistently outperformed the HOTERV core by a ratio of about 1.2 at comparable conditions. The principal reason for this difference is the higher pressure drop of the HOTERV core at the given conditions.

2.3 EVALUATION OF THE DELUGE MODEL

One of the primary objectives of this work was to continue the development and evaluation of an analytical model for predicting the heat transfer from a deluged heat exchanger. This was accomplished with considerable success. In addition, in the course of this work the model was extended to allow prediction of the rate of evaporation and, thereby, the outlet conditions of the air passing through the system.

The principal application of the deluge heat transfer model was to develop correlations used in reduction and presentation of the experimental data. The primary quantity derived empirically from the data was the effective deluge film convective coefficient h_d. When these values of h_d were used in the model equations, predicted correlations were in excellent agreement with the data for a large range of operating conditions. The present experiments have thus shown that, given suitable values for h_d, the deluge model based on the enthalpy difference driving potential will serve as an accurate model for predicting wet performance of a finned, air-cooled heat exchanger.

The present study generated empirical results for h_d as a function of operating conditions that may be used to predict the performance of the Trane core. Furthermore, these results for h_d are quite similar to the previous results obtained for h_d for the HOTERV design, which differed significantly in design and performance from the Trane core. Thus, for design purposes, it is probably safe to use either of these results for h_d for a plate fin design similar to, but different from, either of the above. For a radically different design such as a bundle of cylindrical finned tubes, these results might also suffice for an estimate of performance using the deluge model. However, the validity of this approximation cannot be verified at this time.

The mass transfer extension of the deluge model could not be extensively evaluated in this study because accurate, independent measurements of the deluge water evaporation rates were not obtained. However, from the approximate measurements that were obtained it appeared that the model correctly predicted trends, but that the rate of evaporation was overpredicted by about 20%. This result is highly tentative, and additional measurements are required before a more definitive assessment can be made of this aspect of the model.

SECTION 3

RECOMMENDATIONS

Recommendations arising from the results of this study are of two principal types:

- design and operating criteria for wet/dry cooling systems and
- recommendations of additional tests and analyses.

3.1 RECOMMENDED DESIGN CRITERIA

Based on the results of the present experiments, a number of specific features arise as recommended design/operational criteria. The major findings are as follows.

- For the design conditions selected for the ACT facility, the wavy fin heat exchanger configuration performed better than the slotted fin geometry for both dry and wet operation. These findings thus confirm the selection of the wavy fin geometry for the ACT facility.
- The results of the experiments essentially confirm the selection of the 25^{o} heat exchanger inclination angle for the ACT facility. However, since the performance was found to be relatively insensitive to angle, any angle in the range of 20^{o} to 30^{o} could be used in future designs (or in future modifications of the ACT facility) if other design criteria should make it desirable to do so.
- The onset of water droplet drift from the back of the heat exchanger at higher velocities effectively bounds the maximum air flow rate. To prevent drift, the present tests indicate that the input air superficial velocity should be limited to about 6 ft/sec. A more definitive operational limit will have to be determined in tests of the actual facility.
- The heat transfer performance was found to increase slightly with increasing deluge flow rate in the range $1.5 < \dot{m}_d < 3$ gpm per foot of heat exchanger. However, the enhancement factor Q_w/Q_d was found to be essentially insensitive to $\dot{m}_d$ for this range of flow rates. Thus, the optimum deluge water flow rate may best be specified as the minimum value that provides sufficient flushing action to keep scaling to an acceptable level. This will probably be a very site-specific factor due to changes in water quality.

- In the present tests, the deluge water was sprayed on the very top surfaces of the fins and allowed to trickle down the vertical fins under the combined forces of gravity and shear due to air flow. This technique worked well enough and confirms this choice for the ACT facility. However, previous tests using a packed particle bed which dripped water on the fins worked equally well. Either technique can thus be recommended.

- The tests were performed at a relatively large scale to study the effect of the falling water film over a vertical length that was similar to that of the prototype system. Although some problems were experienced in handling the deluge water, these were specific to the WATA facility and should not be relevant to the prototype design. In general, no operational problems related to the deluge water system were experienced that should significantly detract from the operation or performance of a deluged air-cooled facility.

- Based on the heat transfer and frictional performance observed in this study, the deluge cooling technique appears viable and worthy of serious consideration for cooling tower applications. However, the potential problems related to scaling and corrosion of the wetted surface must be addressed and proven manageable before this technique can be recommended for general use.

3.2 RECOMMENDED ADDITIONAL WORK

As is frequently the case, the tests and analyses performed in this project in answering one set of questions have uncovered others that could not be addressed within the scope of the project. The principal areas recommended for additional work are as follows:

- Dry/wet performance tests should be run of additional heat exchanger designs other than the plate fin configurations. One of the most important parameters to be determined in these tests is the deluge film coefficient for the different geometries. The present plan calls for testing a system based on a bundle of cylindrical finned tubes. Hopefully, other geometries may also be tested in future studies.

- The WATA system should be modified to allow accurate measurement of the instantaneous deluge water evaporation rate. Tests should then be run with the wavy fin heat exchanger and with all future systems to evaluate the accuracy of the mass transfer extension of the deluge model.

- Additional tests should be performed to investigate the effect of primary side temperature. This is one aspect of the model that has not been adequately verified experimentally.

- Another effect that should be studied is alternative means for applying the deluge water to the fins. Other means of improving wetting might be devised.

- Tests should be run to determine the effect of wetting agents (or other additives or impurities in the deluge water) on the heat transfer and pressure drop performance. Preliminary studies run as part of an earlier program indicated increased heat transfer due to addition of a wetting agent. However, this was offset by higher pressure drop. This may be dependent on additive concentration and heat exchanger design. These ideas should be pursued.

- An analysis should be performed to determine a theoretically optimum heat exchanger design for dry/wet applications. If possible, a prototype heat exchanger based on this design should then be tested.

SECTION 4

BACKGROUND

4.1 PREVIOUS WORK IN THE WATA FACILITY

The Water Augmentation Test Apparatus (WATA) was built to experimentally assess the operational characteristics and performance of finned heat exchangers designed for dry cooling when operated with wetted surfaces. Another principal objective of this work was to assist with the development and evaluation of the "deluge" model for predicting the heat transfer enhancement due to wetting.

In the course of the previous studies,[3,4,5] tests were conducted of dry heat transfer performance for a HOTERV plate fin heat exchanger and for two Curtis-Wright chipped fin configurations. Wet performance data were obtained for the HOTERV surface only. In addition, however, limited data were also obtained with one of the Curtis-Wright assemblies operated in the "Separate Channel Augmented Tower" or SCAT configuration.

The dry performance data indicated that the slotted C-W surface had slightly better performance based on the heat rejection rate per unit of fan power. However, the differences in dry performance were insufficient to clearly indicate a preferred choice without detailed economic analysis.

Comparison of the deluged HOTERV surface performance with dry operation of the same system and with the CW systems showed that the enhancement due to deluge can be substantial. Enhancement ratios (Q_w/Q_d at equal air-side ΔP) of 2 to 5 were obtained for typical operating conditions. Thus, the potential for heat transfer enhancement due to deluge was found to be quite significant and worthy of further study.

During the preliminary design and bidding procedures that subsequently led to the design of the ACT facility, it appeared that a plate-fin heat exchanger designed by Trane could provide performance equal to or better than that of the HOTERV system and at lower cost. Thus, it was decided that tests of the dry/wet performance of the Trane plate-fin design would be performed. The preliminary results of these tests contributed to the selection of the Trane design for the dry/wet section of the ACT facility. In addition, results of the tests contributed in several ways to the final design of the facility. The final results of these tests constitute an important part of this report.

4.2 DEVELOPMENT AND EVALUATION OF THE "DELUGE" HEAT TRANSFER MODEL

An important part of the preceding and current test programs has been the development and testing of an approximate analytical model for predicting heat transfer from wetted surfaces. For brevity, the resulting formulation has been referred to as the deluge model. The model has been very useful in planning the test program in reducing and correlating data and in interpreting the final results. The model predicted the qualitative aspects of the HOTERV tests very well. However, because of incomplete development and inadequate means for computing two critical parameters in the model, the predicted heat transfer rates reported in the previous study[3] were generally 20-30% too high as compared to the measurements.

Due to recent advances in the development and interpretation of the deluge model, the predictive accuracy for calculating heat transfer from a wet surface has been greatly improved. In addition, the model has been extended to allow prediction of the rate of evaporation of deluge water and the resultant air outlet conditions.

An up-dated, detailed development of the deluge model that incorporates all of the recent simplifications and refinements is given in Appendix A. A brief outline of the principal steps in the development and a summary of the results will also be given here to provide the background and introduce the terminology that are needed to effectively read and understand the remaining material in this report.

4.2.1 The Surface Heat/Mass Flux Analogy

The analysis of the heat and mass transfer from an element of wetted surface is based on the control volume shown in Figure 1. Equations, 1, 2 and 3 in Table 1 contain expressions for the energy and mass balances for the control volume for dry and wet operations. For conditions where the assumption of heat/mass transfer similarity is valid, it may be assumed that Le≈1 where the convective Lewis number is defined by

$$Le = \frac{h_s}{\sigma_s C_a} \approx 1 \qquad (51)$$

Equations 3 and 4 may then be given approximately by Equations 5 and 6. There are a number of additional assumptions and approximations employed in obtaining these results that are discussed in Appendix A.

The results in Equations 1, 5 and 6 are entirely analogous in form and each of them contains the same heat transfer coefficient h_s. The important difference is that the equations for transport of heat and mass from a wet surface are written in terms of the enthalpy difference and humidity difference instead of the temperature difference. The significance of these results is that dry surface heat transfer data can be used to compute wet heat and mass transfer performance by merely changing the form of the driving potential employed. This is the basis upon which the "deluge" heat/mass transfer model is formulated.

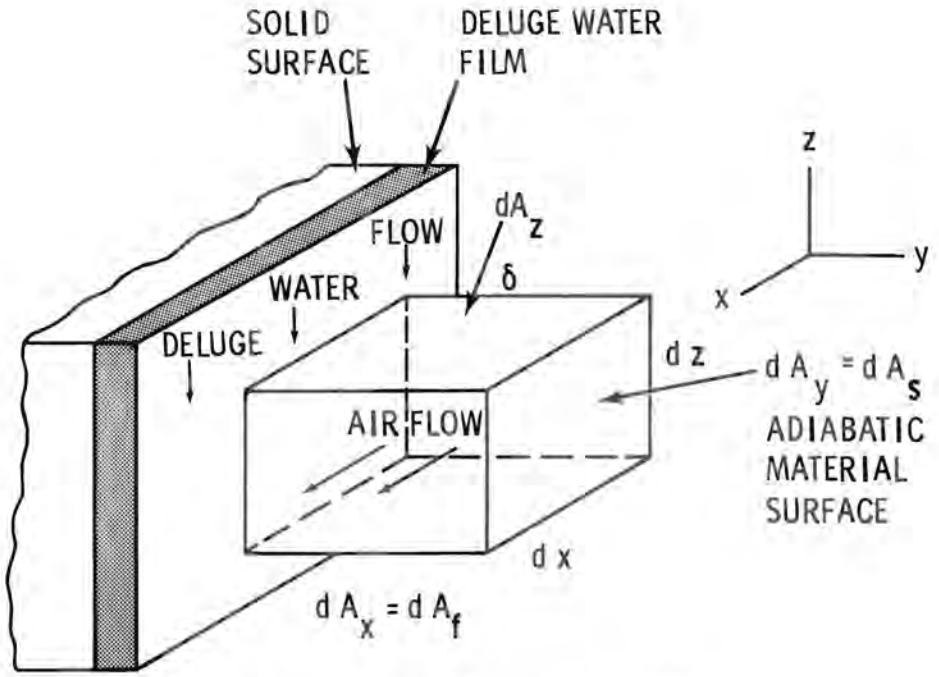

A. CONTROL VOLUME, GENERAL BOUNDARY LAYER

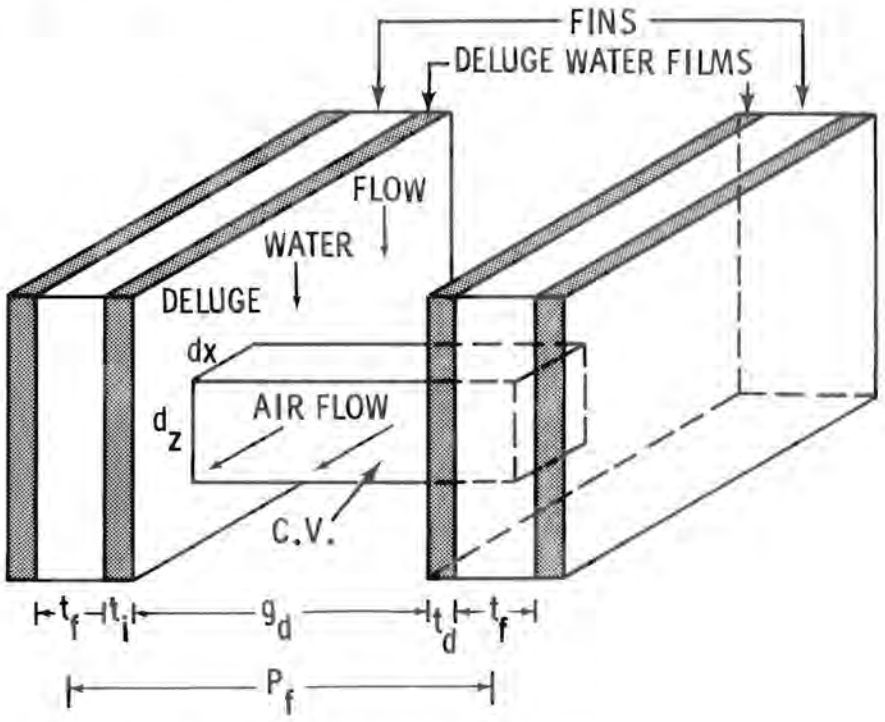

B. CONTROL VOLUME, FINNED SURFACE

Figure 1. Illustration of control volume used for heat/mass balance.

TABLE 1. SUMMARY OF EQUATIONS FOR THE SURFACE MASS/ENERGY BALANCE

$$\frac{dQ}{dA_s} = h_s(T_s - T_\infty) \qquad (1)$$

$$\frac{dQ}{dA_s} \simeq h_s(T_s - T_\infty) + \lambda_s\sigma_s(H'_s - H_\infty) \qquad (2)$$

$$\simeq \sigma_s\left[C_a(T_s - T_\infty)\left(\frac{h_s}{C_a\sigma_s}\right) + \lambda_s(H'_s - H_\infty)\right] \qquad (4)$$

$$\frac{d\dot{m}_w}{dA_s} = \sigma_s(H'_s - H_\infty) \qquad (3)$$

$$\frac{dQ}{dA_s} \simeq \frac{h_s}{C_a}(i'_s - i_\infty) \qquad (5)$$

$$\frac{d\dot{m}_w}{dA_s} \simeq \frac{h_s}{C_a}(H'_s - H_\infty) \qquad (6)$$

$$\frac{dQ}{dA_f} = G_a C_a dT_\infty \qquad (7)$$

$$\frac{dQ}{dA_f} \simeq G_a di_\infty \qquad (8)$$

$$\frac{d\dot{m}_w}{dA_f} \simeq G_a dH_\infty \qquad (9)$$

$$\frac{dT_\infty}{(T_s - T_\infty)} = \left(\frac{h_s D}{G_a C_a \delta}\right)dx \qquad (10)$$

$$\frac{di_\infty}{(i'_s - i_\infty)} = \left(\frac{h_s D}{C_a G_a \delta}\right)dx \qquad (11)$$

$$\frac{dH_\infty}{(H'_s - H_\infty)} \simeq \left(\frac{h_s D}{G_a C_a \delta}\right)dx \qquad (12)$$

The mass/energy balances for the air stream are given in Equations 7, 8 and 9. When combined with Equations 1, 5 and 6 these yield analogous differential equations for the distribution of temperature on a dry surface, Equation 10 and the distributions of enthalpy and humidity on a wet surface Equations 11 and 12. In principle, Equations 10, 11 and 12, may be integrated if the relevant variables can be given as functions of the dimensionless distance χ. However, the information required to perform the necessary integrations would seldom if ever be available except for the simplest heat exchanger configurations (i.e. a flat plate).

4.2.2 Extension to Finned Surfaces

The surface heat/mass transfer analysis has been extended to the treatment of heat transfer from finned surfaces (as illustrated by Figures A-2 and A-3, Appendix A) with introduction of the overall heat/mass transfer coefficients. The results of the analysis are summarized in Table 2. Equations 13, 14, and 15 are the analogous equations for heat/mass transfer based on overall coefficients and overall driving potentials from the primary (tube) side to the free stream (air side) conditions. The analogous expressions assumed for U_o, U_o^* and $U_m^* = C_a \Sigma_o^*$ are given in equations 16, 17 and 18 respectively.

The thermal resistance $1/U_o$ is given in the conventional form as the sum of the thermal resistances of the tube side film $(1/h_p a_p)$, the tube wall (t/ka_t)/and the finned surface $(1/h_s a_s)$ where a_s, the relative effective surface area is given by

$$a_s = \frac{A_{st} + \eta_f A_{sf}}{A_{st} + A_{sf}} \tag{52}$$

The fin efficiency is defined in the conventional manner where the actual fin area A_{sf} is replaced be an equivalent area $\eta_f A_{sf}$ which, when assumed to be uniformly at the fin root temperature T_r, will dissipate the same amount of heat as the actual finned surface. The fin efficiency can be given by a function (Equation 21) or a graph (Figure 2) as a function of the heat exchanger geometry and operating conditions. The function given in Figure 2 for cylinderical fins may also be used for plate fins if the equivalent fin length l_f and equivalent radius r_o are computed such that the resulting area is equal to the actual area of the plate fin configuration.

Equation 17 for U_o^* is analogous to Equation 16 for U_o. However, an additional thermal resistance has been added to account for the deluge water film $(1/h_d a_s^*)$ and the sum of the resistances from the tube side to the air/water interface has been multiplied by a resistance transformation parameter.

The deluge film convective heat transfer coefficient h_d is an effective or "lumped" parameter that incorporates the effects of nonuniform water flow, air flow and surface wetness. The technique employed for determining this parameter from experimental data is described in the subsequent discussion.

TABLE 2. SUMMARY OF MODEL DEVELOPMENT FOR EXTENDED SURFACE

$$\frac{dQ}{dA_s} = U_o(T_p - T_\infty) \quad (13) \qquad \frac{dQ}{dA_s} = U_o^* \left(\frac{i_p' - i_\infty}{C_a}\right) \quad (14) \qquad \frac{dm_w}{dA_s} = \Sigma_m^* (H_p' - H_\infty) \quad (15)$$

$$U_o = \left[\frac{1}{h_p a_p} + \frac{t}{k a_t} + \frac{1}{h_s a_s}\right]^{-1} \quad (16) \qquad U_o^* = \left[\xi\left(\frac{1}{h_p a_p} + \frac{t}{k a_t} + \frac{1}{h_d a_s^*}\right) + \frac{1}{h_s a_s^*}\right]^{-1} \quad (17) \qquad C_a \Sigma_m^* = \left[\xi_m\left(\frac{1_m}{h_p a_p} + \frac{t}{k a_t} + \frac{1}{h_d a_m^*}\right) + \frac{1}{h_s a_m^*}\right]^{-1} \quad (18)$$

$$\xi = \frac{(i_p' - i_r')}{C_a(T_p - T_r)} \quad (19) \qquad \xi_m \tilde{\simeq} \xi \quad (20)$$

$$\eta_f = f\left(\frac{r_i}{r_o}, Bi_f^{1/2}\right) \quad (21) \qquad \eta_f^* = f\left(\frac{r_i}{r_o}, Bi_f^{*1/2}\right) \quad (22) \qquad \eta_m^* = f\left(\frac{r_i}{r_o}, Bi_m^{*1/2}\right) \quad (23)$$

$$Bi_f = \frac{1_f^2}{k y_b} h_s \quad (24) \qquad Bi_f^* = \frac{1_f^2}{k y_b}\left[\frac{1}{h_d} + \frac{1}{\xi h_s}\right]^{-1} \quad (25) \qquad Bi_m^* = \frac{1_f^2}{k y_b}\left[\frac{1}{h_d} + \frac{1}{\xi_m h_s}\right]^{-1} \quad (26)$$

$$\frac{dT_\infty}{(T_p - T_\infty)} = \left(\frac{U_o A_s}{\dot{m}_a C_a}\right) dx \quad (27) \qquad \frac{di_\infty}{(i_p' - i_\infty)} = \left(\frac{U_o^* A_s}{\dot{m}_a C_a}\right) dx \quad (28) \qquad \frac{dH_\infty}{(H_p' - H_\infty)} = \left(\frac{\Sigma_o^* A_s}{\dot{m}_a}\right) dx \quad (29)$$

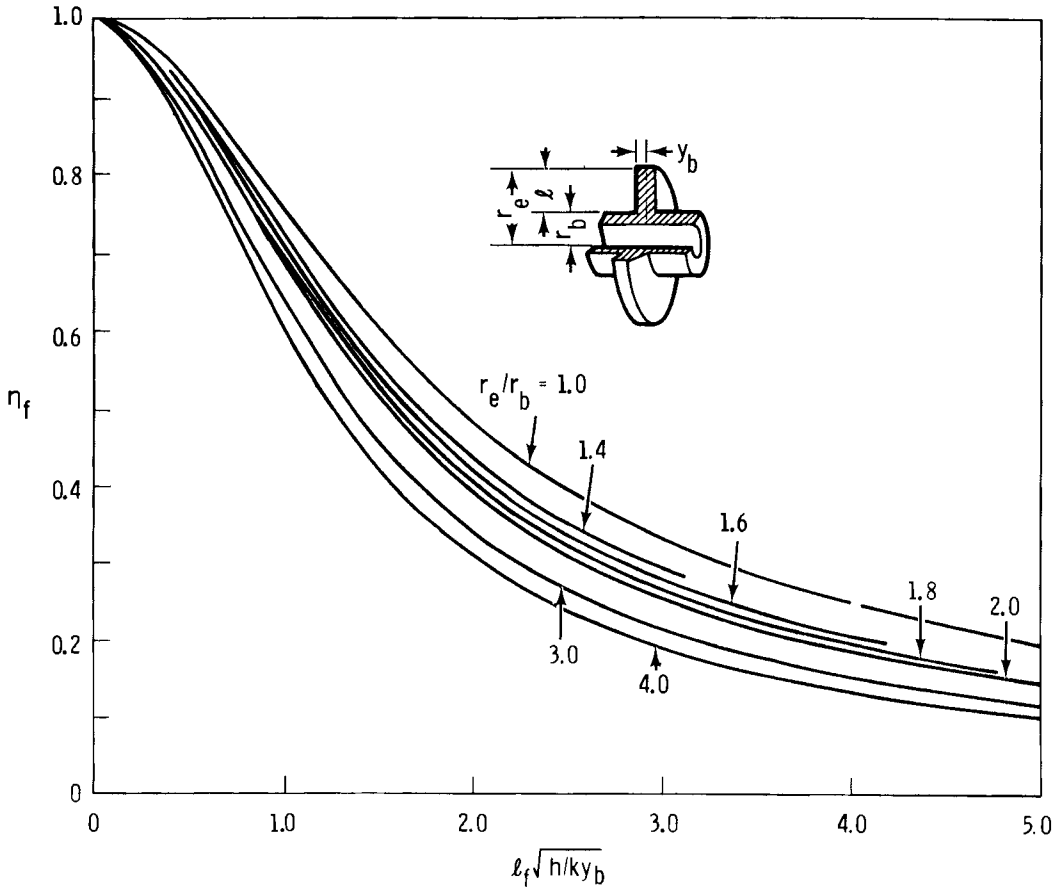

Figure 2. Fin efficiency solution for an annular fin (also used to model plate fin with equivalent radius).

The transformation of the inside thermal resistances is required to match the internal expression for Q based on the temperature driving potential to the surface heat flux based on the enthalpy potential. The relevant derivation is given in Appendix A. The resulting definition for ξ is,

$$\xi = \frac{(i_p' - i_r')}{C_a(T_p - T_r)} \tag{19}$$

The evaluation of this parameter and the analogous expression for ξ_m are discussed in detail in Appendix A.

The relative effective surface area for wet operation a_ξ^* is analogous to a_s. The wet fin efficiency may be computed from the function or graph for the dry efficiency by the transformation of variables given by Equations 22 and 25.

An overall mass transfer coefficient $U_m^* = C_a\Sigma_m^*$ is defined by Equation 18 in a manner completely analogous to the expression for U_o^*, Equation 17. It

is assumed that the actual internal resistance to heat transfer can be converted to an "effective" resistance to mass transfer by multiplication with a resistance transformation parameter ξ_m. This is completely analogous to the transformation wherein the equation for U_o^* was obtained from the expression for U_o. The efficiency η_m^* and area A_m^* are then determined by the transformation of variables given by Equations 23 and 26. In many cases, it may be assumed that $\xi_m \approx \xi$ and thus $\eta_m^* \approx \eta_f^*$ which greatly simplifies the model. A general, vigorous technique for computing ξ_m is described in Appendix A.

When the equations for dry surface heat flux, equation 13 and wet surface heat/mass flux, Equations 14 and 15 are equated to the respective heat/mass gains of the air, Equations 1, 5 and 6, differential Equations 27, 28 and 29 are obtained that describe the air property variations with distance in the airflow direction. For suitable conditions these expressions can be integrated to obtain the distributions of temperature, enthalpy and humidity in a heat exchanger. However, closed form solutions would probably be possible in only the simplest applications. (see for example the analysis in the next section).

4.2.3 Analysis of a Wetted Plate-Fin Condensor

The expressions in Equations 27, 28 and 29 will now be integrated for a plate fin condensor in cross-flow. The principal assumptions are,

- the primary or tube side temperature is constant
- the air mass flux G_o is uniform in any plane normal to the flow
- the NTU parameters N, N* and N_m^* are constant

The results of the integrations are summarized in Table 3.

Equations 30, 31 and 32 give the distributions of the air temperature in a dry heat exchanger and the air enthalpy and humidity in a wet heat exchanger. In addition, using the computed values of i_∞, H_∞ and psychometric charts, the distribution of the dry bulb temperature in a wet core can also be predicted. This is the analytical analog to the graphical procedure developed by Mickley[6].

The total heat/mass transfer from the heat exchanger is obtained by a second integration where the results are given in terms of the effectiveness ϕ, ϕ^* and ϕ_m^*. The analogous expressions for heat and mass transfer are given by Equations 39, 40 and 41 where the corresponding expressions for the effectiveness are given by Equations 45, 46 and 47. The advantage to this approach is that the heat/mass transfer is given in terms of the inlet conditions without the need of the outlet properties.

Equations 13, 14 and 15 can also be integrated to obtain alternate equivalent expressions for the heat and mass transfer, Equations 42, 43 and 44. The only disadvantage of this approach is that both inlet and outlet conditions appear in the log mean property differences defined by Equations 48, 49 and 50. This generally requires an iterative solution technique.

TABLE 3. SUMMARY OF MODEL EQUATIONS FOR A DELUGED CONDENSOR IN CROSS FLOW

$$\theta(x) = \frac{T_{p1} - T_{\infty}(x)}{T_{p1} - T_{\infty 1}} \quad (30)$$

$$\theta^*(x) = \frac{i'_{p1} - i_{\infty}(x)}{i'_{p1} - i_{\infty 1}} \quad (31)$$

$$\theta_m^*(x) = \frac{H'_{p1} - H(x)}{H'_{p1} - H_{\infty 1}} \quad (32)$$

$$= e^{-Nx} \quad (33)$$

$$= e^{-N^*x} \quad (34)$$

$$= e^{-N_m^*x} \quad (35)$$

$$N = \frac{U_o A_s}{\dot{m}_a C_a} \quad (36)$$

$$N^* = \frac{U_o^* A_s}{\dot{m}_a C_a} \quad (37)$$

$$N_m^* = \frac{\Sigma_o^* A_s}{\dot{m}_a} \quad (38)$$

$$\dot{Q}_o = \dot{m}_a c_a \phi (T_{p1} - T_{\infty 1}) \quad (39)$$

$$\dot{Q}_o = \dot{m}_a \phi^* (i'_{p1} - i_{\infty 1}) \quad (40)$$

$$\dot{m}_o = \dot{m}_a \phi_m^* (H'_{p1} - H_{\infty 1}) \quad (41)$$

$$= U_o A_s \Delta T_{1m} \quad (42)$$

$$= U_o^* A_s \frac{\Delta i_{1m}}{C_a} \quad (43)$$

$$= \Sigma_m^* A_s \Delta H_{1m} \quad (44)$$

$$\phi = 1 - e^{-N} \quad (45)$$

$$\phi^* = 1 - e^{-N^*} \quad (46)$$

$$\phi_m^* = 1 - e^{-N_m^*} \quad (47)$$

$$\Delta T_{1m} = \frac{(T_{p2} - T_{\infty 2}) - (T_{p1} - T_{\infty 1})}{\ln \left| \frac{T_{p2} - T_{\infty 2}}{T_{p1} - T_{\infty 1}} \right|} \quad (48)$$

$$\Delta i_{1m} = \frac{(i'_{p2} - i_{\infty 2}) - (i'_{p1} - i_{\infty 1})}{\ln \left| \frac{i'_{p2} - i_{\infty 2}}{i'_{p1} - i_{\infty 1}} \right|} \quad (49)$$

$$\Delta H_{1m} = \frac{(H'_{p2} - H_{\infty 2}) - (H'_{p1} - H_{\infty 1})}{\ln \left| \frac{H'_{p2} - H_{\infty 2}}{H'_{p1} - H_{\infty 1}} \right|} \quad (50)$$

4.2.4 Evaluation of ξ, h_d and ξ_m

To apply the deluge model for prediction of heat/mass transfer, values of ξ and h_d must be specified. An explicit expression (Equation 19) has been derived for ξ. However, precise evaluation of ξ requires knowledge of the root temperature T_r which varies with core design and operating conditions in a manner that is not easily predicted.

Figure 3 illustrates temperature profiles in a simple geometry that show how T_r can vary. The characteristics of the three profiles are as follows:

1. $T_\infty < T_r < T_p$: relatively low heat transfer and evaporation rates, representative of conditions of low ITD, high humidity and low h_s, dominated by sensible heat transfer with relatively little evaporation

2. $T_r \approx T_\infty$: high heat/mass transfer rates, low ITD, low humidity and high h_s, little or no sensible heat flux to the air, thus air humidity rises but temperature is unchanged

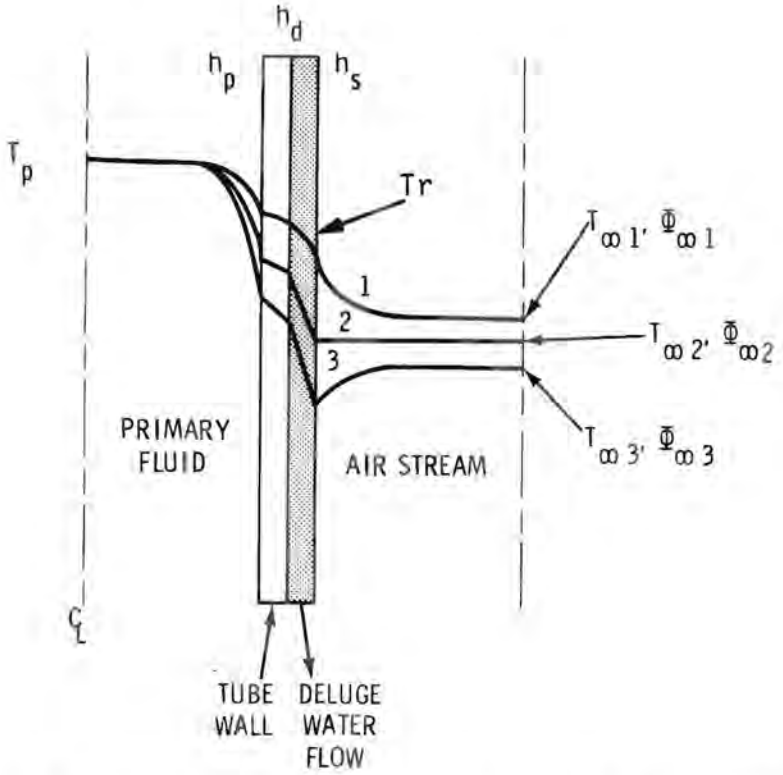

Figure 3. Simplified schematic of temperature profiles that may exist for deluged heat exchanger operation.

3. $T_r < T_\infty$: very high heat transfer and evaporation rates, low ITD, low humidity high h_s, air stream is cooled evaporatively.

All of these conditions have been observed in the experiments. Variations in T_r of 10°F to 20 °F can result in 10-30% variation in ξ with nearly proportional variations in U_o^*. Thus, values of T_r used in evaluating ξ should be as accurate as possible. When T_r is not known, equation 19 can still be used to estimate ξ (i.e. by assuming $T_r = T_\infty$ or some other reasonable value). When practical, however, values of T_r and ξ should be computed by an iterative procedure such as that used to extract T_r and h_d from the data as discussed below.

As mentioned above, the deluge film coefficient h_d is a lumped parameter that incorporates the effects of nonuniformities in airflow, deluge water flow, surface wetness and all other forms of ignorance not specifically accounted for elsewhere. It is thus probably impossible to predict this parameter from first principles. In addition, it is extremely unlikely that empirical correlations exist that would be useful for this application (at least none have been found). Thus, there is presently no recourse for determining h_d except by extracting it from experimental data.

According to the deluge heat/mass transfer model, the heat rejected by the core for given operating conditions can be given by any of the following expressions,

$$\frac{Q}{A_s} = \frac{\left(\frac{i'_p - \bar{i}'_r}{C_a}\right)}{\xi\left(\frac{1}{h_p a_p} + \frac{t}{k a_t} + \frac{1}{h_d a_s^*}\right)} \tag{53}$$

$$\frac{Q}{A_s} = h_s a_s^* \left(\frac{i'_r - \bar{i}_\infty}{C_a}\right) \tag{54}$$

$$\frac{Q}{A_s} = \left(\frac{\dot{m}_a \phi^*}{A_s}\right) \frac{(i'_p - i_\infty)_1}{C_a} \tag{55}$$

Equation 53 gives the heat transfer from the tube side to the root, Equation 54 gives the heat transfer from the root to the air and Equation 55 gives the heat transfer in terms of the overall enthalpy difference. If the model is to be internally consistent, values of h_d and ξ must be used that simultaneously satisfy all three of these expressions. (In fact, only two of these expressions are independent, since, for example, the first two can be used to obtain the third.)

For a given set of operating conditions defined by values of (h_p, h_s, $\dot{m}_a$, T_p, T_∞, H_∞, $\dot{m}_d$) and the corresponding measured value of Q for that condition, any two of the above equations constitutes a set of two simultaneous equations with two unknowns. The solution of these equations will yield unique values of T_r, h_d for each data set. Because of the complex interrelationships of the variables in these equations, an iterative solution such as that described in Appendix A is required. The results obtained by this procedure are presented in Section 6.

The values of T_r and h_d thus determined are empirical results determined from experimental data according to an assumed heat transfer formulation; the deluge model. The values of h_d that result are empirical in exactly the same sense that h_s and h_p are. Furthermore, all of these heat transfer coefficients are "lumped" parameters in that they account for nonuniformities in geometry, flowrate and surface conditions in some average way that cannot be precisely defined. The only difference in h_d is that the amount of ignorance "lumped" into this parameter is somewhat greater because of the additional effect of nonuniform wetting.

The procedure used to derive h_d values from the data also yields corresponding values of T_r (and thereby of ξ) for each data set. Although the fin root temperature T_r has a physical interpretation, as illustrated in Figure 3, the values of T_r extracted from the data are only approximately related to any actual temperatures in the heat exchanger. However, the same would be true of root temperatures calculated for a dry operation of the same system since the same type of assumptions and approximations are involved.

At one time it was suspected that the temperature of the deluge water dropping off the core (T_d, a measured parameter) could be used to approximate T_r and thus to compute ξ and h_d. However, when this approach was used, predicted values of U_o were high by 20-30%.[3] Furthermore, the model was internally inconsistent because calculation of the root condition from the inside would not match that obtained from the surface to the air. This approach was then abandoned in favor of the approach just described.

The analysis in Appendix A contains many details of the above analysis including justification for the approximations employed. The theoretical basis for data correlations used in Section 6 are also developed. For these and other details concerning the basis and use of the model, the reader may consult Appendix A.

SECTION 5

EXPERIMENTAL APPARATUS AND PROCEDURES

5.1 DESCRIPTION OF WATA LOOP

All testing took place in the Water Augmentation Test Apparatus (WATA), an experimental test facility designed by PNL and shown in Figure 4. Figure 5 shows a schematic diagram of the facility. The WATA consists of three fluid loops: the air loop, circulation water loop, and augmentation water loop. These loops come together in the heat exchanger test section.

The air loop is an open-ended single-pass loop designed to provide uniform airflow through the test section at a desired temperature and humidity and at approach velocities from 3 ft/sec to 16 ft/sec. Outside air is brought in through a centrifugal blower whose output is variable from 2100 cfm to 12000 cfm. After leaving the blower, the air passes through a steam heating unit and then through a steam humidification section to provide inlet air at the desired wet and dry bulb temperatures. The air then flows through a restricted mixing section before passing through a vaned expansion section with a 2 ft x 6 ft outlet. A screen pack at the expansion section outlet helps maintain flow uniformity. The air then passes through a vaned 2 ft x 6 ft 90° elbow, and another screen pack, and then through a 4-ft approach section of the same cross section as the 2 ft x 6 ft test core.

From the test core section the air flows through a 3-ft section of 2 ft x 6 ft duct, through a contraction, through a flexible duct, then into an 18-in. diameter, 20-ft long section of straight duct before being exhausted to the outside. The straight section is equipped with an Annubar flow sensor used to measure the air mass flow rate through the test section.

The air loop has been designed to permit flexibility in core orientation and airflow direction. Figure 6 illustrates the means provided to vary the core orientation.

The circulation loop provides the heat to be rejected by the test core. A centrifugal pump capable of up to 365 gpm flow pulls water from a 400-gal storage tank. Part of the flow is passed through two SCR-controlled electric circulation heaters providing a total of 135kW of heat. The heated water is then mixed with the remainder of the circulation water flow and fed to the test core inlet manifold. After being cooled in the test core, the circulation water returns to the storage tank and is ready for recirculation.

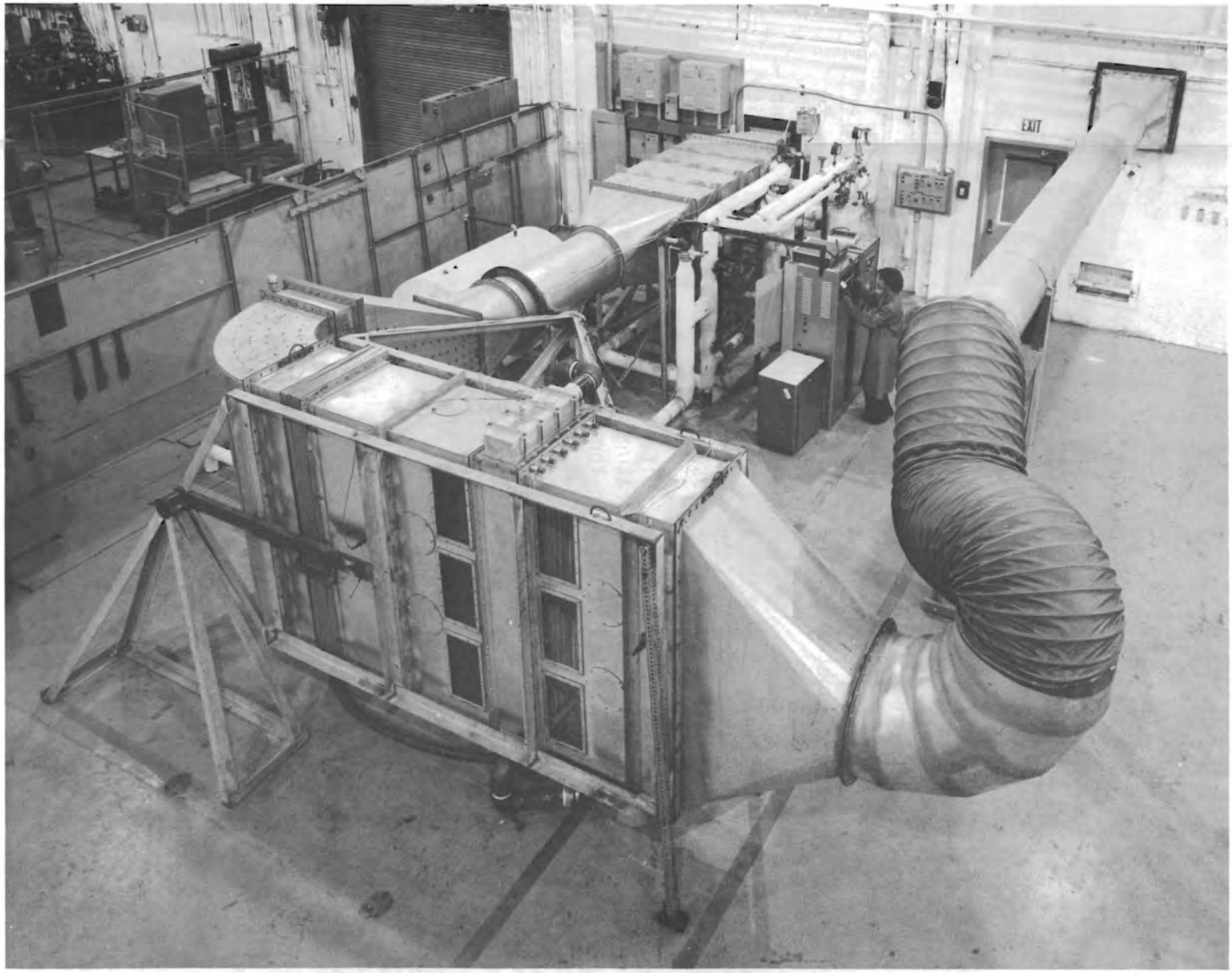

Figure 4. WATA test apparatus.

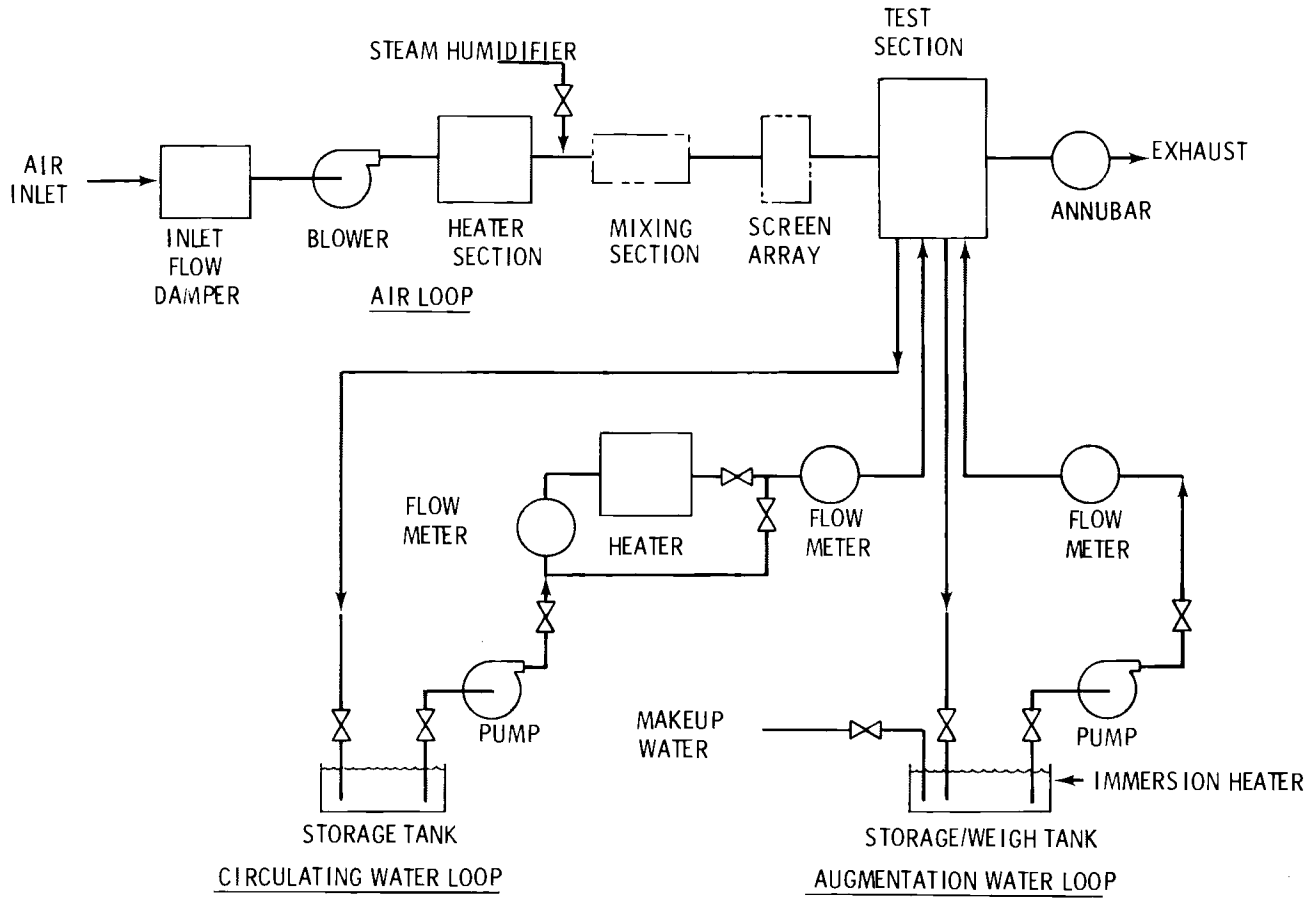

Figure 5. Schematic of WATA test apparatus.

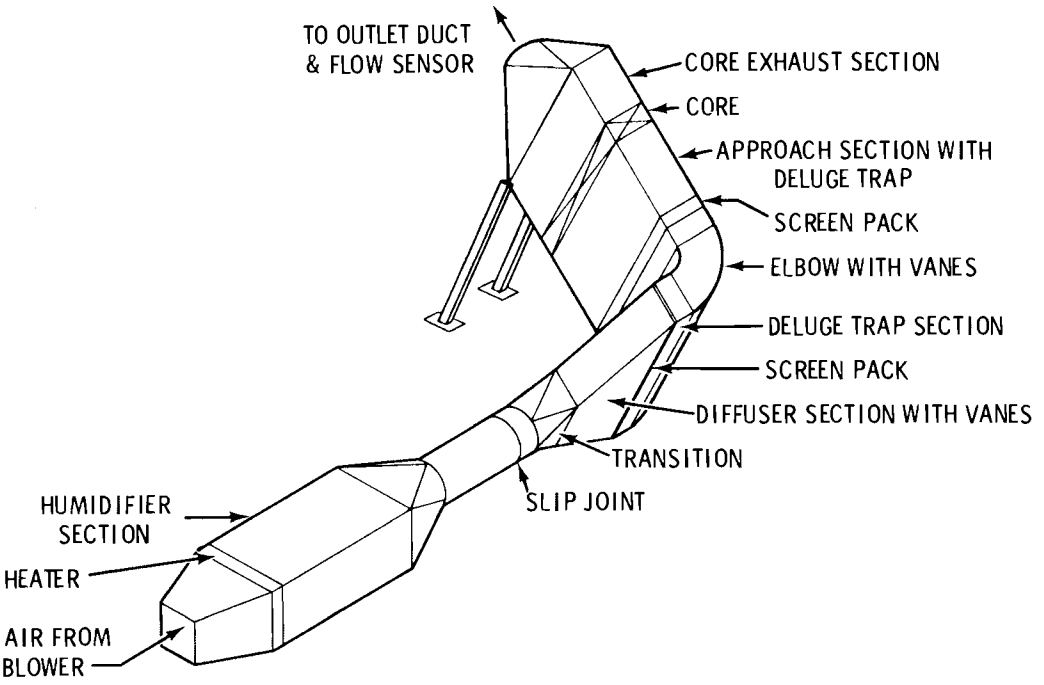

Figure 6. WATA air ducting upward airflow at any angle up to 45°.

The augmentation loop is used for evaluating deluged heat exchangers for integrated dry/wet towers. A centrifugal pump with a 25-gpm (maximum) capacity draws water from a 40-gal weigh tank and pumps it to the deluge injection point located at the top of the deluged test core. After the deluge water passes over the air-side surfaces of the core, it is collected in a catch basin at the base of the test core. A second pump then returns the deluge water to the weigh tank. Water may be added to the weigh tank from a deluge storage tank when the water in the weigh tank has been depleted by evaporation on the test core.

The three loops come together in the test core. The test core section consists of a 6-ft high x 2-ft wide x 1-ft deep duct section surrounding the specific heat exchanger core being tested. Specific cores tested will be discussed in subsequent sections.

5.2 INSTRUMENTATION

Five parameters are measured in the WATA facility:

5.2.1 Temperature

Calibrated shielded copper constantan thermocouple probes (Type T) accurate to $\pm 0.5^{\circ}F$ are located as listed below:

a) blower inlet
b) in the airflow 17 in. upstream of the test core (6)
c) in the airflow 17 in. downstream of the test core (6)
d) in the airflow adjacent to the Annubar

e) exposed to room air adjacent to the test core
f) circulation water storage tank (2)
g) 135-kW heater inlet (2)
h) 135-kW heater outlet (2)
i) core inlet manifold (3)
j) core outlet manifold
k) augmentation water storage tank
l) augmentation water weigh tank
m) augmentation water injection point
n) augmentation water collection basin

5.2.2 Differential Temperature

Two thermocouples are used to measure the differential temperature in each of two locations:

1) inlet to outlet of the 135-kW heater

2) inlet to outlet of the core

These thermocouples were calibrated individually but they were picked to have closely matching calibration curves. The resulting emf's were measured with a Doric microvoltmeter. Uncertainty in these measurements were estimated at $\pm 0.5^{o}F$.

5.2.3 Air Dewpoint

Air dewpoint upstream and downstream of the test core was determined using two General Eastern Model 1200 EP optical hygrometers fed by aspirated probes. Two probes were located 15 in. upstream of the core and five probes were located 33 in. downstream of the core. Under laboratory controlled conditions these units have a claimed accuracy of $\pm 0.44^{o}F$. Error in the data logger sampling technique caused the actual error to be about $\pm 1.0^{o}F$.

5.2.4 Air Flow

Total airflow is measured with an 18-in. calibrated Annubar with a manufacturer's claimed accuracy of $\pm 4\%$ of reading. Readout is accomplished through a Dwyer Model 246 inclined manometer with a claimed accuracy of ± 0.02 in. H_2O. Nonuniformity in the flow distribution upstream from the annubar increased the uncertainty in the measured airflow rate to about $\pm 10\%$. Airflow uniformity was checked by traverses in front of the test section using a Thermo Systems Model 1054B linearized hot film anemometer with a manufacturer's claimed accuracy of $\pm 1\%$ of reading.

5.2.5 Water Flow

Cox turbine flowmeters, calibrated to an accuracy of $\pm 0.5\%$ of flow, are used to measure three water flow rates:

a) total deluge flow rate

b) total circulation water flow rate

c) circulation water flow rate through the 135-kW circulation heater.

5.2.6 Pressures

Static pressure is measured upstream of the test core and downstream of the test core with a Wallace and Tiernan precision aneroid manometer claimed accurate to ±0.03 in. Hg. Ambient barometric pressure is measured with the same device. Air-side pressure drop across the core is measured with a Dwyer Model 246 inclined manometer claimed accurate to ±0.02 in. H_2O. Four static pressure probes are located 21 in. upstream of the core and four are located 21 in. downstream of the core. The downstream probes are in fully recovered flow.

5.3 TEST CORE SPECIFICATIONS

Table 4 contains a list of the important dimensions for the Trane core. A sketch of its general construction is shown in Figures 7 and 8. The surface is made of aluminum and is contained in a steel frame work.

TABLE 4. TRANE CORE SPECIFICATION SHEET

Heat Exchanger Dimensions

Height:	6 ft	
Width:	2 ft	
Depth:	0.375 ft	
Tube Orientation:	Horizontal	
Number of Tubes:	144	
Tube Cross Section Dimensions:	5/8" x 0.049 circular	
Airside Fins:	0.0085 in. (10 fins/in.)	
	Ammonia Side	Air Side
Frontal Area:	--	12 ft^2
Minimum Flow Area:	0.0939 ft^2	6.408 ft^2
Fin Area:	N/A	931.00 ft^2
Total Surface Area:	39.74 ft^2	974.14 ft^2
Hydraulic diameter	0.0439 ft	0.009724 ft

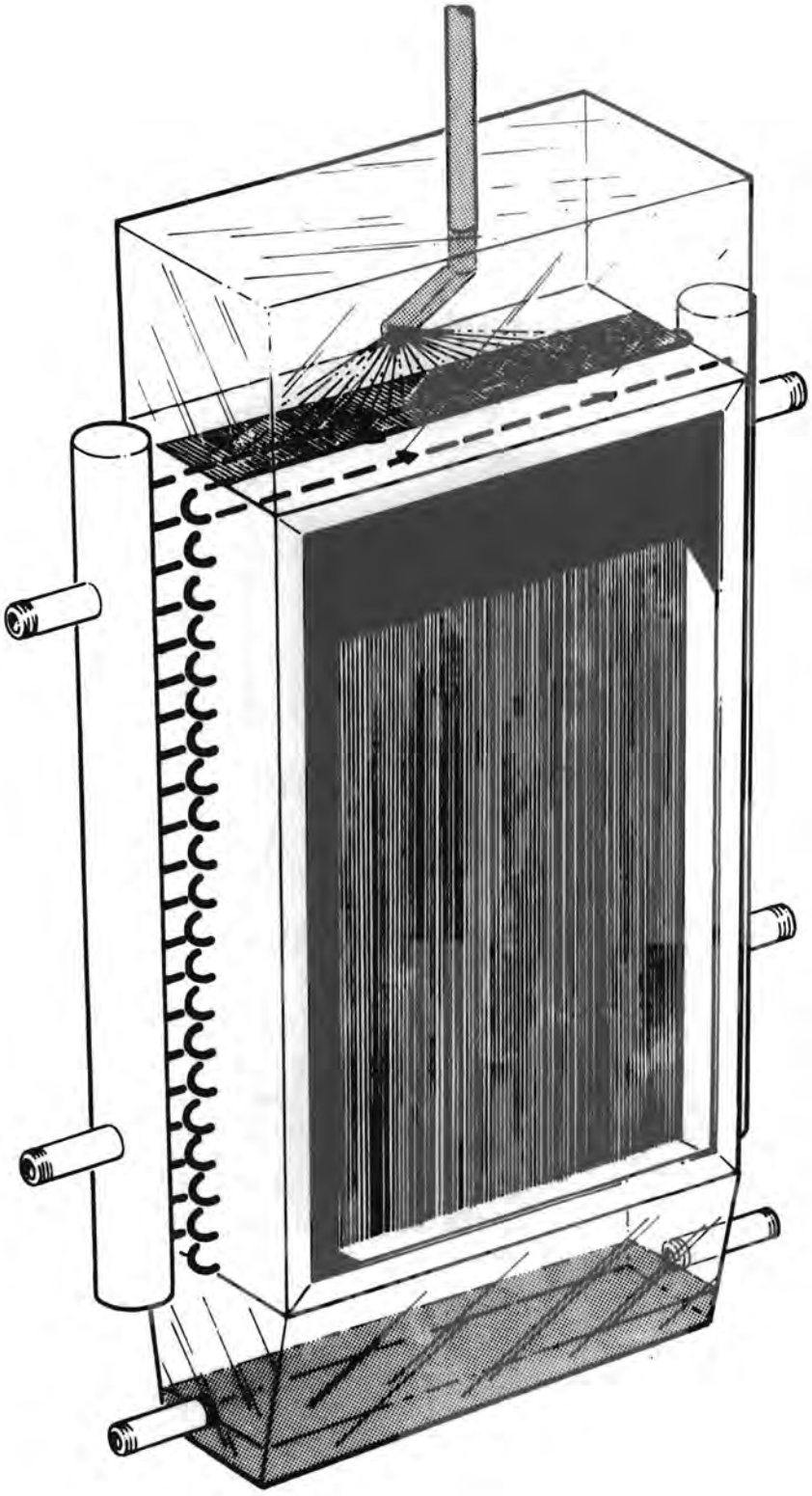

Figure 7. Trane test core assembly.

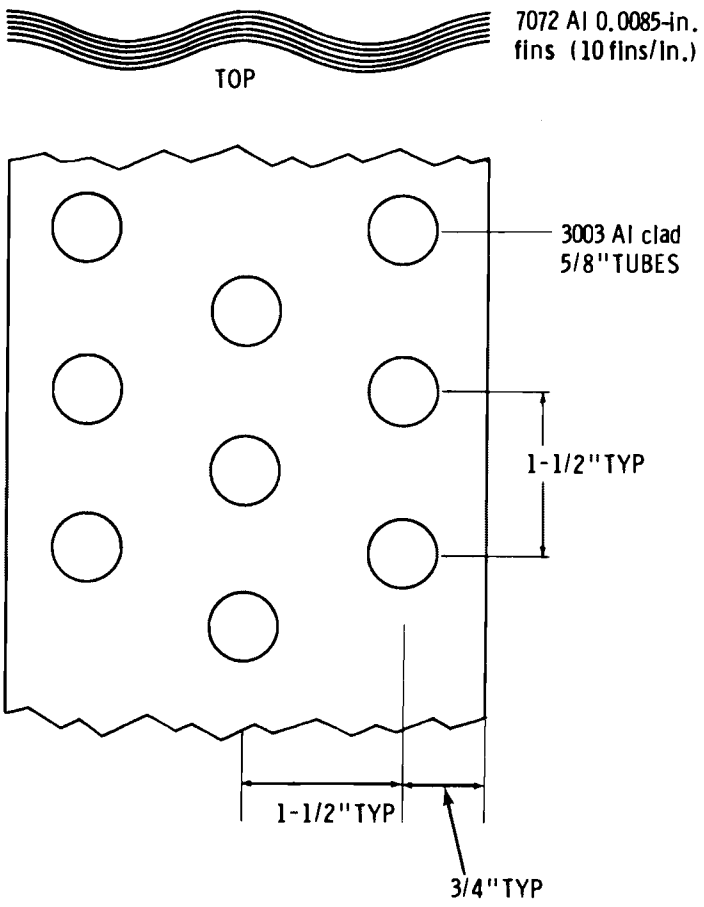

Figure 8. Trane plate fin heat exchanger design.

Deluge distribution is accomplished by forcing the water through a flat spray "floodjet" nozzle size #40 manufactured by Delavan Inc. The nozzle is housed in an air tight plastic box which allows for proper location and orientation of the nozzle. A plastic deflection plate in the box insures that a majority of the spray impinges on the core. Water is allowed to enter and leave the test section through 4" gaps in the top and bottom surfaces of the steel frame. A plastic box at the bottom of the test section serves to collect the unevaporated deluge water.

5.4 UNCERTAINTY ANALYSIS SUMMARY

Any experimentally derived value has an uncertainty associated with it. That uncertainty is caused by the inherent uncertainty in the measured variables and parameters used to derive the value. The purpose of an uncertainty analysis is to estimate the probable uncertainty in an experimentally derived value based on the uncertainty of the measurements used to derive it. In this way the unexpected magnitude of scatter or inconsistency in the experimental results can be estimated. If the actual observed inconsistency is

appreciably greater than that predicted, problems such as the existence of uncontrolled variables may exist in the experimental facility or procedure. This may also indicate the methods being used to analyze the data or the theory to which the results are being compared do not fully account for all the controlling variables. An uncertainty analysis aimed at predicting probable experimental uncertainty is particularly valuable in the WATA test program where the analytical methods being used to predict deluged performance are as yet unproven and may not fully account for all variables.

The probable uncertainty for the WATA test results to be presented in Section 6 is indicated by bars showing the uncertainty range for representative data points. Where data points are very close together, uncertainty bias are shown on representative points. Probable uncertainties (δR) have been determined using the method suggested by Kline and McClintock[7] in which

$$\delta R = \left[\left(\frac{\partial R}{\partial X_1} dX_1\right)^2 + \left(\frac{\partial R}{\partial X_2} dX_2\right)^2 \ .... + \left(\frac{\partial R}{\partial X_n} dX_n\right)^2\right]^{1/2} \tag{56}$$

where

R = the experimental result, a function of several variables (X_i)

δR = the probable uncertainty in R at 20:1 odds

δX_i = the uncertainty in X_i where $X_i = X_i \pm \delta X_i$ at 20:1 odds

and where $\frac{R}{\partial X_i}$ has been evaluated approximately using the expression

$$\frac{\partial R}{\partial X_i} \triangleq \lim_{\Delta X_i \to o} \left[\frac{R(X_i + \Delta X_i) - R(x_i)}{\Delta X_i}\right] \tag{57}$$

$$\simeq \frac{R(X_i + \delta X_i) - R(X_i)}{\delta X_i} \tag{58}$$

It should be noted that the determination of values for δX_i to be used in evaluating δR requires some judgment on the part of the experimenters. Uncertainties in the individual variables measured in the WATA facility have been estimated based on instrument manufacturers' claims, observed instrument fluctuation noted from repeated readings under steady-state conditions, and past experience. The major sources of uncertainty have been found to be the measurement of temperature rise across the circulation heater and the measurement of air dewpoint temperature upstream and downstream of the test cores. Uncertainty in the circulation heater temperature rise affects the uncertainty of both dry and deluged results, while dewpoint temperature uncertainty affects only deluged results. A complete calculation of the uncertainty for certain important parameters is given in Appendix C.

5.5 SUMMARY OF DATA REDUCTION TERMINOLOGY, EQUATIONS, AND PROCEDURES

5.5.1 Dry/Wet Pressure Drop

The values for pressure drop across the core during both wet and dry operation are commonly represented by a non-dimensional friction factor f or loss coefficient f_o. Equation 59 was used to reduce the pressure drop data to fanning friction factors.

$$f = \frac{2g_c \rho_m \Delta P A_c^3}{\dot{m}_a^2 A_s} - \frac{\sigma^2 A_c N'E}{A_s} \tag{59}$$

where ΔP = total frictional pressure drop (lb/ft^2)

N' = number of coil banks

E = contraction and expansion losses

$$= \frac{1.75}{\sigma_f^2} - \frac{2.75}{\sigma_f} + 1 \tag{60}$$

σ_f = fin free area ratio

$$= 1 - FPI \cdot t_f \tag{61}$$

FPI = fins/inch

The first term in Equation 59 is an overall friction factor or loss coefficient and the second term accounts for the expansion and contraction losses. Thus, Equation 59 can be rewritten in terms of f_o:

$$f = f_o - \frac{\sigma^2 A_c N'E}{A_s} \tag{62}$$

It was assumed that Equation 59 was appropriate for use with both wet and dry pressure drop data. This is technically not true, since the wet film increases the apparent thickness of the fins and thus increases the expansion and contraction losses.

The air flow rate is calculated using Equation 63 which is an empirical formula supplied by the annubar manufacturer

$$\dot{m}_a = 90326 \sqrt{\Delta P_{ann}} \sqrt{\rho} \tag{63}$$

ΔP_{ann} = manometer reading of pressure drop across the annubar (in. H_2O)

Dry air densities were used in the above calculations in place of moist air densities. Since ρ is directly proportional to $\dot{m}_a^2$, any errant effect this substitution might have is cancelled out when calculating f_o or f.

5.5.2 Dry Heat Transfer

All individually recorded temperatures were recorded 4 times at one minute intervals. These four values were then averaged and the average was used in the calculations. In the cases where thermocouples were located at several positions to measure the same temperature, the positional average as well as the time average temperature was used. For instance, the air temperatures at the inlet and outlet to the core were each measured in six different locations. With each temperature measured four times, there were 24 temperatures for the inlet and 24 temperatures for the outlet. The average of these 24 was used in each case as the core inlet and outlet temperatures.

Emf readings for the differential temperatures were measured in microvolts (μV) and are converted to ^oF by dividing by the constant 24 $\mu V/^oF$ (for Type T thermocouples). Inlet and outlet air temperatures ($T_{\infty 1}$, $T_{\infty 2}$) and inlet water temperatures (T_{p1}) are measured directly. The outlet water temperature (T_{p2}) is the inlet water temperature minus the ΔT_p(core) measured differentially. These four temperatures are used to determine the ΔT_{lm} in Equation 48. ΔT_{core} was generally 2^oF or less. Thus the assumption for much of the analysis that T_p is constant is valid.

The total rate of heat rejection from a given test core may be determined from the equation

$$Q_{REJ} = \dot{m}_p C_p \Delta T_c \tag{64}$$

where

Q_{REJ} = rate of test core heat rejection, Btu/hr

$\dot{m}_p$ = circulation water mass flow rate, lb_m/hr

C_p = circulation water specific heat, Btu/lb_m F

ΔT_p = temperature drop of circulation water across the core.

However, to insure fully turbulent circulation water flow in the test core and to approximate the near isothermal core tube temperature that would be found in an ammonia cooling tower, it is desirable to maintain high circulation water flow rates during testing. This results in ΔT_p values of only 1 to 2°F. Because of the high percentage uncertainty that would result from measuring such a small temperature drop, an alternative means for determining Q_{REJ} was used based on the following equation:

$$Q_{REJ} = \dot{m}_h C_p \Delta T_h + Q_{PUMP} - Q_{LOSSES} \quad (65)$$

$$= \dot{m}_h C_p \Delta T_h + Q_{PERIPHERAL} \quad (66)$$

where

Q_{REJ} = rate of test core heat rejection, Btu/hr

$\dot{m}_h$ = circulation water mass flow through the circulation heater, lb_m/hr

C_p = circulation water specific heat, Btu/lb_m-°F

ΔT_h = temperature rise across the circulation heater, °F

Q_{PUMP} = rate of heat addition to circulation water by the circulation pump, Btu/hr

Q_{LOSSES} = rate of heat lost to the atmosphere through piping, tank walls, and manifolds, Btu/hr

$Q_{PERIPHERAL} = Q_{PUMP} - Q_{LOSSES}$

During testing, $\dot{m}_h$ was adjusted to give a value of ΔT_h of over 10°F as measured by a differential thermocouple circuit. This insured an acceptably small uncertainty in the measurement of ΔT_h. For the test core, a curve was generated relating $Q_{PERIPHERAL}$ to the average temperature difference between room air and circulation piping at a constant circulation water flow rate. These curves were generated by well insulating the air-side heat transfer surfaces of the test core and measuring the rate of temperature change of the known circulation water inventory for various circulation water temperatures at zero heater input. Thus,

$$Q_{PERIPHERAL} = m_p C_p \frac{\Delta T}{\Delta t} \tag{67}$$

where

m_p = circulation water inventory, lb_m

$\frac{\Delta T}{\Delta t}$ = change in average water temperature over time interval Δt, $^oF/hr$

Once a curve was generated, the value of $Q_{PERIPHERAL}$ could be determined for any test condition and added to the circulation heater rate to obtain the core heat rejection rate. For all cores tested, $Q_{PERIPHERAL}$ was positive (i.e., the pump added more heat than was lost by the piping). Typically, $Q_{PERIPHERAL}$ was less than 10% of the total Q_{REJ}.

The previous information may be used collectively to determine an overall dry heat transfer coefficient (U_o) by using Equation 42. Equation 16 may then be used to determine an average air-side coefficient h_o which includes the fin efficiency.

$$h_o = \left(\frac{1}{U_o} - \frac{1}{h_p a_p} - \frac{t}{k_f a_t}\right)^{-1} \tag{68}$$

The water-side heat transfer coefficient was calculated using the Dittus-Boelter correlation[8] for turbulent flow of a liquid being cooled.

$$h_p = 0.023 \frac{k}{D_h} Re^{0.8} Pr^{0.3} \tag{69}$$

Under nominal operating conditions the velocity of the water on the primary-side of the Trane core was about 10 fps. At this velocity the water is fully turbulent and h_p is calculated to be about 2200 $Btu/hr\text{-}ft^2\text{-}^oF$.

As discussed in Section 4, the fin efficiency can be extracted to yield the surface coefficient, h_s.

$$h_s = \left(\frac{A_s}{A_{st} + \eta_f A_{sf}}\right) h_o \tag{70}$$

Since η_f depends on h_s, determination of both η_f and h_s for a given h_o must be done by iteration.

The heat transfer capabilities of a surface are commonly given in the literature in terms of a Colburn factor. This may be calculated both with and without efficiency as shown in equations 71 and 72.

$$j_o = \frac{h_o}{G_o C_a} Pr^{2/3} \tag{71}$$

$$j' = \frac{h_s}{G_o C_a} Pr^{2/3} \tag{72}$$

5.5.3 Wet Heat Transfer

Temperatures were recorded and used exactly the same way as described in the previous sections with just one exception. The thermocouple located closest to the downstream distribution box was recorded but not averaged in with the rest. Air circulation into the distribution box and back out caused this particular thermocouple to read excessively low.

All calculations for wet heat and mass transfer were done on the computer (see Appendix D). A routine given in Reference 9 was used to calculate all the needed air properties from the measured dry bulb and wet bulb temperatures. This was done by calculating the appropriate saturation pressures using the following formula given by Keenan and Keyes:(10)

$$\log_{10}\left(\frac{P_{ws}}{218.167}\right) = \frac{-\beta}{T}\left(\frac{a + b\beta + c\beta^3}{1 + d\beta}\right) \tag{73}$$

where

p_{ws} = saturation pressure, atm

$\beta = 647.27 - T$

T = absolute temperature, ^oK

a = 3.2437814

b = 5.86826×10^{-3}

c = 1.1702379×10^{-8}

d = 2.1878462×10^{-3}

Total heat transferred from the circulating water to the air was determined as previously discussed. During wet heat transfer, a certain amount of heat is also being added to the deluge water if total equilibrium has not been reached. In this case Q_{REJ} becomes

$$Q_{REJ} = \dot{m}_h C_p \Delta T_h + Q_{peripheral} - Q_{deluge} \tag{74}$$

where $Q_{deluge} = \dot{m}_d C_p (T_{d2} - T_{d1})$

$$U_o^* = \frac{C_a Q_{rej}}{A_s \Delta i_{\ell m}} \tag{75}$$

In general it was not practical to wait for total equilibrium so that T_{d1} and T_{d2} were usually slightly different.

There are two fundamentally different, although equivalent, means for using the overall heat transfer coefficient for the prediction of heat transfer. These are:

- the log mean temperature difference (LMTD) and the analogous log mean enthalpy difference (LMED) approaches
- The NTU-effectiveness approach.

The analogous equations used in these two approaches are summarized in Table 3.

Calculation of the heat transfer by the LMTD (or LMED) technique requires a trial and error solution to determine the appropriate outlet stream conditions. In the NTU approach, Q is computed using only the known inlet conditions. However, an equation for the effectiveness ϕ must be available for this calculation. In the WATA studies, the primary side flow rate was very high to simulate the operation of a condenser. For this case the Trane core effectiveness can be modeled by Equation 45 or 46 (note that the crossflow correction has been neglected).

The above heat transfer calculational schemes provide alternative means for determining U_o^* from the data. From Equation 42 we obtain Equation 75 where Q_{rej} is the heat transferred from the circulating water to the air. (See Equation 74).

The NTU technique provides two alternative means for determining U_o^*. From Equations (32), (40) and (46) we obtain

$$U_o^* = - \frac{\dot{m}_a^* C_a}{A_s} \ell n \left| 1 - \frac{Q_{rej}}{\dot{m}_a^* \Delta i_1} \right| \tag{76}$$

Or, by using the definition of ϕ^* in Equation 40, we obtain

$$U_o^* = - \frac{\dot{m}_a^* C_a}{A_s} \ell n \left| 1 - \frac{\Delta i_\infty}{\Delta i_1} \right| \tag{77}$$

Equation 76 depends on measurement of the heat rejection and the inlet enthalpy difference. Equations 75 and 77 depend on the air stream enthalpy rise which, in this study is not precisely measured. Thus, Equation 76 is likely to be most accurate. Theoretically, all three of the above determinations of U_o^* should give the same results. Thus, a comparison of the three results gives a good check on the internal consistency of the data.

For experiments with deluge heat transfer, the enhancement ratio Q_{wet}/Q_{dry} is of particular interest. This is the ratio of heat transferred under deluge operation to the heat transferred under dry operation with all inlet conditions the same and with the same overall core pressure drop. Comparison is done in this manner since actual operation of dry/wet cooling towers will have part of the tower wet and part of the tower dry simultaneously; thus equal pressure drops.

To obtain this enhancement ratio, the measured value of Q_{rej} under wet operation is used. The dry heat transfer coefficient is then calculated for the same ΔP. With this value of U_o^* and the inlet conditions under which Q_{rej} was measured, Equations 36, 39, and 45 are used to calculate Q_{dry}.

Predicted values of the various parameters are calculated as discussed in Section 4. Sample calculations are given in Appendix B.

5.5.4 Wet Mass Transfer

Experimental difficulties prevented direct measurements of the amounts of deluge water which was evaporated. This value was calculated indirectly however using Equation 78

$$\dot{m}_w = \dot{m}_a (H_{\infty 2} - H_{\infty 1}) \tag{78}$$

Using this value for $\dot{m}_w$ an overall mass transfer coefficient can be calculated using Equations 44 and 50.

$$\Sigma_{01}^* = \frac{\dot{m}_w}{A_s \Delta H_{\ell m}} \tag{79}$$

Similar to the heat transfer calculations Σ_m^* may be determined a second way using Equations 38 and 47.

$$\Sigma_{02}^* = \frac{-\dot{m}_a}{A_s} \ln \left| 1 - \phi_m^* \right| \tag{80}$$

The only difference between Equations 79 and 80 is that 80 assumes that the primary side of the heat exchanger can be modelled as a condensor. Thus the two values are very nearly identical and only one is plotted in Section 6.

SECTION 6

TEST RESULTS

6.1 DESCRIPTION OF TESTS PERFORMED

Prototypic tests were performed to investigate the dependence of heat transfer and pressure drop on several independent parameters. These parameters are:

1) inlet temperature difference (ITD)

2) air side inlet relative humidity (Φ)

3) air side mass flux (G_o)

4) deluge flow rate (m_d)

5) core angle (θ_c)

A complete list of the tests done is given in Table 5. Tests #1-#9, #11, #12, and #14 were done twice. A third run was done for #4 and #5 only. All data available was plotted in the following figures. Insufficient data were taken to make any qualitative decision to whether the data from a certain test was "good" or "bad".

6.2 DRY/WET PRESSURE DROP RESULTS

Pressure drop under dry operation is significantly dependent only on G_o. Under wet operation ΔP is dependent on both G_o and $\dot{m}_d$. For the isothermal tests the ITD was set at 0 ($T_\infty = T_p = 100^oF$) to minimize any effect heat transfer might have on the pressure drop during wet operation. The core angle was set at the nominal ACT design of 25^o and ambient humidity was used.

Figure 9 gives the results of ΔP as a function of G_o and $\dot{m}_d$. Data for dry heat transfer are represented by the line $\dot{m}_d = 0$. These tests were done several times in order to establish the apparent uncertainty in measuring ΔP. The bars in Figure 9 indicate this uncertainty.

Figure 10 gives the same results in terms of a fanning friction factor f (see Section 3). The solid line indicates the correlation given by the Trane Co. for their surface.

TABLE 5. TEST MATRIX OF WATA TEST PROGRAM FOR TRANE CORE

$\dot{m}_d$ \ V_o	3	4.5	6
2	1	2	3
3	4	5	6
5	7	8	9

$T_p = 120^0F$
$\theta_c = 25^0$
$T_{\infty l} = 90^0F$
$\Phi = 50\%$

ITD \ Φ	25	50	75
20	10	11	12
30	13	5	14
40	X	15	16
50	X	X	17

$T_p = 120^0F$
$\theta_c = 25^0$
$V_o = 4.5$ fps
$\dot{m}_d = 3.0$ gpm

V_o \ θ_c	20	25	30
3	18	4	23
4.5	19	5	24
6	20	6	25

$T_p = 120^0F$
$T_{\infty l} = 90^0F$
$\Phi = 50\%$
$\dot{m}_d = 3$ gpm

$\dot{m}_d$ \ θ_c	20	25	30
2	21	2	26
3	19	5	24
5	22	8	27

$T_p = 120^0F$
$V_o = 4.5$ fps
$T_{\infty l} = 90^0F$
$\Phi = 50\%$

WET HEAT TRANSFER

$\dot{m}_d$ \ V_o	3	4.5	6	9	12	15
0		TEST COMPLETED BUT NOT NUMBERED				
2					X	X
3					X	X
5					X	X

$T_{pl} = 100^0F$
$T_{\infty l} = 100^0F$
$\theta_c = 25^0$
Φ = AMBIENT

PRESSURE DROP TESTS

V_o	3	4.5	6	9	12	15
X	TESTS COMPLETED BUT NOT NUMBERED					

$T_{pl} = 125^0F$
$T_{\infty l} = 85^0$
$\theta_c = 25^0$
Φ = AMBIENT

DRY HEAT TRANSFER

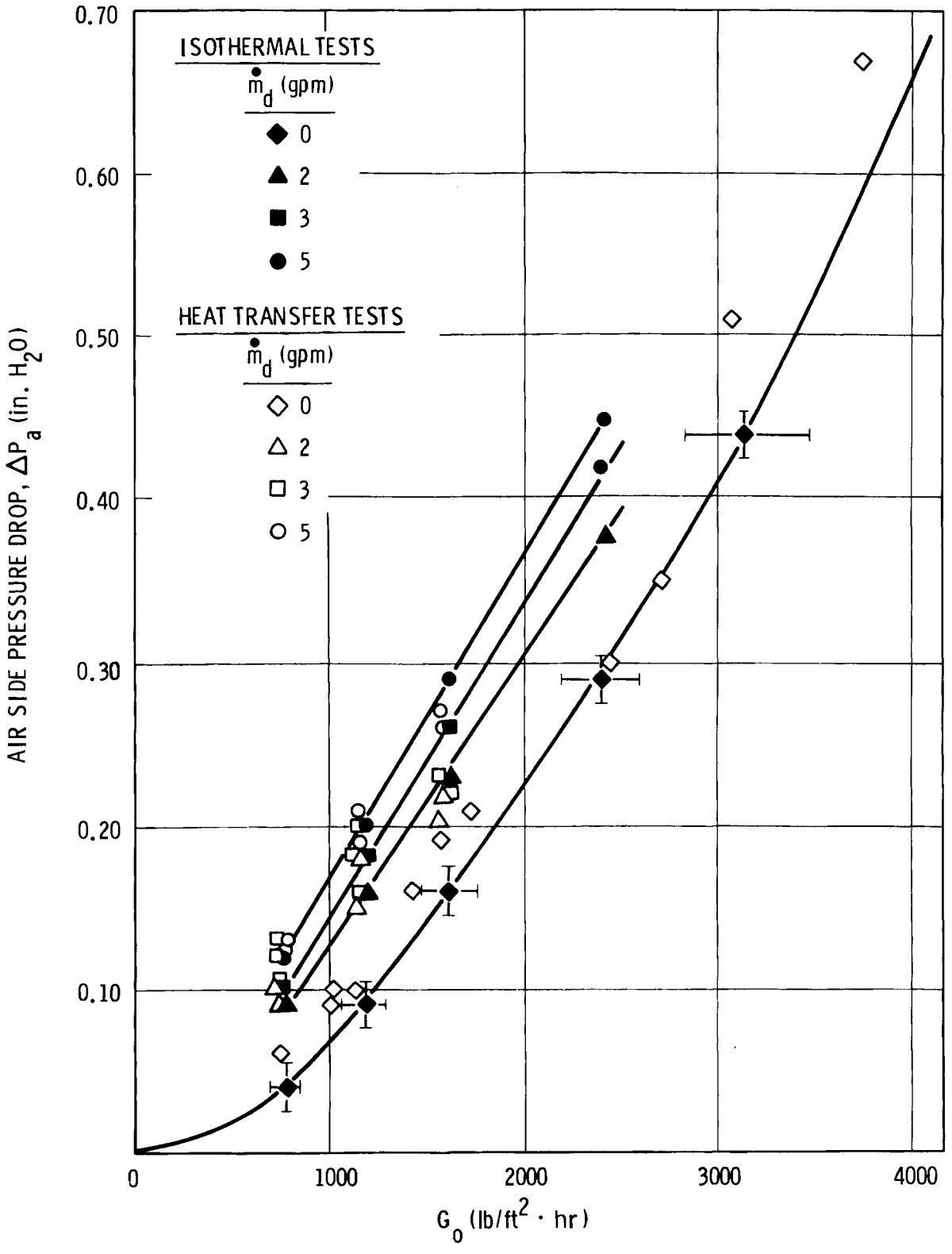

Figure 9. Pressure drop across core.

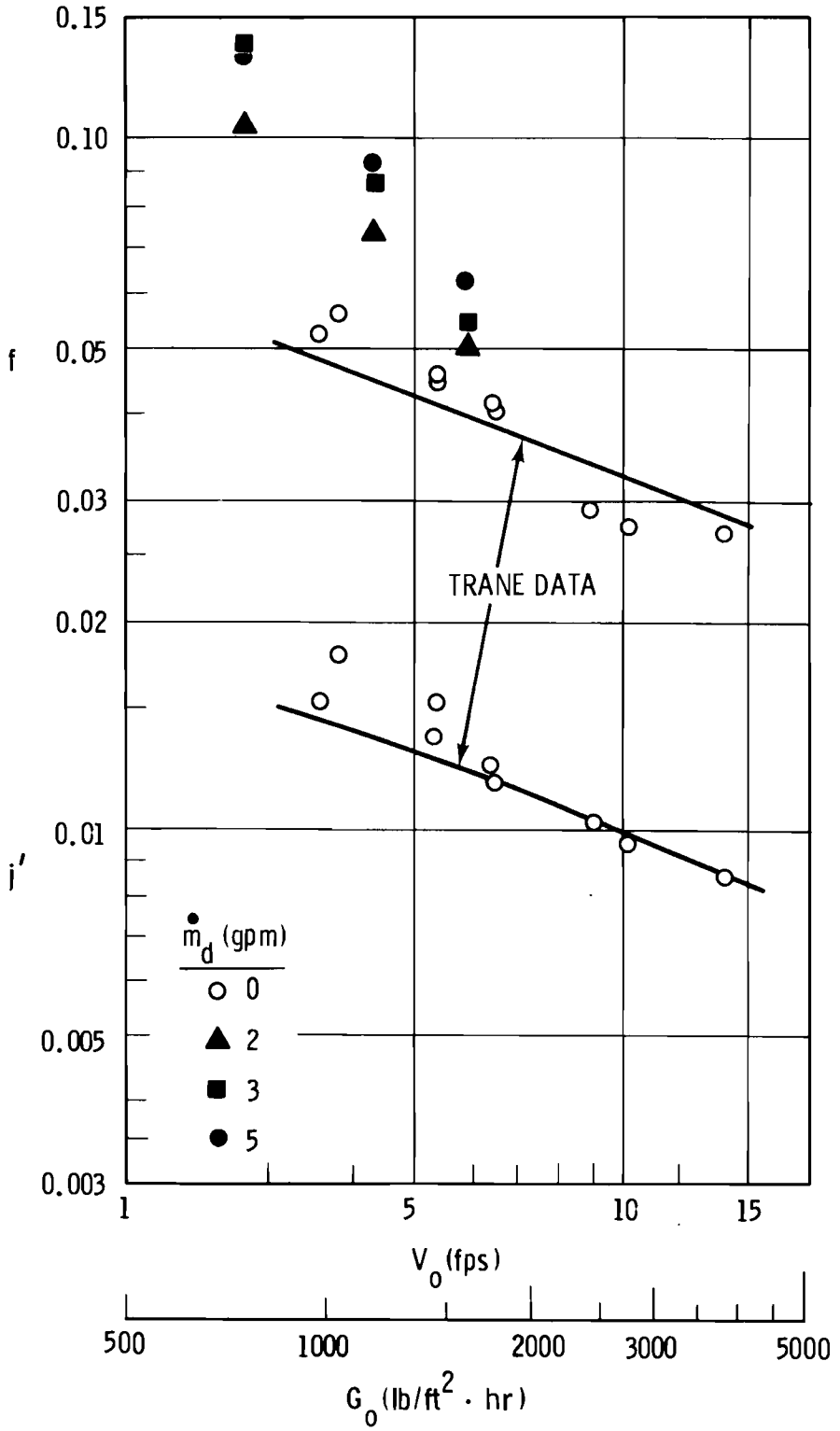

Figure 10. Plots of f and j versus V_0 and G_0 for wet and dry heat transfer.

The data shown are in relatively good agreement with the correlation. However in both cases the slopes of the WATA data appear to be slightly greater than that of the Trane correlations.

6.3 DRY HEAT TRANSFER RESULTS

Heat transfer tests without deluge water were done for a wide range of velocities as indicated in Table 5. The results are shown in Figure 11 in terms of a surface heat transfer coefficient with and without efficiency (h_o and h_s, respectively) and an overall heat transfer coefficient, U_o. The uncertainty in U_o was calculated to be about 10% (see Appendix C) and is shown with bars in Figure 11. All data points lie within the uncertainty bands.

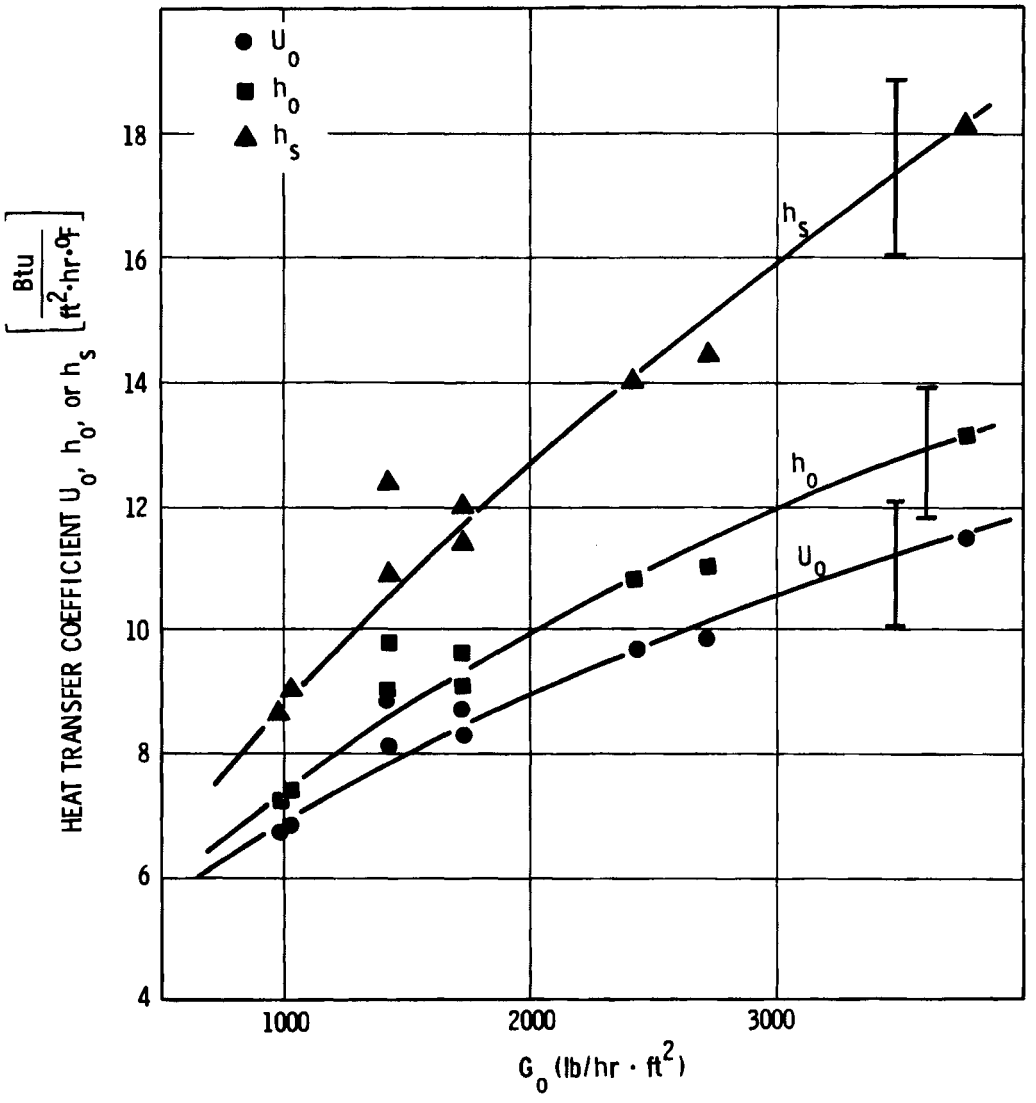

Figure 11. Plots of U_o, h_o, and h_s versus G_o

The U_o values were also converted to j values as shown in Figure 10. These can be compared to the correlation given by the Trane Co. indicated by the solid line. In both cases fin efficiency effects have been removed.

Measured values of j agreed well with the correlation at high velocities, but tended to be higher than the correlation at low velocities.

6.4 WET HEAT TRANSFER RESULTS

The results of the wet heat transfer tests are presented as plots of Q_{wet}/Q_{dry}, U_o^* and h_d^* as functions of the various independent operating parameters. The experimental values of U_o^* were computed using Equation 76 since this expression results in the least experimental uncertainty. The experimental values of h_d^* were computed from the experiments by a technique outlined in Section 4 and described in Appendix A.

Figure 12 shows the measured heat transfer per unit ITD, $Q/(T_p-T_\infty)$, as a function of the nondimensional inlet driving potential ,

$$\Gamma = \frac{(i'_p - i_\infty)_1}{C_a(T_p - T_\infty)_1} \tag{81}$$

Increasing Γ corresponds to increasing ITD and/or decreasing humidity, both of which contribute to a larger driving potential for heat transfer. A plot of Γ as a function of conditions is given in Figure A-5 of Appendix A.

This parameter is also useful for correlating other aspects of the heat exchanger performance as shown in the subsequent discussion.

The data in Figure 12 show that Q/ITD rises linearly with increasing Γ. The majority of the data were for V_o = 4.5 fps. One point each is plotted for V_o = 3.0 fps and V_o = 6.0 fps. A line predicting the relationship between Q/ITD and Γ is also shown for each of the three velocities. The Equation used to calculate this is given in Appendix A.

To make these predictions it is necessary to assume values for both ξ and h_d^*. As discussed in Appendix A, the value for ξ does not change substantially with any of the independent parameters except Tp. Since all of the tests done on the Trane core were at the same Tp, a constant value of 9.5 (see Figure 24) is used for ξ in all of the theoretical calculations. For predictions in Figure 12 h_d^* values are taken from Figures 13 and 16. These values were: h_d^* = 18 at V_o = 3.0; h_d^* = 26 at V_o = 4.5; and h_d^* = 24 at V_o = 6.0.

It is apparent that the theory is in excellent argreement with the data. This good agreement is not coincidental since the h_d^* values were obtained

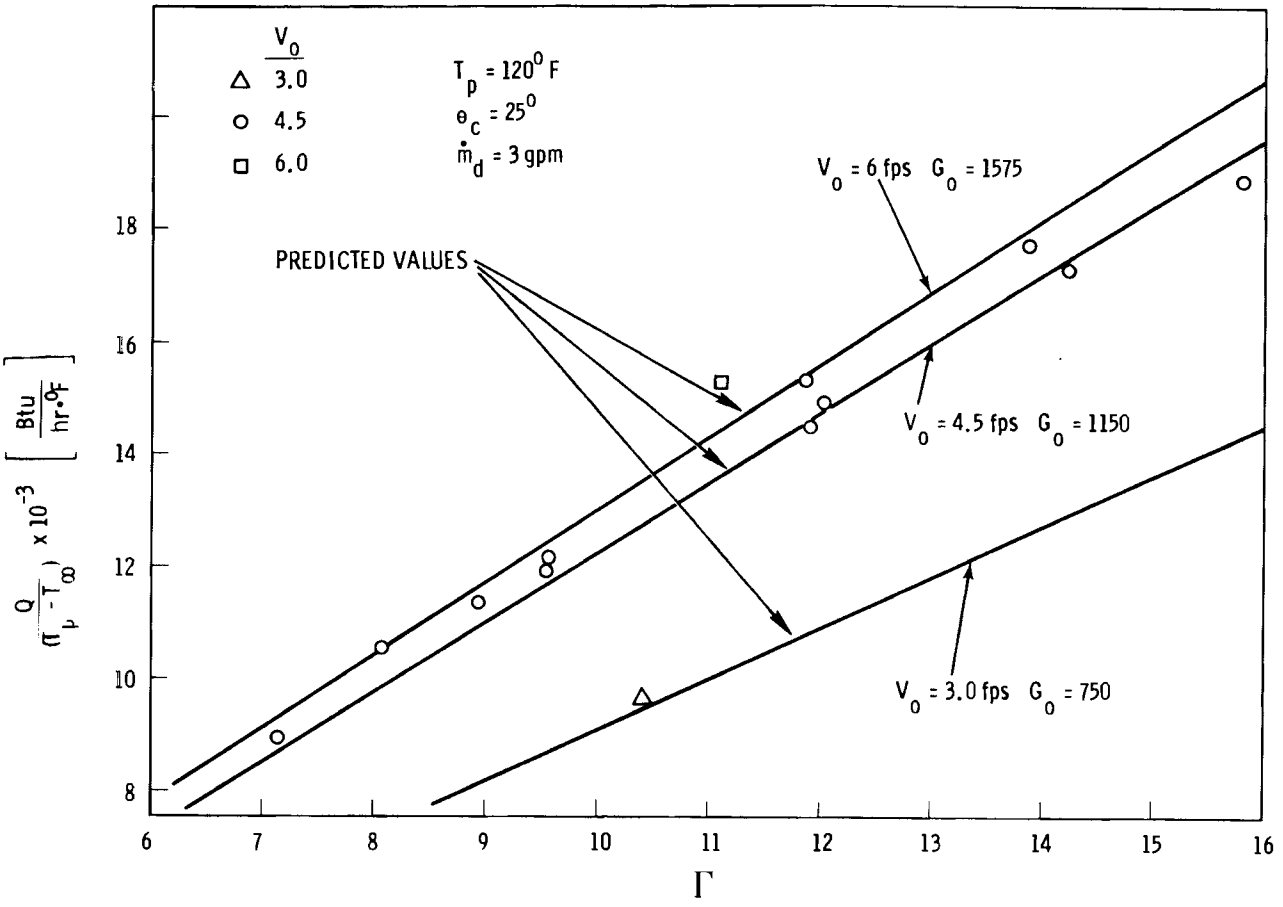

Figure 12. Normalized heat transfer versus Γ.

from the same experiments. The agreement does substantiate the validity of the model. Uncertainties in the predicted values of h_{d*} are very difficult to quantify but are reasonably large.

The data for h_d^* and U_0^* vs G_0, $\dot{m}_d$ and θ_c are shown in Figures 13, 14 and 15. It is apparent from these figures that both h_d^* and U_0^* increase with increasing G_0 and increasing $\dot{m}_d$. There appears to be very little if any effect of core angle on either parameter to within the experimental uncertainty. In Figure 13, h_d^* appears to have a slight maximum or at least a leveling off at $G_0 \approx 1000$. However, the data scatter is too great to conclude that the apparent maximum is real.

Predicted lines for U_0^* are shown in each of the three figures. As discussed above $\xi = 9.5$. For Figures 13 and 15 h_d^* values were taken as 18, 24, and 24 corresponding to G_0 values of 750, 1150, and 1575 respectively. For Figure 14 h_d^* values were 20, 24, and 28 corresponding to m_d values of 2.0, 3.0, and 5.0 respectively. The good agreement between the predictions and the data is assured because of the method for determining h_d^* (see Section 4 and Appendix A for discussion). The method forces U_0^* (predicted) values to equal U_0^* (experimental) values.

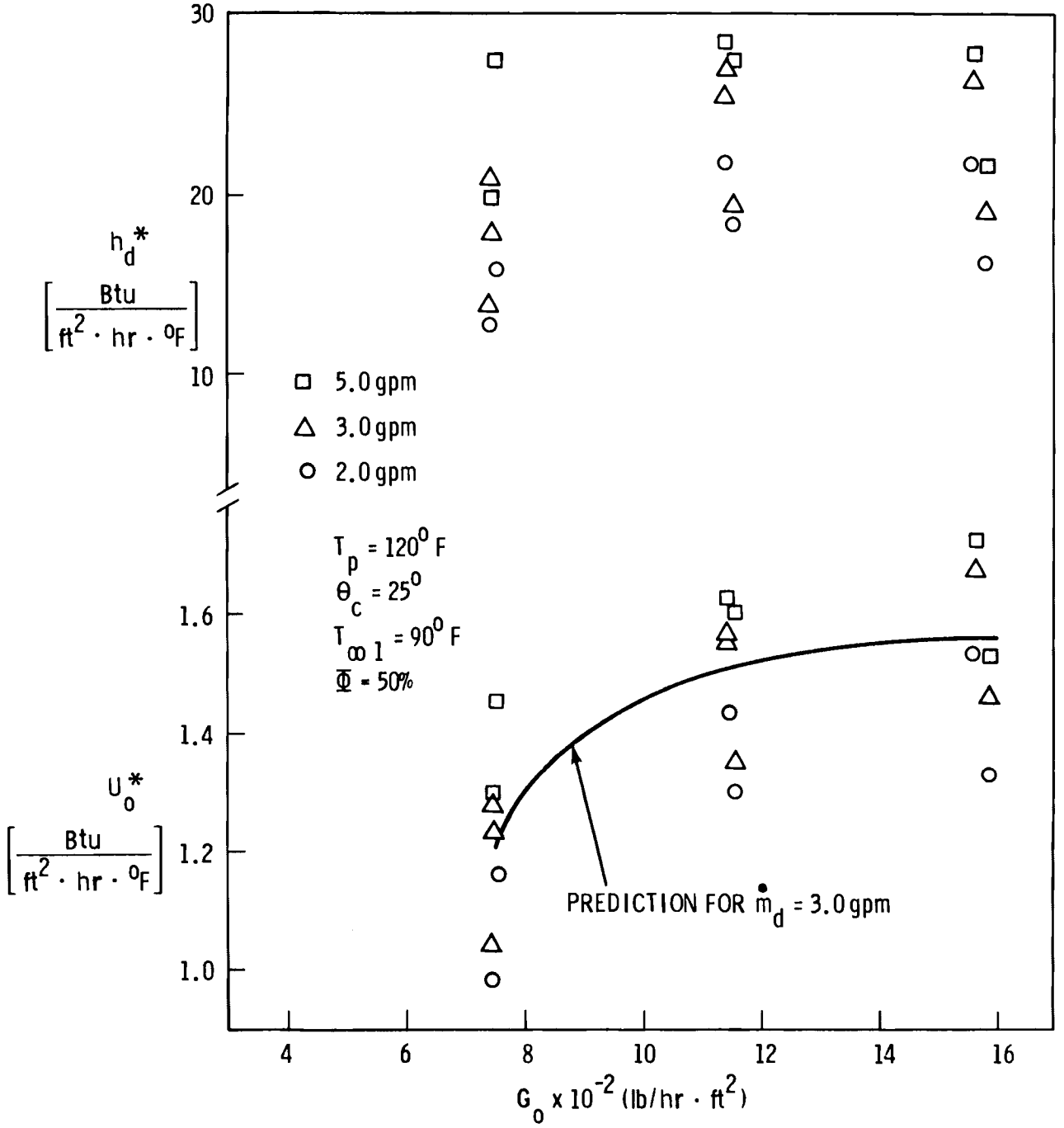

Figure 13. Plots of h_d^* and U_o^* versus G_o and $\dot{m}_d$.

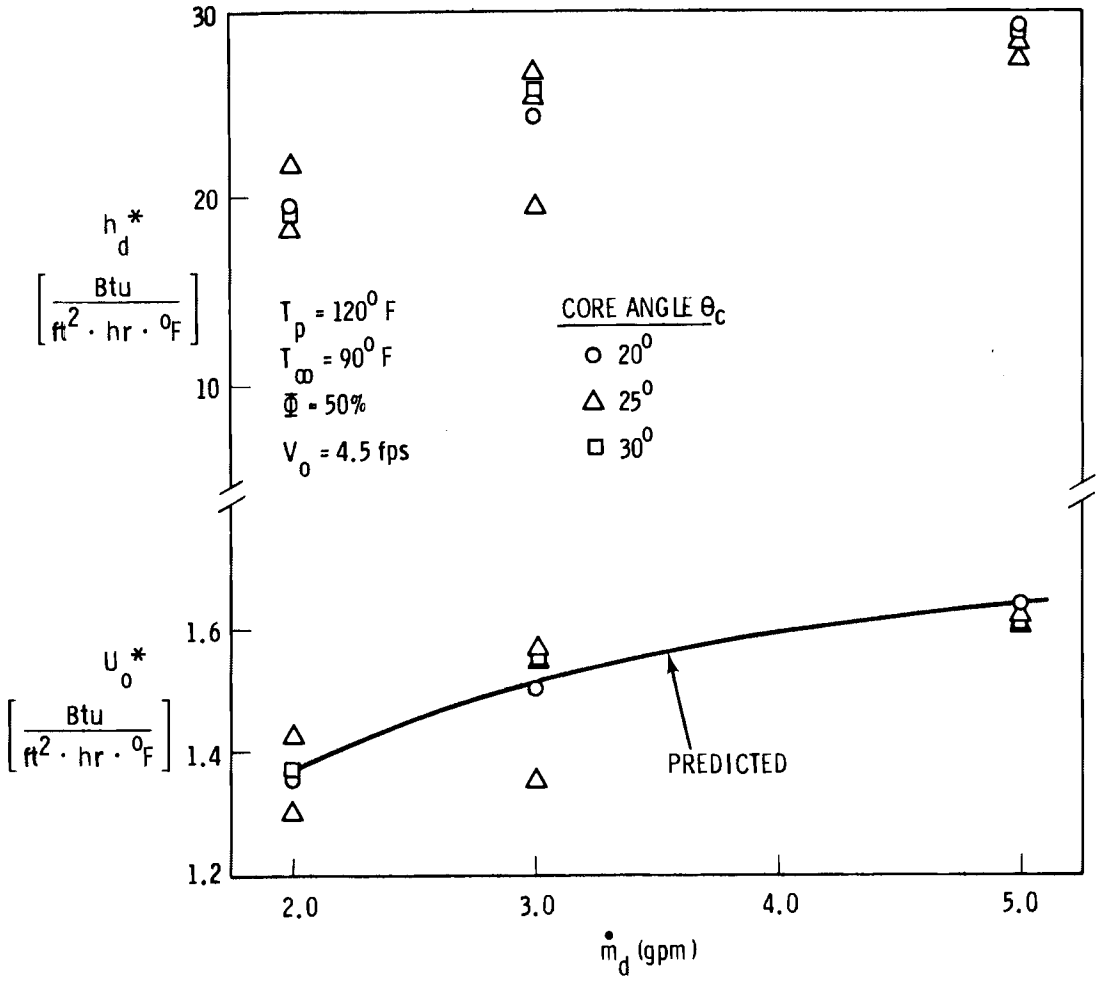

Figure 14. Plots of h_d^* and U_0^* versus $\dot{m}_d$ and θ_C

The dependences of h_d^* and U_0^* on the nondimensional driving potential Γ are shown in Figure 16. There is an apparent tendency for h_d^* and U_0^* to decrease with increasing Γ. However, because of the experimental uncertainty, it is not apparent whether this effect is real. High values of Γ result in high rates of heat flux and thus greater tendency toward drying of the surface. This would tend to reduce h_d^* and thus U_0^*. The tendency toward decreasing values of these parameters with increasing Γ is thus plausible.

There are other important parameters that correlate with Γ. Figure 17 shows the results for (T_p-T_r) and ξ as a function of Γ. These results were determined simultaneously with h_d in analysis of the data (see Appendix A). It is seen that the ratio $(T_p-T_r)/(T_p-T_\infty)$, increases linearly with Γ. This is exactly as predicted by the model. The resistance transformation parameter ξ is seen to be essentially independent of Γ for the range of conditions shown at a fixed value of T_p. This is potentially a very useful result that

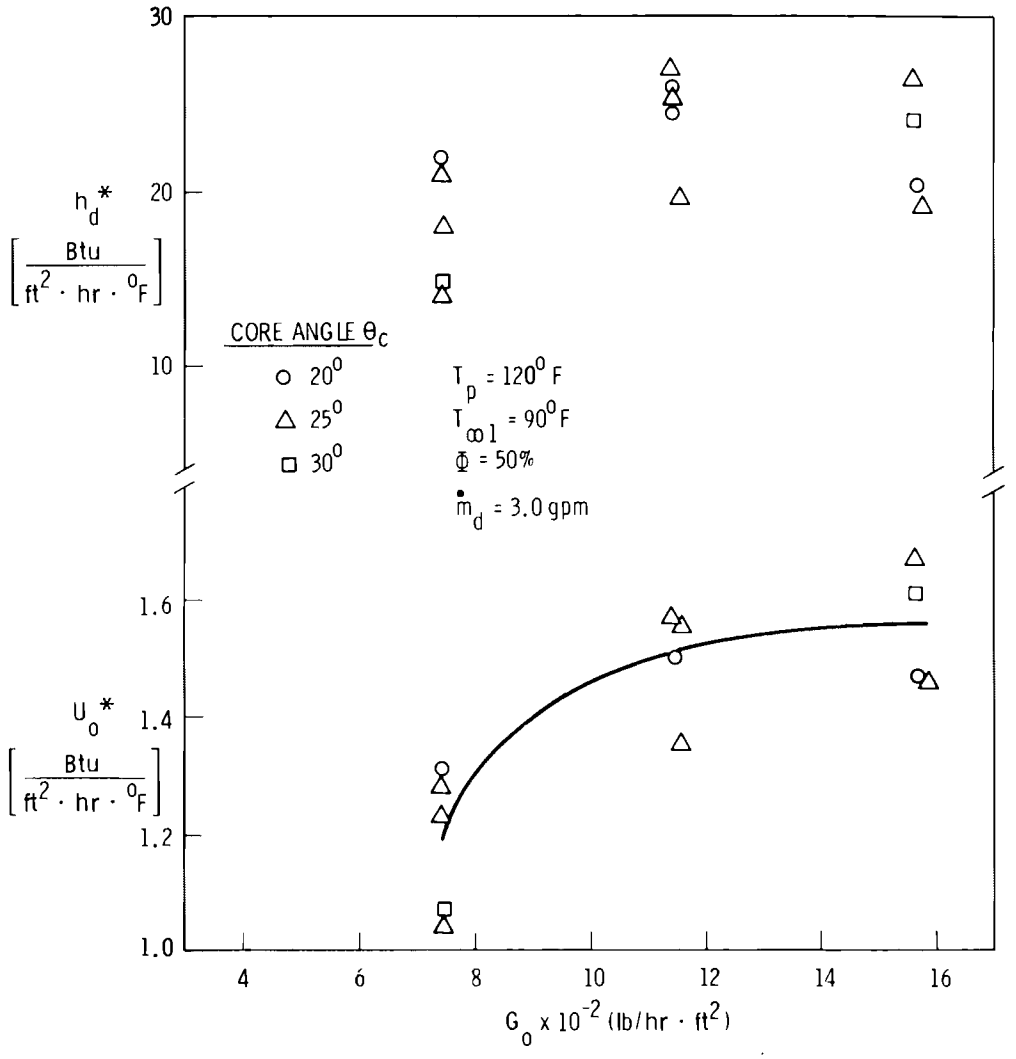

Figure 15. Plots of h_d^* and U_o^* versus G_o and θ_C.

can be used to devise an approximate means for evaluating ξ when the root conditions are not known. This is discussed further in the subsequent discussion.

Since the prediction of $(T_p-T_r)/(T_p-T_\infty)$, comes from the same formulation as the prediction of Q/ITD, the assumptions used are exactly the same. Again the model predicts the experimental data very well. Although the predictions indicate a change in slope with different air flow rates, the data tend to show that the value of T_r is independent of air flow rate.

One of the most important parameters used for characterizing the performance of a deluged heat exchanger is the ratio of wet to dry heat transfer, Q_w/Q_d. To best evaluate a real operating condition, the comparison is made for the same core temperature, the same inlet air conditions and the

same air side pressure drops. The predicted value of this ratio is given by Equation 82.

$$\frac{Q_w}{Q_d} = \left(\frac{\dot{m}_a^*}{\dot{m}_a}\right)\left(\frac{\phi^*}{\phi}\right)\Gamma \qquad (82)$$

where Γ is the ratio of input driving potentials discussed above.

The data for Q_w/Q_d for the Trane core and the corresponding predictions is given in Figure 18. It is apparent that the data correlate very well with Γ and that the prediction is in excellent agreement with the data. The same assumptions apply here as were used in Figure 16.

Additional results of Q_w/Q_d for the Trane core are shown in Figures 19 and 20 as a function of G_o, θ_c and $\dot{m}_d$. There appears to be very little dependence of Q_w/Q_d on the air flowrate G_o as shown in Figure 19. The predicted dependence of Q_w/Q_d shows a very slight reduction in enhancement at higher airflows, but the effect is well within the expected uncertainty.

The data in Figure 20 show the dependence of Q_w/Q_d on $\dot{m}_d$ and the predicted value based on the model. There may be a slight maximum in Q_w/Q_d at

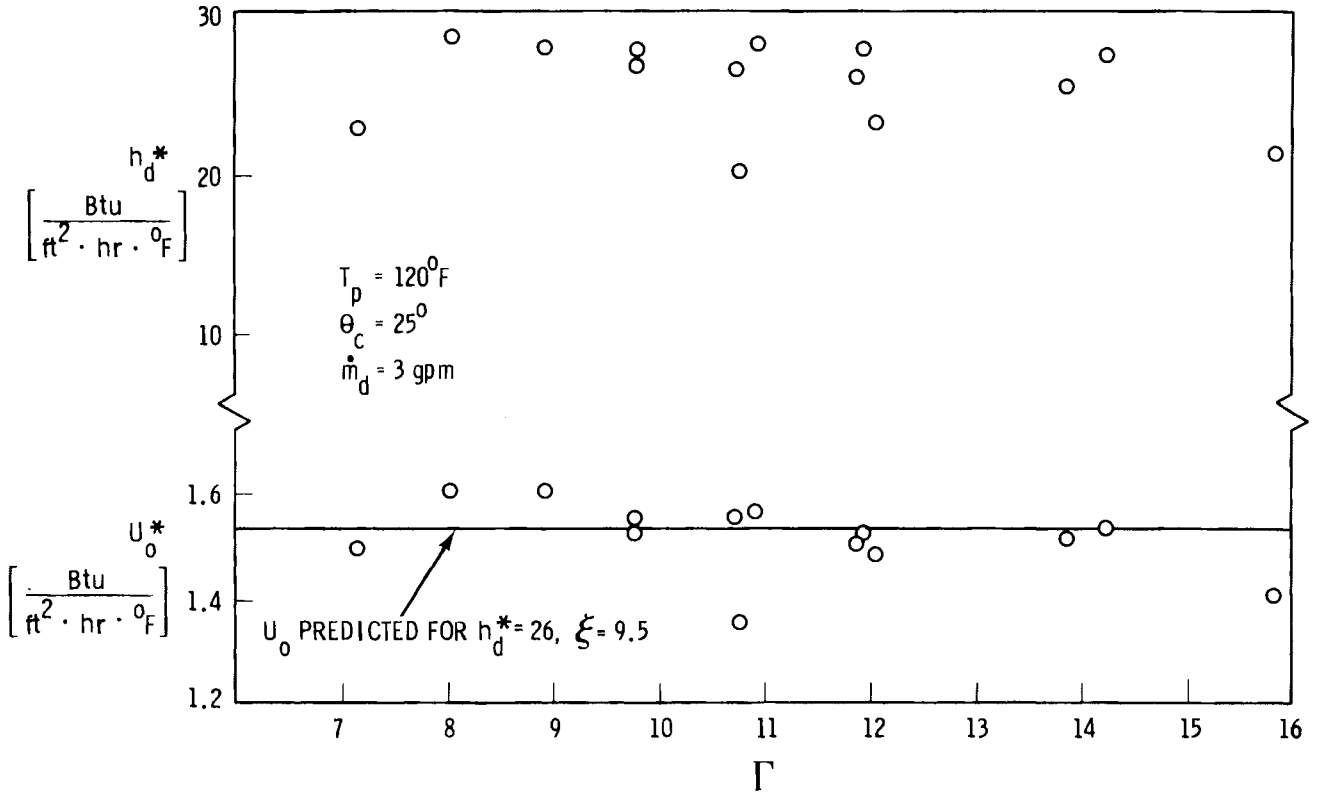

Figure 16. Plots of h_d^* and U_o^* versus Γ.

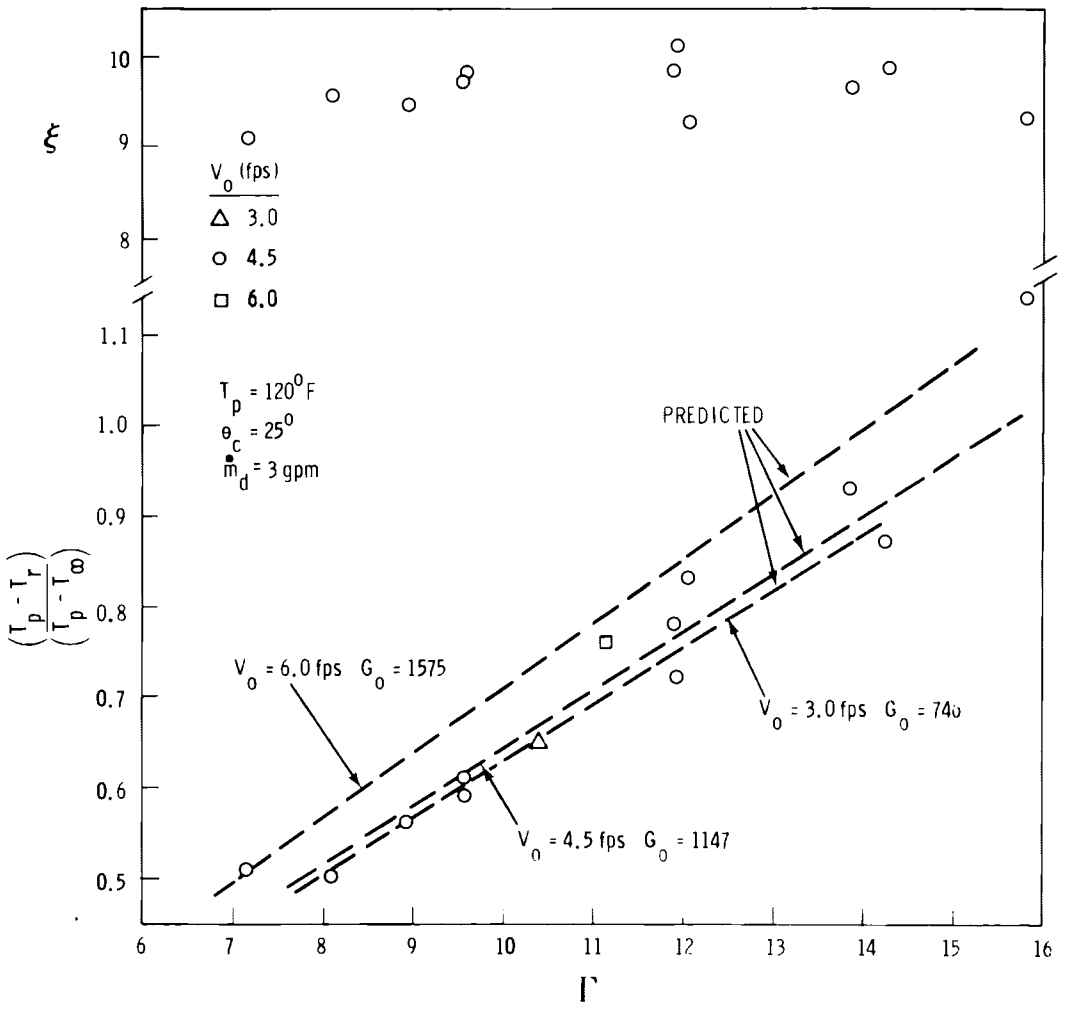

Figure 17. $(T_p-T_r)/(T_p-T_\infty)$ and ξ versus Γ.

$\dot{m}_d \approx 4$ gpm, however this effect may or may not be real. The predicted values for Q_w/Q_d also show the maximum but to within the expected uncertainty, the enhancement appears to be essentially independent of $\dot{m}_d$.

The assumptions made for predictions in Figures 19 and 20 correspond to those made for Figures 13, 14, and 15.

6.5 WET MASS TRANSFER RESULTS

According to the model developed in Appendix A, the rate of evaporation of water from the surface of the heat exchanger to the air can be described in terms of an overall mass transfer coefficient Σ_m^* that is analogous to the overall heat transfer coefficient U_o^*. Although the experiments were not designed to obtain an accurate measurement of the deluge water evaporation rate, an estimate of evaporation rate was obtained from the measured

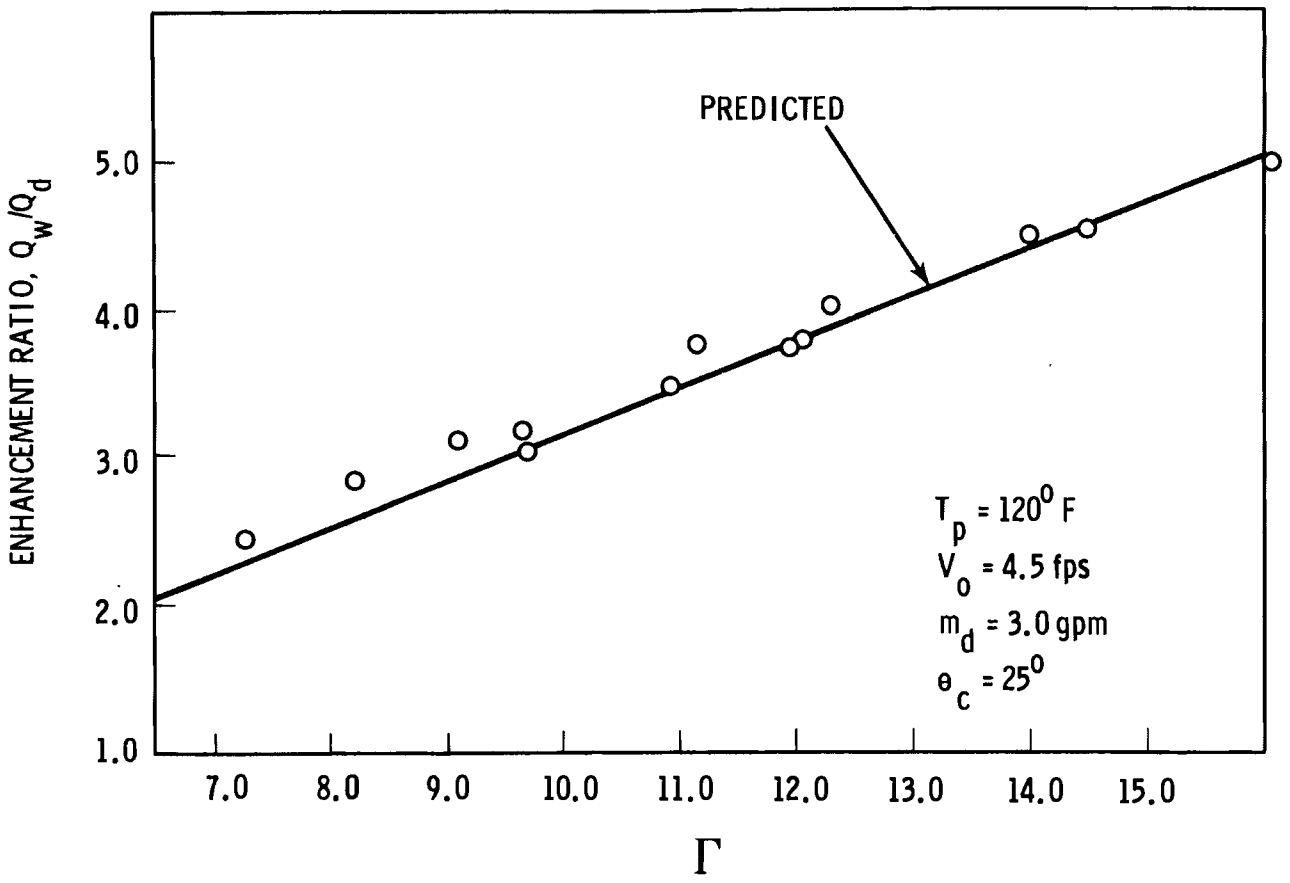

Figure 18. Plot of Enhancement Ratio versus Γ.

difference in the air moisture content across the core by Equation 15. Two values of Σ_{m1}^* were then computed using the log mean humidity approach (Σ_{m1}^* Equation 79) and the effectiveness approach (Σ_{m2}^*, Equation 80) where Σ_m^* was calculated with

$$\phi_m^* = \frac{H_{\infty 2} - H_{\infty 1}}{H_p' - H_{\infty 1}} \tag{82}$$

The results for Σ_{m1}^* and Σ_{m2}^* determined from the measurement were very nearly equal. This was expected since the difference between the two methods of calculation is only the assumption that T_p = constant (i.e., as in a condensor). The values for Σ_{m1}^* are plotted in Figures 21 as a function of Γ for $T_p = 120^0$F, $V_o \approx 4.5$ ft/sec and $\dot{m}_d = 3$ gpm. Predicted values of Σ_m^* determined with Equation 39 were computed for each measurement and plotted in Figure 21 for comparison. A general predicted value for Σ_m^* is also shown by a line at $\Sigma_m^* = 6.56$. This value is calculated based on the same assumptions as used in Figure 16 with the additional assumption that $\xi_m = 0.95\xi$. The later is taken from Figure 23. The difference between the individual predicted points and the general predicted line is the values of h_d^* used in the calculation.

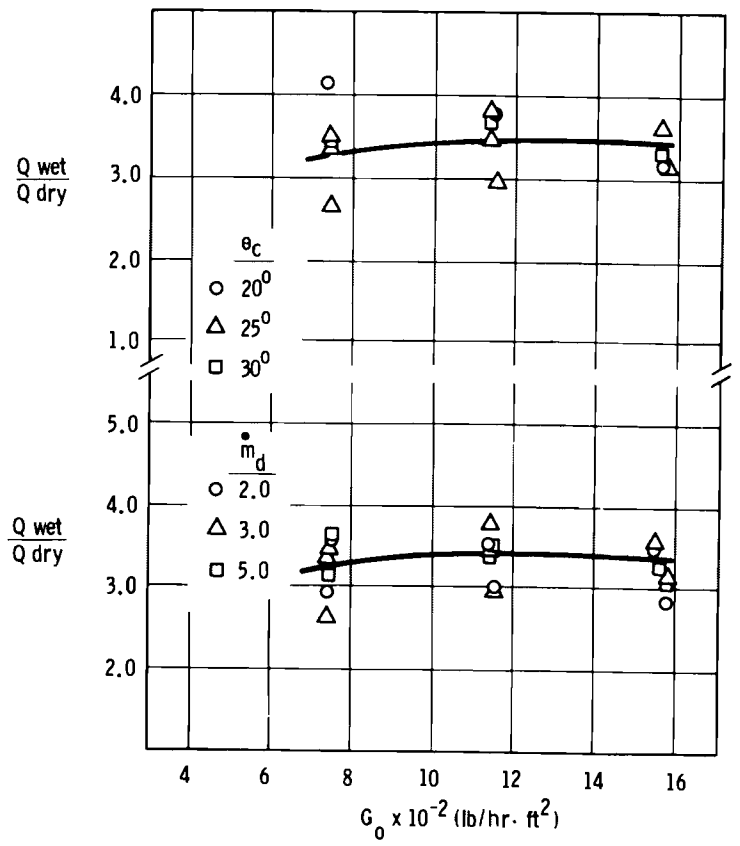

Figure 19. Plot of enhancement ratio versus G_o, $\dot{m}_d$, and θ_c.

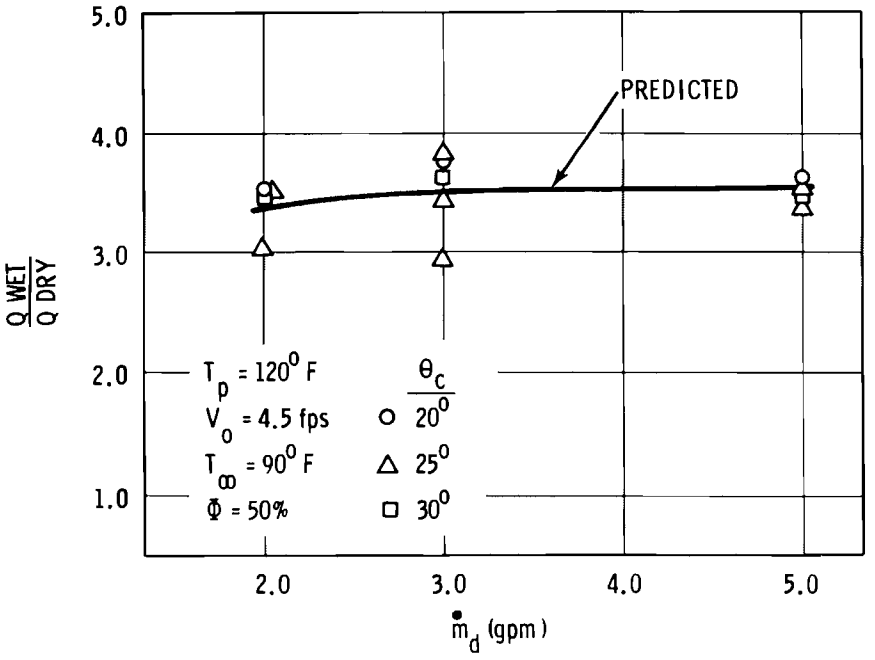

Figure 20. Plot of enhancement ratio versus $\dot{m}_d$ and θ_c.

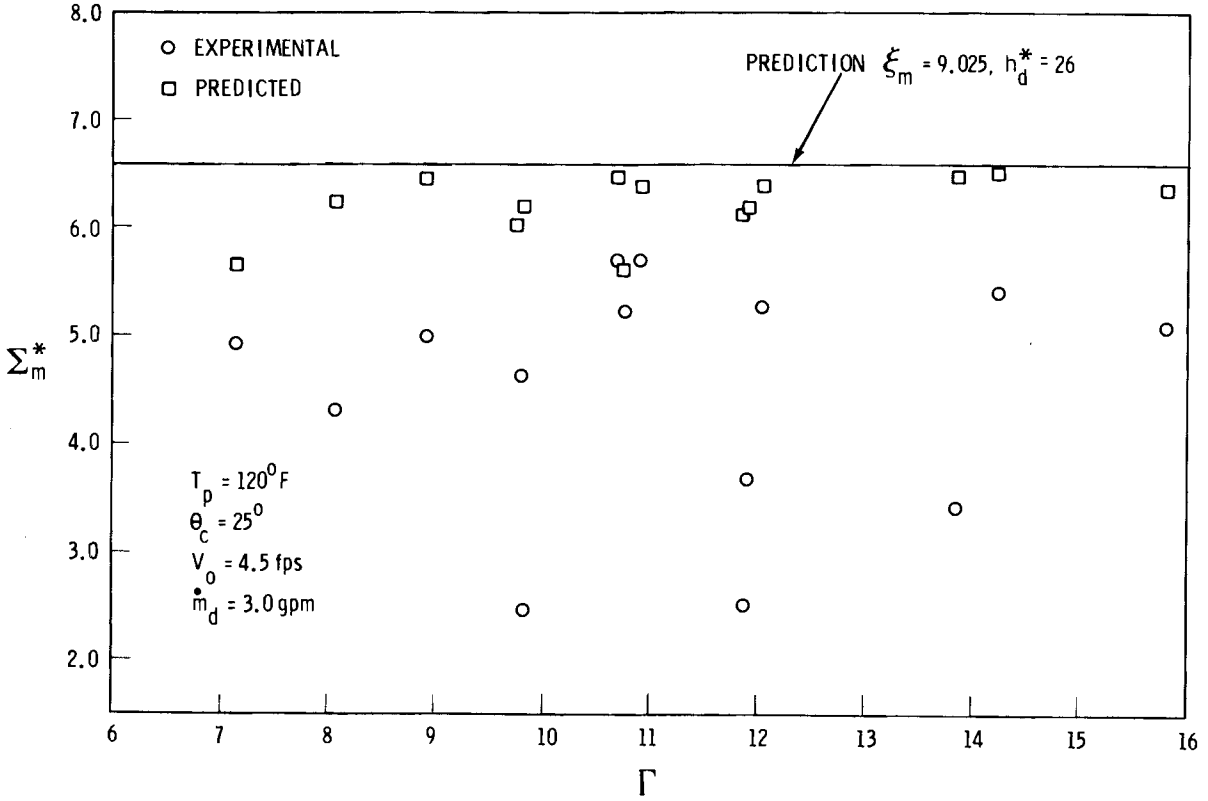

Figure 21. Plot of Σ_m^* versus Γ.

The uncertainty and the resultant data scatter are large because Σ_m^* is based on the difference between two humidity measurements both of which have substantial uncertainty. The outlet humidity in particular is doubtful because nonuniformity in the outlet air conditions could not be adequately accounted for. Since the data scatter exceeds the estimated uncertainty it is also possible that there were other unaccounted for variations in the tests. The data scatter was sufficiently great that no attempt was made to fit a curve to the data in Figure 21.

Because of the extreme data scatter no detectable trend with Γ can be inferred from the data in Figure 21. The predicted values of Σ_m^* appear to increase slightly with increasing Γ, but the effect is small. Ignoring some of the anomolously low values of Σ_m^*, it appears that the deluge model over predicts the data by about 20-30%. It is not apparent to what extent the fault is in the data or in the model.

The data for Σ_m^* as a function of G_o are given in Figure 22. Again Σ_{m1}^* is shown and the theoretical prediction is given for comparison. There appears to be a tendency for increasing Σ_m^* with increasing G_o, similar to the result for U_o^*. The theoretical prediction is still somewhat higher than the data at low air flowrate but is in better agreement with the data at the higher flowrates.

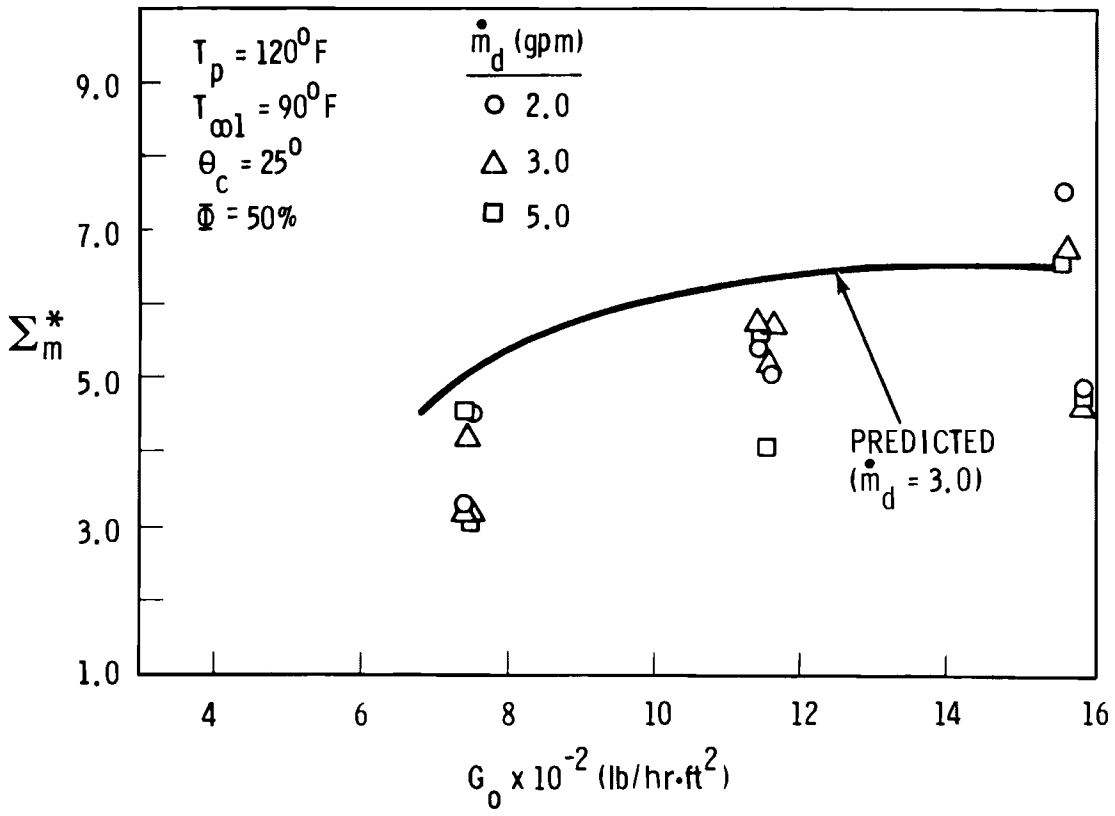

Figure 22. Plot of Σ_m^* versus G_0 and $\dot{m}_d$.

The data in Figure 23 illustrate the relationship between ξ and ξ_m as derived by the procedure described in Appendix A. For ξ, this is the same results as shown in Figure 17. For the most part, it can be seen that ξ and ξ_m are essentially equal to within the expected uncertainty. However, at larger values of Γ, ξ_m is noticeably smaller than ξ. These results are essentially in agreement with the prediction computed in Appendix A. The conclusion to be reached is that it is probably sufficient to assume $\xi_m = \xi$ except for conditions where the driving potential for evaporation and heat transfer is very high. Since the prediction of ϕ^* and ϕ_m^* gives the outlet air stream conditions in terms of $i_{\infty 2}$ and $H_{\infty 2}$ respectively, the outlet dry bulb temperature can also be predicted. Figures 24 and 25 present ϕ^*, ϕ^*_m, and ϕ in terms of experimental data and theoretical predictions. The experimental data was calculated from measured inlet and outlet conditions. Although experimental values agree reasonably well with the theory for ϕ^* and ϕ^*_m, a large discrepancy exists for values of ϕ. From a psychometric chart one can see that the dry bulb temperature is very sensitive to the values of enthalpy and humidity. The discrepancy is probably due to both experimental uncertainties and inadequacies in the model.

From the limited data presented here, it appears that the deluge model tends to overpredict the rate of evaporation. However, because of the large uncertainty in the measurements, more and better data are required before any definite judgments should be made.

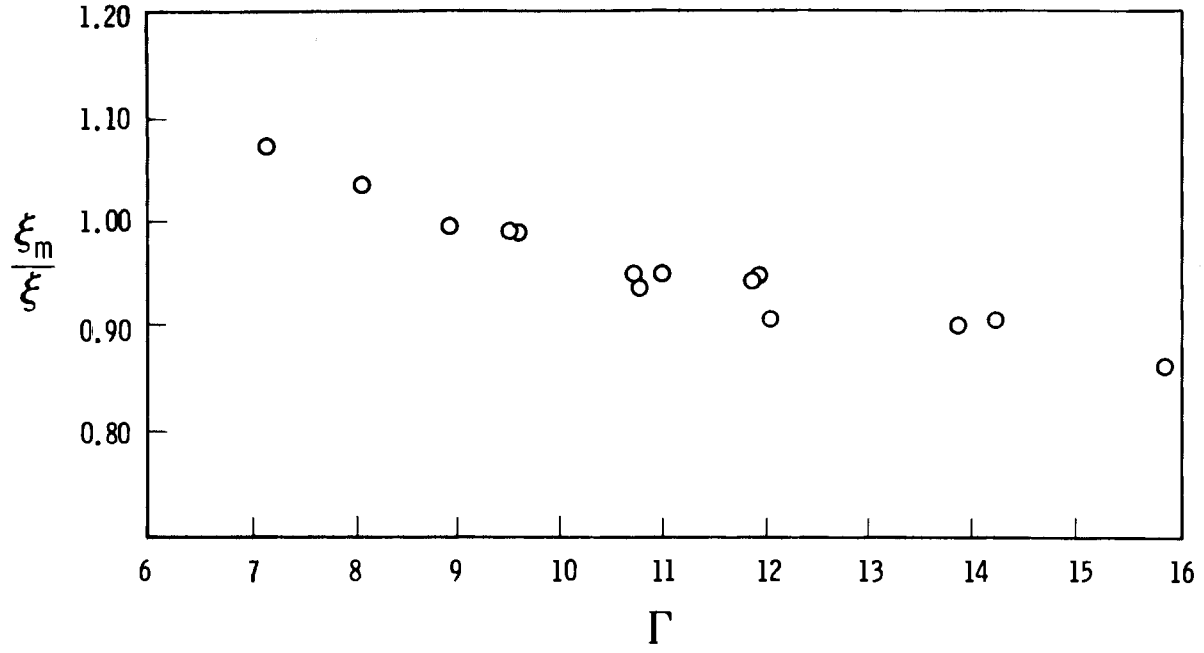

Figure 23. Plot of ξ_m/ξ versus Γ.

An additional parameter of interest in evaluating the performance of a deluged heat exchanger is fraction of heat transfer that is attributable to evaporation. Denoting Q_o as the total heat flux and Q_u as that due to evaporation (the latent heat component), the ratio Q_v/Q_o may be calculated for each operating condition using

$$\frac{Q_v}{Q_o} = \frac{Q_o - \dot{m}_d C_a (T_{\infty 2} - T_{\infty 1})}{Q_o} \tag{83}$$

The results of this computation for the present experiment are given in Figure 26, plotted as a function of Γ. A technique for predicting Q_v/Q_o is derived in Appendix A and predicted results for the conditions of the experiments are plotted with the data in Figure 26.

From Figure 26 it can be seen that the data correlate quite well with Γ and that the prediction is in good agreement with the data. It can be seen that the proportion of the total heat flux attributable to evaporation increases at high Γ (i.e., low humidity high air flowrate, low ITD). For values of $\Gamma \gtrsim 20$, $Q_v/Q_o \gtrsim 1$ for the conditions shown in Figure 26. For these values of Γ the air is actually cooled by evaporation and the sensible heat flux to the air is negative. None of the present experiments achieved this condition, however; some of the tests performed in previous work[3] resulted in core outlet air temperatures below the inlet conditions. These results are relevant to optimizing the operating conditions to get the maximum cooling value from the water used.

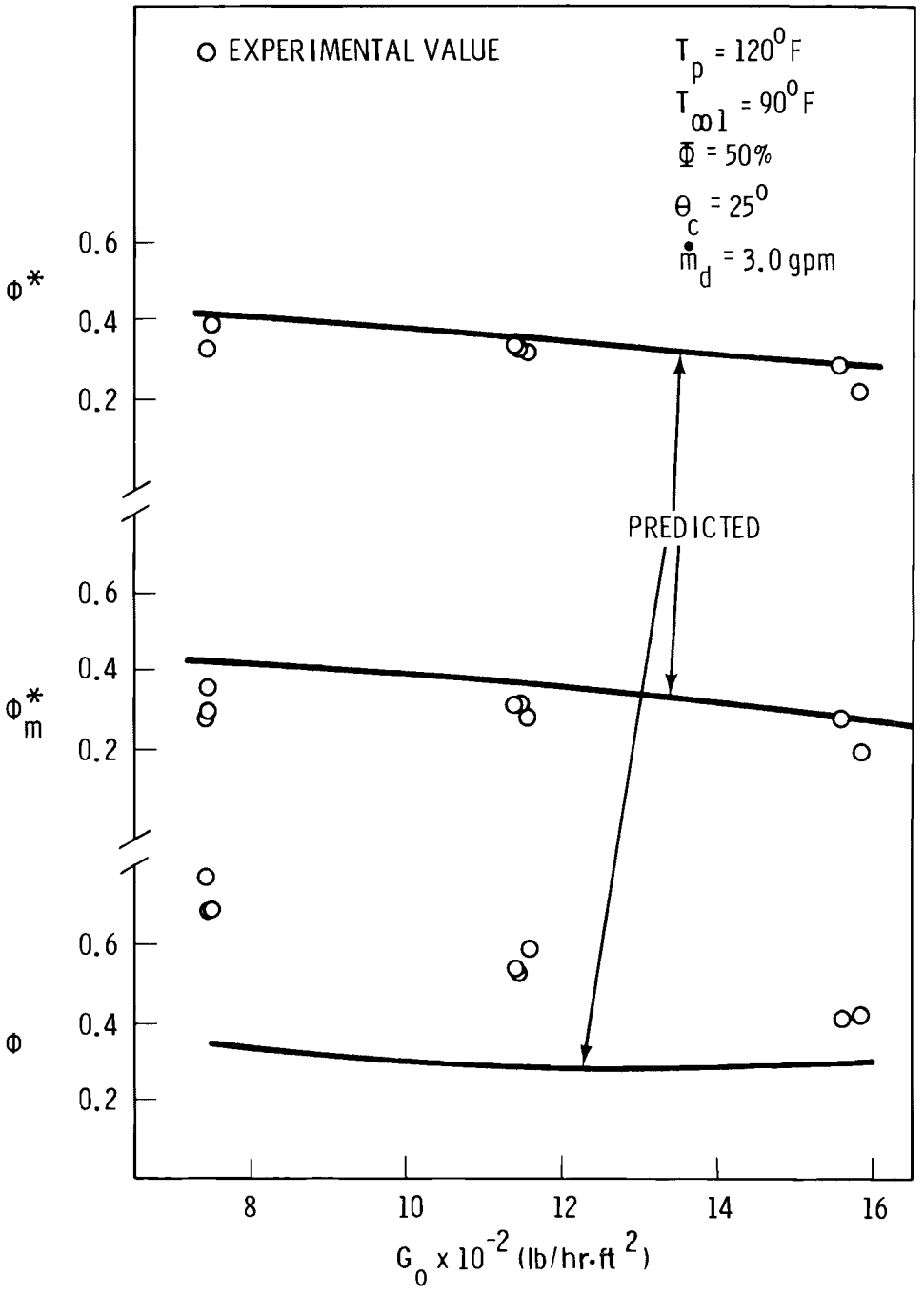

Figure 24. Plot of effectiveness ratio versus G_o.

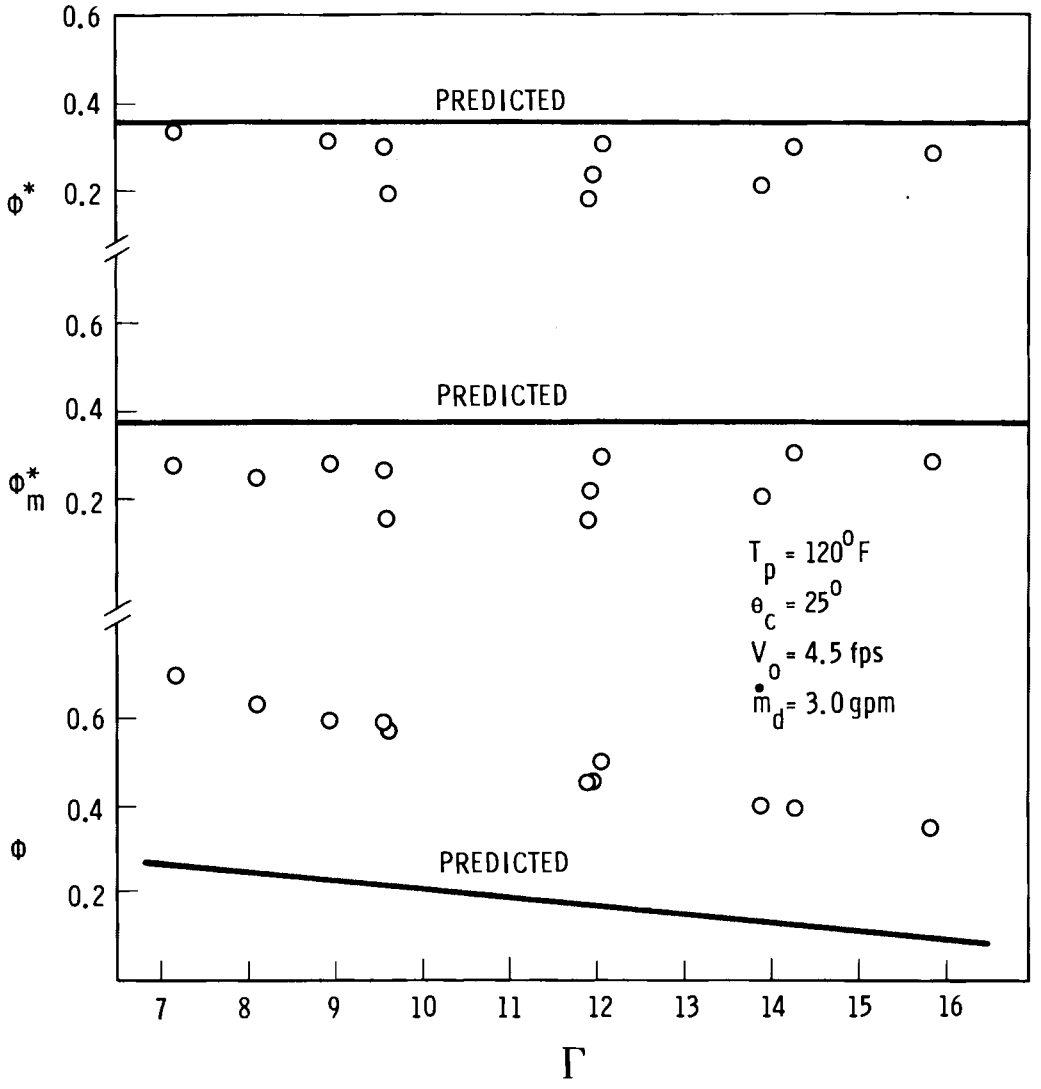

Figure 25. Plot of effectiveness ratio versus Γ.

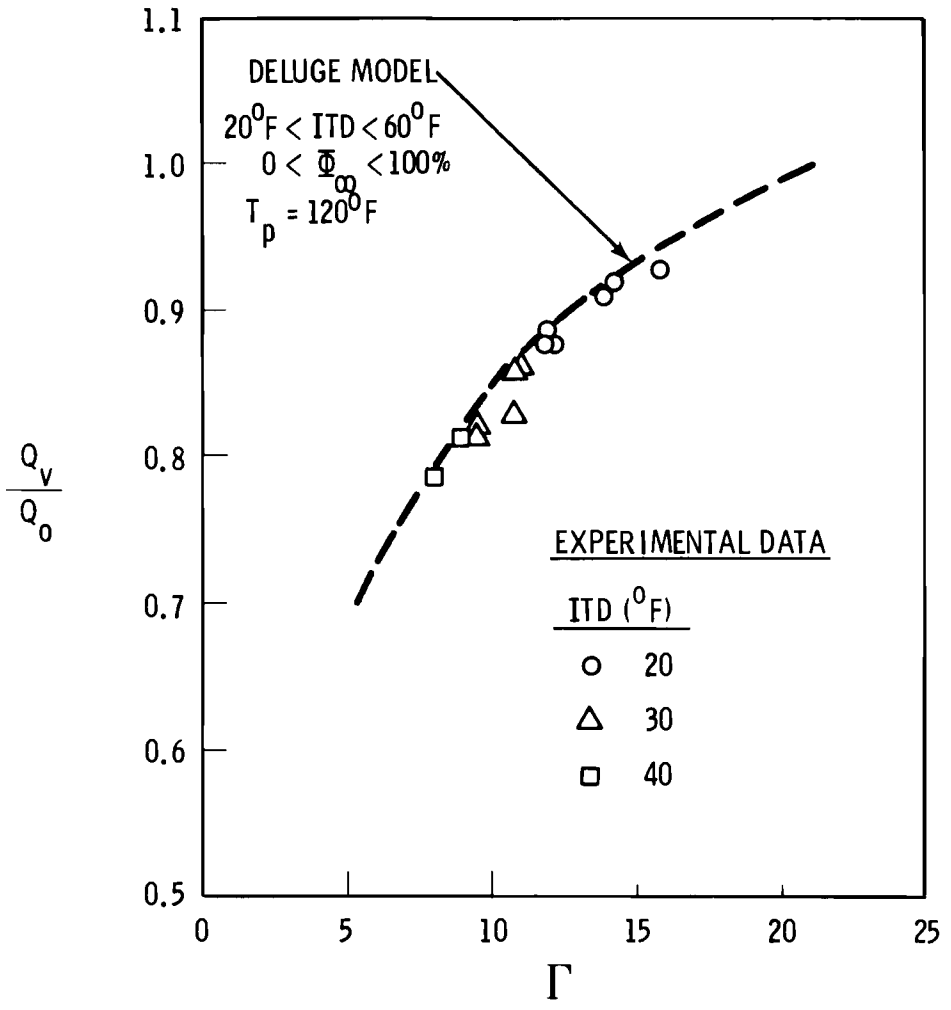

Figure 26. Comparison of predicted and experimental values of Q_V/Q_o.

SECTION 7

COMPARISON OF SIMILAR HEAT EXCHANGER SURFACES

As noted earlier, one of the prime objectives for testing the Trane core was in order to compare it to other cores designed for similar applications. This section will compare performance of various cores both under dry and wet operatng conditions.

7.1 DRY/WET PRESSURE DROP CHARACTERISTICS

Pressure drop characteristics are important because of their influence on system costs due to fan power consumption. Figure 27 gives the total pressure drop across each core for the HOTERV and Trane surfaces under both wet and dry conditions. The wet operation is with 1.5 gpm per lineal foot of core or 3 gpm total for the WATA test section. Under dry conditions at an air mass flux less than 2000 $lb/hrft^2$ the pressure drop of the two cores is essentially equal within present experimental error. Above 2000 $lb/hrft^2$ the HOTERV core has an increasingly larger pressure drop. Under wet operation the pressure drops are nearly equal at very low mass flow with the HOTERV core pressure drop becoming quickly much larger. At G_o = 2000 $lb/hrft^2$ the HOTERV core pressure drop is approximately twice as large as that for the Trane core.

This same data is plotted in Figure 28 in terms of a loss coefficient or friction factor. The method of reduction is discussed in Section 5. The friction factor for the HOTERV core is essentially constant with that for the Trane core being larger at $G_o < 2000$ and smaller for $G_o > 2000$. Also shown in Figure 28 are values of j_o for both cores. These values are equal within experimental error.

7.2 COMPARISON OF DRY HEAT TRANSFER PERFORMANCE

The performance of the Trane heat exchanger surface operating in the dry mode may be compared with that of the HOTERV and the two Curtiss-Wright exchangers reported in reference 3. Several methods of presenting this comparison have been discussed in the literature. Cox and Jallouk[11] suggested combining the heat transfer and pressure drop performance by plotting an air-side standardized heat transfer rate (Q per unit ΔT) as a function of the fan power or the fan power per unit heat transfer rate. the heat transfer rate was expressed in terms of a unit of surface area (air-side) or a unit of heat exchanger volume. In reference 3 the heat transfer rate was related to a third parameter, the frontal area.

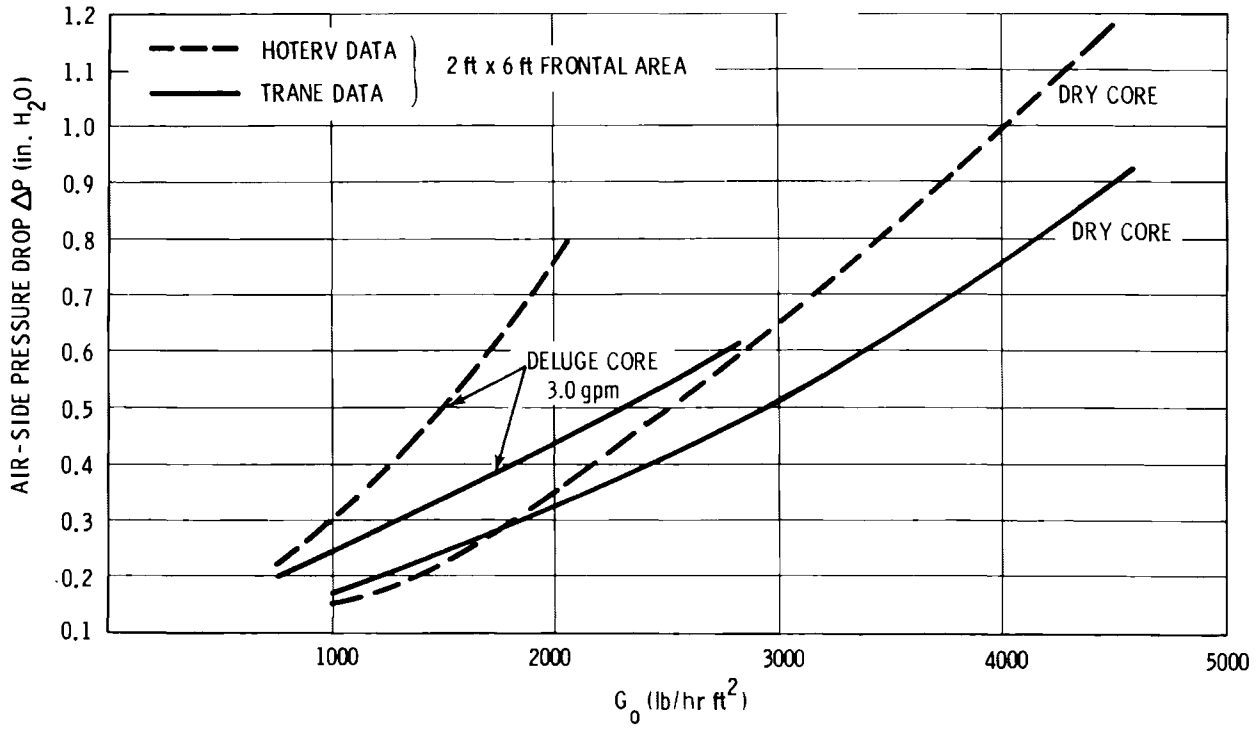

Figure 27. Comparison of TRANE and HOTERV pressure drop data.

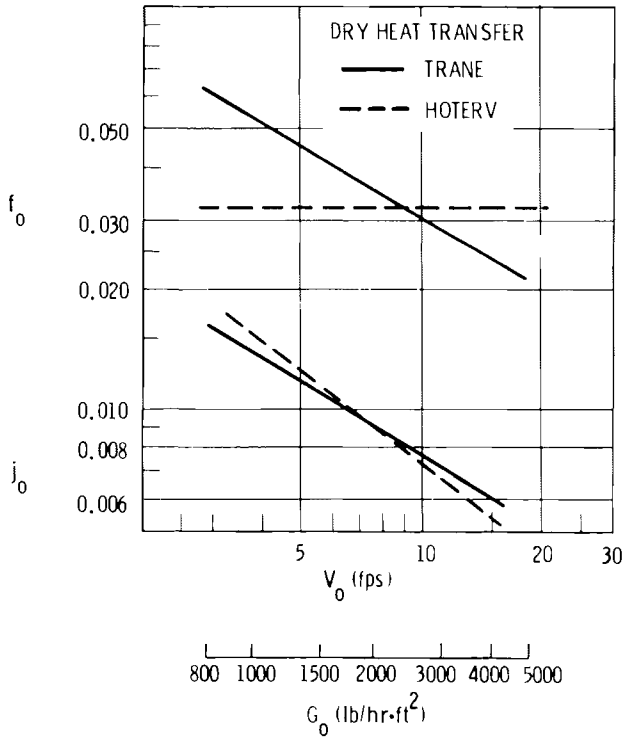

Figure 28. Comparison of f_o and j_o for HOTERV and TRANE cores.

The standardized heat transfer rate of Cox and Jallouk is essentially a heat transfer coefficient and consequently it does not reflect the incentives for high air flow at a given power expenditure which will reduce the air temperature range through the heat exchanger and thus increase the effective temperature difference.

A more meaningful comparison of heat exchangers is the total heat transferred per unit of frontal area as a function of the power expended per unit of frontal area. If this is divided by the depth of the exchanger, the total heat transferred is related to the required volume of the heat exchanger. These comparisons for the Trane surface and the three surfaces previously studied[3] are shown in Figure 29.

The expression used for this comparison is the following (see Appendix E for derivation):

$$\frac{Q}{C_p \Delta T_i A_f L} = \frac{C_1}{L} \left\{1 - \exp\left[- C_2 P^{-n/(3-m)}\right]\right\} P^{1/(3-m)} \tag{83}$$

where

$$C_1 = \sigma \left[\frac{1000\,\mu g_c}{2LV^2 f_r} \left(\frac{D_h}{1000\mu}\right)\right]^{(1+m)^{1/(3-m)}} \tag{84}$$

$$C_2 = \left(\frac{C_1}{\sigma}\right)^{-n} \left(\frac{1000\mu}{D_h}\right)^{(1+n)} \left(\frac{4\,LP_r^{-2/3jr}}{1000\mu}\right) \tag{85}$$

P = power per square ft of frontal area; i.e., $\frac{P_{(total)}}{A_f}$

j_U = j-factor based on the overall heat transfer coefficient, U

j_r = j_U evaluated at Re = 1000

f_r = f_o evaluated at Re = 1000

m,n = constants from the fit of f_o and j_U vs Re number; i.e.,

$$f_o = f_r\,(Re/1000)^{-m} \tag{86}$$

$$j_u = j_r\,(Re/1000)^{-m} \tag{87}$$

(The expression for j_U is assumed to contain the influence of fin efficiency and inside film coefficients.)

All other terms are included in the nomenclature.

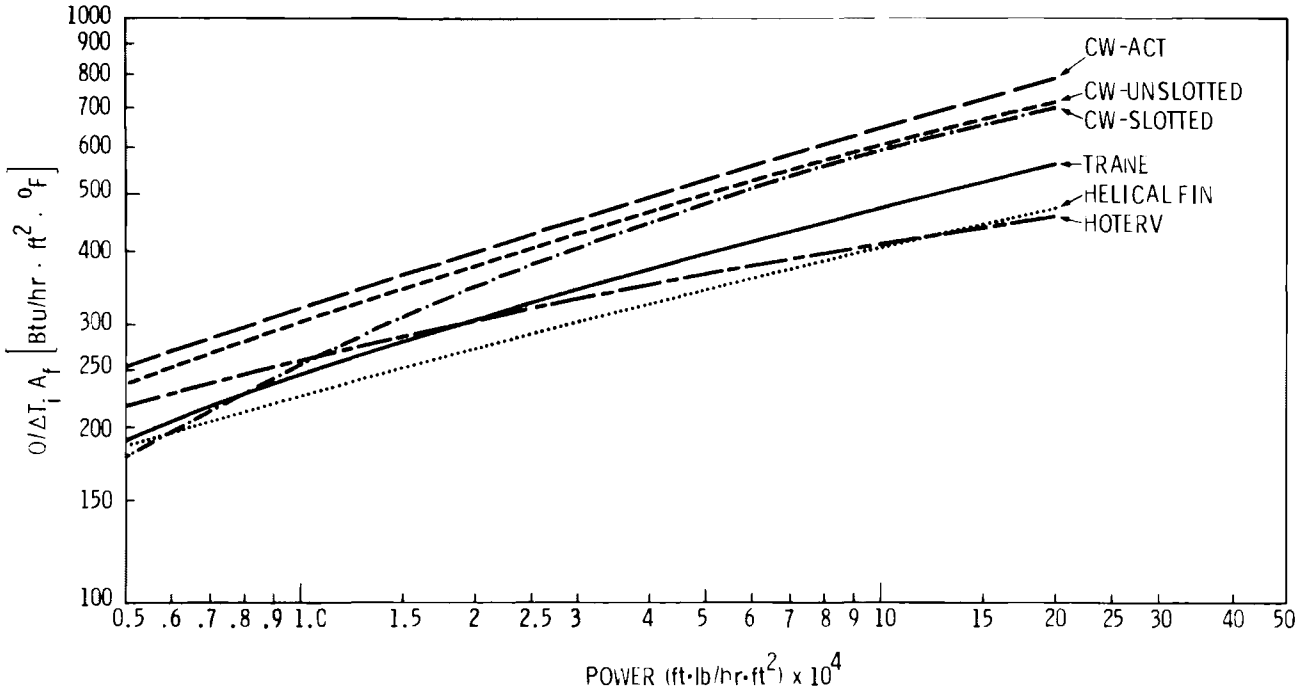

Figure 29a. Comparison of heat exchanger performance per unit frontal area on the basis of equal power input.

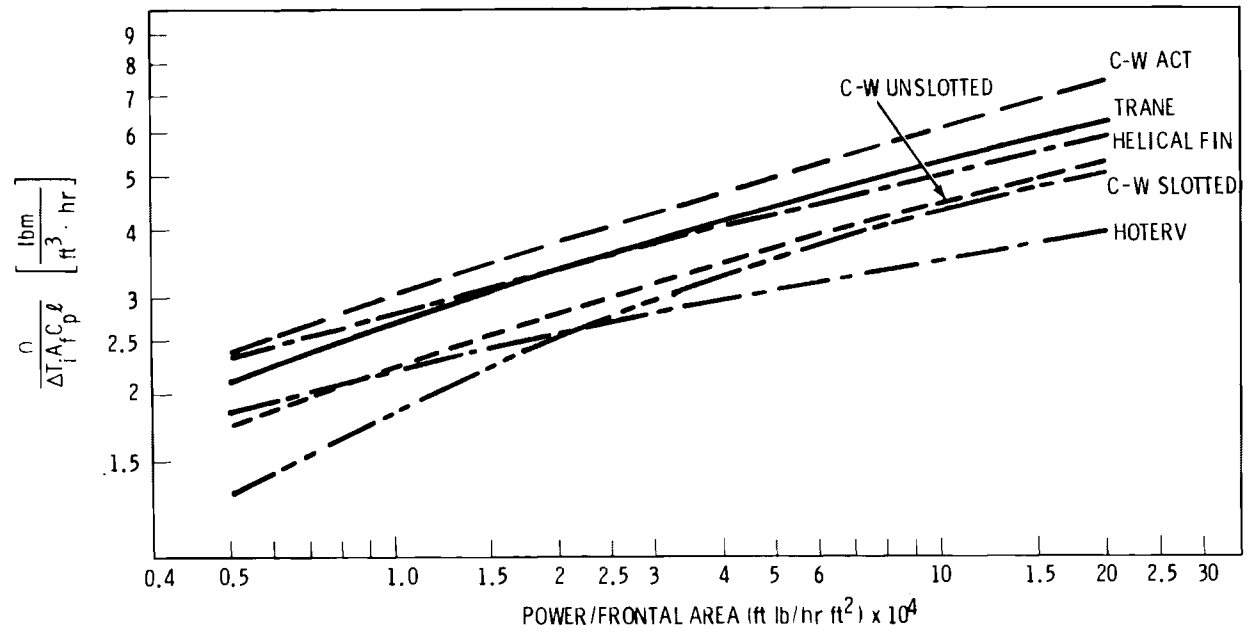

Figure 29b. Comparison of heat exchanger performance per unit volume on the basis of equal power input.

This expression is obtained by combining the Equations for: (1) fan power as a function of mass velocity, (2) the rate of heat transfer, and (3) the air-side heat balance for an isothermal heat exchanger (e.g., a condenser). A similar expression for a heat exchanger with temperature range on the liquid side is shown in Appendix E, together with the development of Equation 83.

Figure 29 includes curves for three different widths of Curtiss-Wright exchangers; one 5.4 inches thick, as proposed for the Advanced Concepts Test (ACT) facility, and the other two 6.9 inches, as tested in the WATA loop. Of these one has slotted fins, the other unslotted fins. Table 6 lists the design parameters used in these calculations.

On the basis of these comparisons, the relative performance of the Trane and HOTERV heat exchangers depends on the power available. At the design point of the unit being produced for the ACT facility, the Trane exchanger is about four percent more effective than the HOTERV under the same power-expended conditions which is within the uncertainty band of the data. The Curtiss-Wright surface shows slightly better performance characteristics when compared on the basis of 5.4-inch depth being supplied to ACT. On the basis of volumetric performance, the 6.9-inch depth unslotted surface tested in the WATA loop shows superior performance.

Typical power levels used with these surfaces are roughly 10^4 ft lbs/hr-ft^2. The rather sharp "knee-effect" in the curves of $Q/\Delta T_i C_p$ versus power is shown more clearly on a linear plot of these parameters, Figure 30. Typical data obtained in the WATA loop are also shown.

TABLE 6. CHARACTERISTIC DIMENSIONS OF HEAT EXCHANGERS

	Helical Finned Tubes	HOTERV	TRANE	CURTISS-WRIGHT Plate Fin	CURTISS-WRIGHT Slotted Fin	CURTISS-WRIGHT ACT
Description	Tube diameter = 0.42 in. Fin dia. (outside)= 0.861 in. Fin pitch: 8.72 in^{-1}. Five rows staggered 0.975 in X 0.80 in.	Plate fin - slotted. Tube dia: 0.764 in. Fin pitch: 8.76 in^{-1}. Six rows staggered 2.36 in X 0.984 in.	Plate fin wavy. Tube dia.: 0.625 in. Fin pitch: 10 in^{-1}. Three rows staggered equilateral 1.5 in.	Extended channel w/skived fins. Fin pitch: 9 in^{-1}. In-line channel w/plain fins.	Extended channel w/skived fins. Fin pitch: 12 in^{-1}. In-line channel w/slotted fins.	Extended channel w/skived fins. Fin pitch: 10 in^{-1}. In-line channel w/slotted fins.
D_h ft	0.01452	0.0127	0.00972	0.01455	0.01088	0.0133
s, ft^2/ft^3	136.0	155.2	216.0	172.0	221.0	216.0
σ	0.494	0.493	0.534	0.629	0.603	0.719
L, ft	0.3384	0.492	0.375	0.575	0.575	0.4478
f_r	0.0531	0.032	0.0300	0.0254	0.0217	0.0327
m	0.23	0.0	0.600	0.691	1.133	0.473
b	0.226	1.205	0.117	0.5002	3.509	0.169
n	0.4	0.684	0.3544	0.5911	0.901	0.402
j_r	0.0113	0.00680	0.00568	0.00755	0.00619	0.00867
n'	0.565	0.811	0.697	0.629	0.919	.499
n_f	$.99^+$	included in j_H	included in j_H	included in j_H	included in j_H	included in j_H

f_r is the value of f_o at Re = 1000.

j_r and n' are the constants for $j_U = j_r\left(\frac{Re}{1000}\right)^{-n'}$ which is calculated from $j_H = bRe^{-n}$ assuming a resistance of 0.02 for the tube wall and inside film coefficient.

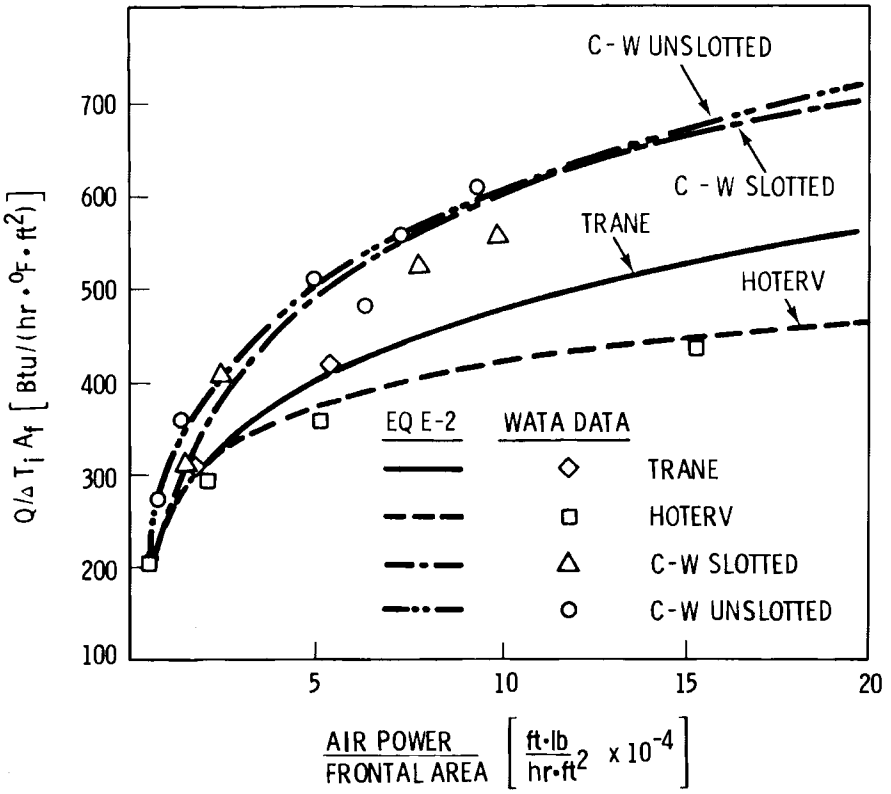

Figure 30. Comparison of TRANE, HOTERV, and heat exchangers on the basis of equal power.

7.3 COMPARISON OF WET HEAT TRANSFER PERFORMANCE

Wet heat transfer performance may be compared on the same basis as discussed in Section 6. The enhancement ratio is important because it is a measure of the gain in heat transfer due to deluging. Figure 31 repeats the data given in Figure 18 and includes data for the HOTERV core.

The results for the Trane and HOTERV cores in Figure 31 are not directly comparable because they are for different operating conditions. The Trane data are for T_p = 120°F and V_o = 4.5 fps whereas the HOTERV data are for T_p = 110°F and V_o = 6 fps. Both data sets use the same deluge rate of 3.0 gpm.

Another important factor to consider when comparing performance of the two cores is the inside heat transfer coefficient used in determining U_o*. Both cores were tested with water as the primary fluid. Because of the different internal construction of the two cores, the primary-side heat transfer coefficients were considerably different (Trane - 2200 Btu/hr-ft^2-°F HOTERV - 625 Btu/hr-ft^2-°F). During real operation in a cooling tower, for instance the ACT facility, the primary side fluid will be ammonia vapor and the condensing coefficients will be very nearly equal.

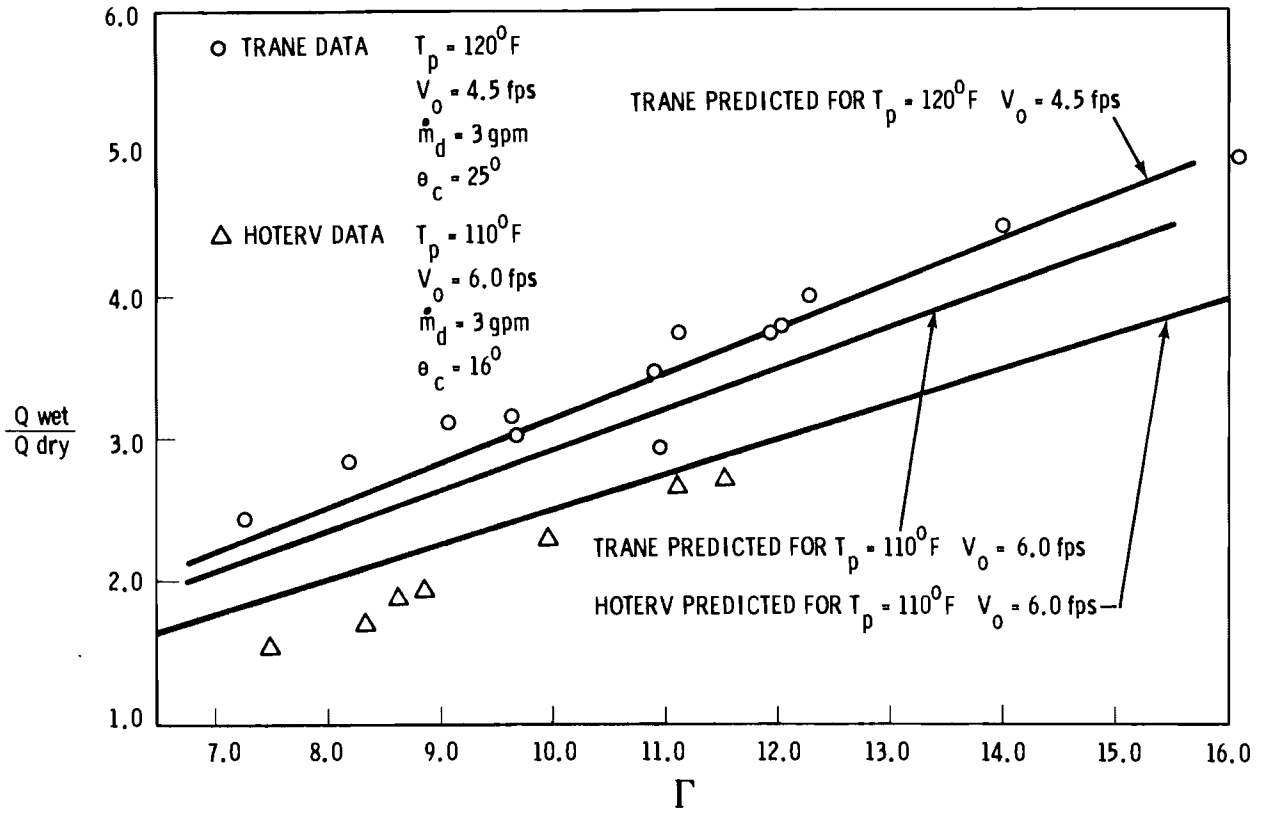

Figure 31. Plot of enhancement ratio versus Γ.

For the reasons mentioned above, in order to compare the two cores directly, a predicted line was calculated for the Trane core for identical operating conditions as the HOTERV core (T_p = 110°F; V_o = 6.0 fps; h_p = 625 Btu/hr-ft^2-°F). The line shown in Figure 31 falls below the other Trane data and above the HOTERV data. The uncertainty in this prediction is unknown but qualitatively the conclusion from this graph would be that the Trane core performs as good and probably better than the HOTERV core under identical operating conditions.

A predicted line for the HOTERV data was also calculated and shown in Figure 31. The same h_d* and ξ values were used as for the Trane calculation. These values may not be applicable, however the prediction agrees reasonably well with the data.

The same type of calculations was done for U_o* and Q/ITD. They are shown in Figures 32 and 33 as a function of air mass flux G_o. Qualitatively the conclusions are the same as for Figure 31. The Trane core seems slightly better in performance than the HOTERV core under identical operating conditions.

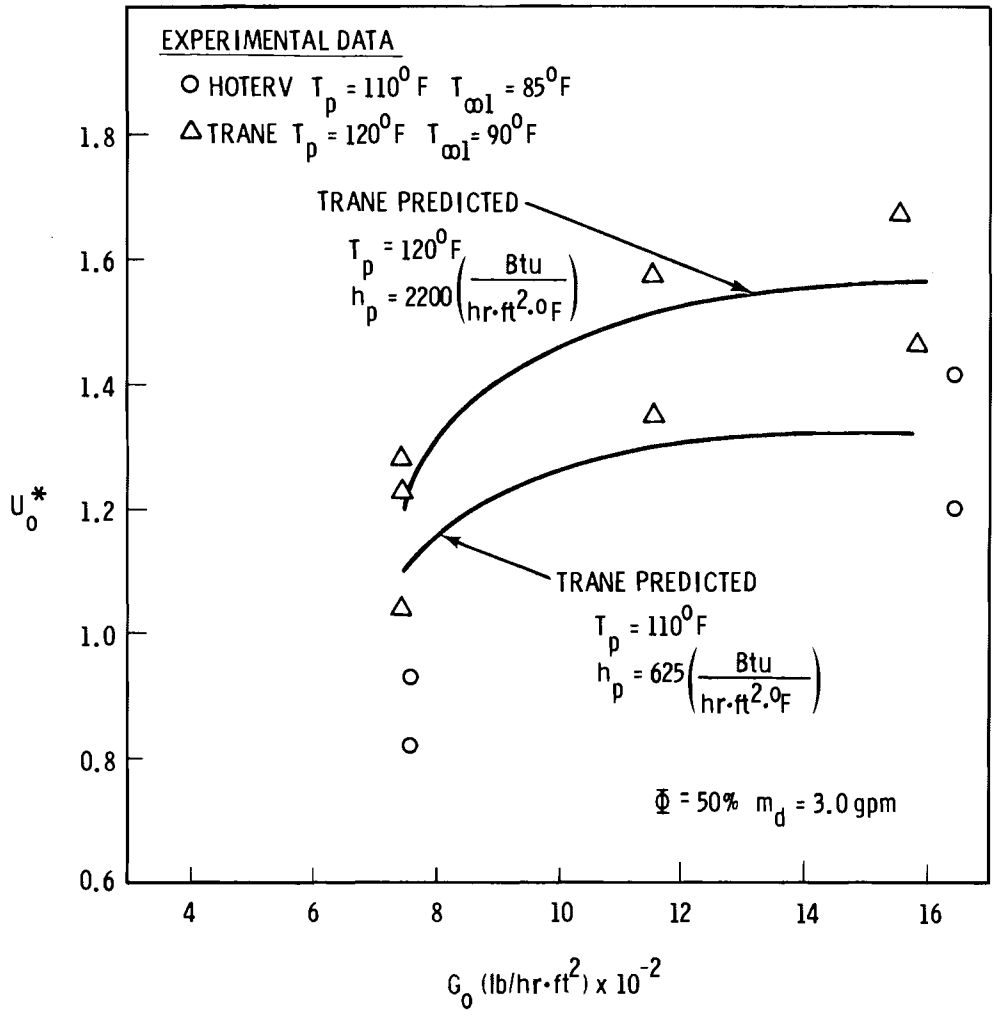

Figure 32. Plots of U_o^* and G_o for HOTERV and TRANE surfaces.

Predicted values for the HOTERV core in Figures 32 and 33 differs significantly from the corresponding experimental data. This indicates that using the same h_d^* and ξ values as for the Trane core is not a good approximation. Other analysis indicates that the primary error is in the h_d^* values.

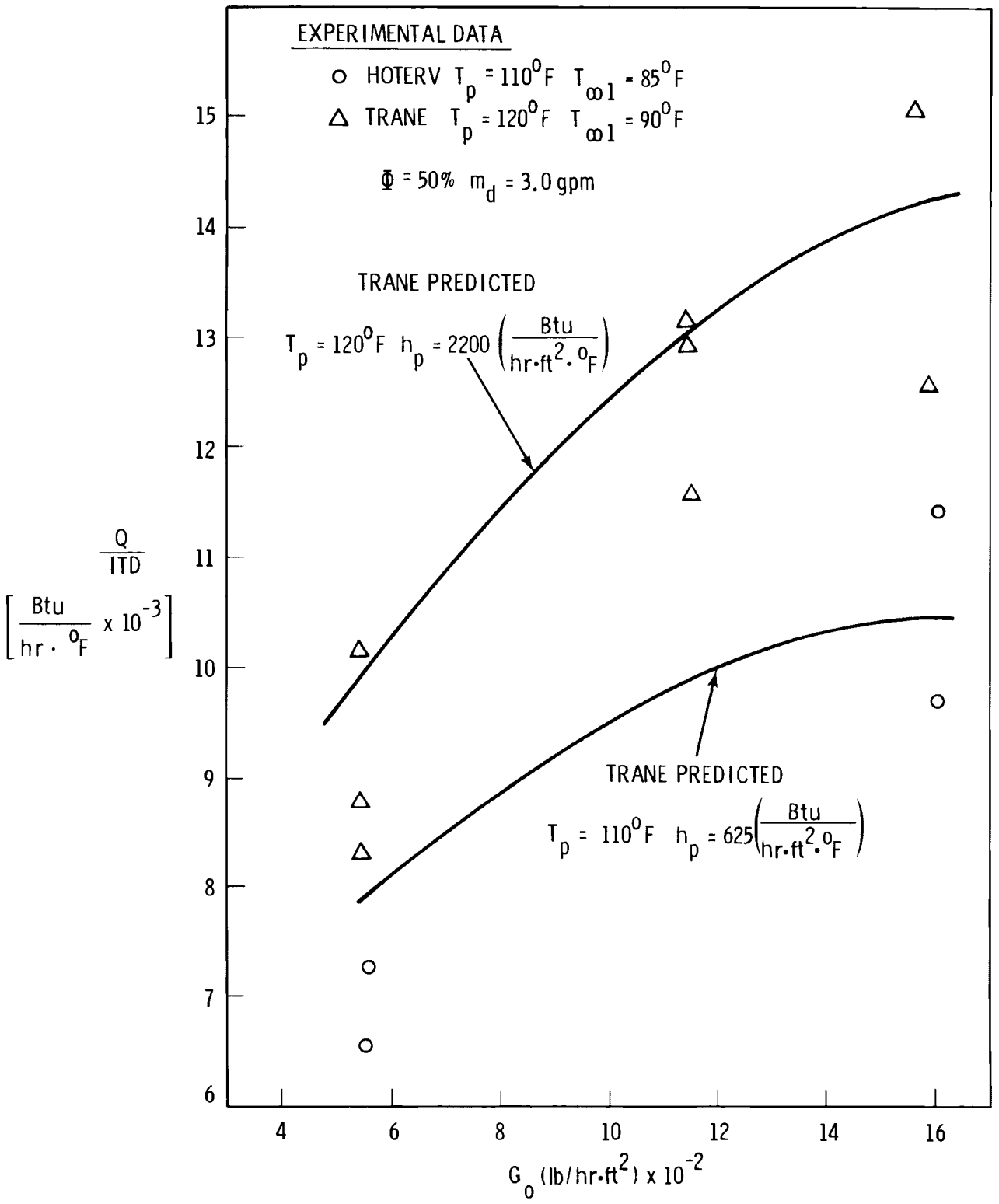

Figure 33. Plots of Q/ITD versus G_o for both HOTERV and TRANE surfaces.

SECTION 8

SUMMARY AND DISCUSSION OF RESULTS

8.1 SUMMARY OF PARAMETERS AFFECTING PERFORMANCE

8.1.1 Dry/Wet Pressure Drop

The data in Figures 9 and 10 depict the measured pressure drop performance of the test core as a function of the air and deluge water flow rates. The present results for f (dry) are in good agreement with the results reported by Trane. The slight difference in slope of the f versus G_0 curves may be due to edge effects since the test case used by Trane (1' by 1') was smaller than that used by PNL (2' x 6').

The wet data for Δp and f illustrate increasing flow friction with increasing deluge water flow rate. From Figure 10 it is clear that the slope of f versus G_0 becomes steeper (more negative) with increasing deluge water flow rates. Data are not shown for wet performance at $V_0 >$ 6 ft/sec because the higher air flow rates resulted in drift of water droplets off the back of the core, an unacceptable operating condition.

8.1.2 Dry Heat Transfer Results

The dry heat transfer data presented as U_0, h_0 and h_s are given in Figure 11 and as the Colburn factor j in Figure 10. The present data for j are generally in good agreement with the Trane results. However, as with f, the slope of the present data for j versus G_0 is somewhat greater than the Trane results possibly because of the difference in the sizes of cores tested.

8.1.3 Wet Heat Transfer Results

The wet heat transfer performance results are presented in various forms in Figures 12-26. Where possible, predictions obtained with the deluge model are also provided for comparison. The presentation of wet heat transfer data is substantially more complex than dry data because there are a larger number of variables that must be accounted for.

A parameter commonly used to characterize heat exchanger performance is the ratio Q/ITD. For dry operation with a given heat exchanger, this ratio is dependent upon the air flow rate and is essentially independent of the core temperature for the range of conditions normally of interest for dry cooling. For wet operation, Q/ITD is dependent on both core temperature

T_p and the air inlet conditions $T_{\infty 1}$, $\Phi_{\infty 1}$. For fixed air and deluge flow rates Q/ITD has been found to correlate with the dimensionless inlet driving potential Γ as shown in Figure 12. The predicted values of Q/ITD generated with the deluge model are also in excellent agreement with the data.

The deluge model employs an overall heat transfer coefficient U_o^* that is completely analogous to U_o. The experimental results for U_o^* are given in Figures 13-16. It can be seen in Figure 13 that U_o^* increases with increasing G_o but that the dependence of U_o^* on G_o diminishes at higher flow rates.

Figures 13 and 14 show that U_o^* is also an increasing function of deluge water flow rate but that the rate of increase diminishes with increasing m_d. Referring to Figures 9 and 10, it can be seen that pressure drop also increases with increasing G_o and/or $\dot{m}_d$. It is not apparent from these results alone to what extent optimums in air flow and deluge water flows exist. For example, the benefits of increased heat transfer may be offset by losses due to increased consumption of power to run fans and pumps.

The results in Figures 14 and 15 indicate that U_o^* at $\theta_c = 25^o$ was higher than at 20^o but that increasing the core angle beyond 25^o resulted in no further benefit for the operating conditions tested. The conclusion to be drawn from these results is that there is no apparent incentive (with respect to heat transfer performance only) to increase θ_c beyond 25^o. However, in the WATA experiments, the air does not experience the acceleration/deceleration effects in passing through the test section that it would in passing through the A-frame arrangement that will be used in the ACT facility. Consequently, this influence of core angle on air flow distribution and resulting effects on heat transfer performance and pressure drop are not present in the WATA data. However, since the observed dependence on θ_c is small, considerable design flexibility probably exists.

The dependence of U_o^* on the inlet and core conditions is shown in Figure 16 as a function of the normalized driving potential Γ. Although there may be a slight trend in the data for decreasing U_o^* with increasing Γ, to within the accuracy of the present experiments, U_o^* may be assumed independent of the air inlet conditions.

One of the most important yet ill defined parameters in the "lumped" deluge heat transfer model is the deluge film coefficient h_d (or $h_d^* = h_d A_s^*$ which includes effects of wet fin efficiency). All of the known film flow heat transfer correlations predict substantially higher values of h_d than were observed. It is postulated that the nature of the incomplete wetting of the surface together with possible bridging of the fin gaps in some regions of the core account for the apparent discrepancy. Unfortunately, to evaluate h_d one must resort to assumptions that do not explicitly account for the influences of partial wetting or bridging even if it was possible to measure these effects. Thus, the only credible means for

determining the "effective" h_d is empirically from the results of experiments such as those reported here.

The results for h_d^* (including the effects of fin efficiency) determined from the experiments are presented with the data for U_o^* in Figures 13-16. The data show that for the conditions tested, h_d increases with increasing air flow and/or deluge water flow much like U_o^*. There may be a slight maximum in h_d^* at $G_o \sim 0.012$ (lb/hr ft^2), however, the observed effect is within the uncertainty and is thus inconclusive. These results also suggest that the degree of surface wetting is improved by higher deluge flow rates and increased air velocity but that the benefits achieved diminish as the flow rates are increased. This might be due to increased bridging and the resultant reduction in the effective air-water interface area.

The data in Figures 14 and 15 illustrate little clear dependence of h_d^* on core angle θ_c consistent with the result for U_o^*. Similarly, the data in Figure 16 indicate no significant dependence of h_d^* on the ambient operating conditions.

Another parameter of critical importance to the deluge model is the resistance transformation parameter ξ whereby the internal thermal resistances are converted to a form compatible with the surface enthalpy driving potential. The definition of ξ is

$$\xi = \frac{(i'_p - i'_r)}{C_a(T_p - T_r)} \tag{19}$$

where "r" denotes the fin root conditions. The root condition T_r, i'_r (and thus ξ through Equation 19) were determined empirically in the same procedure used to extract the values of h_d^* already discussed. The corresponding results for the root conditions and ξ are shown in Figure 17.

The primary to root temperature difference divided by the ITD was found to be linearly related to Γ for given core temperature and flow conditions. The data in Figure 17 are seen to be well correlated and in good agreement with the deluge model prediction. In addition, the values of $T_p - T_r$ were found to be unaffected by core angle and only slightly dependent on the air and deluge water flow rates.

The results for ξ in Figure 17 show no significant dependence on . The value of ξ is however dependent on the core temperature T_p. For the range of variables tested, ξ showed no significant dependence on θ_c, G_o or $\dot{m}_d$. This is an important result because it implies that for a given T_p, ξ may be assumed constant.

One of the simplest and yet most meaningful parameters used to characterize the performance of a deluged heat exchanger is the enhancement ratio Q_w/Q_d. For this calculation Q_d is the heat rejection rate of

the heat exchanger in question at the same core temperature, inlet air conditions and air side pressure drop as in the wet operation corresponding to heat rejection rate Q_w. The ratio Q_w/Q_d represents the approximate relative improvement in the heat transfer performance of a wet section of heat exchanger as compared to a dry section operating in parallel with it at the same conditions. Since the wet and dry sections operate in parallel with a common source of fan induced air flow, the flow through each section will be self regulated in response to the same overall pressure drop. Values of Q_w/Q_d determined in the present experiments and the corresponding predicted values computed with the deluge model are presented in Figures 18-20.

Values of Q_w/Q_d for widely varying conditions of air temperature and humidity were found to correlate very well with the parameter . These results are shown in Figure 18 along with the predicted correlation based on the deluge model. The agreement of theory and experiment is excellent.

The data in Figures 19 and 20 for Q_w/Q_d show no significant dependence on G_o, $\dot{m}_d$ or θ_c to within the uncertainty of the experimental data. This is a very important result because it implies that the heat transfer performance is relatively insensitive to several important design and operating parameters. Thus, for example, alteration of the core angle from the nominal 25^o chosen for the ACT design could be accomodated, if necessary without loss of performance. Similarly, it should be possible to vary G_o and $\dot{m}_d$ to optimize constraints such as minimizing fan power, droplet drift and/or scale formation without significantly altering the heat transfer enhancement.

The predicted values of Q_w/Q_d are also shown in Figures 18-20 for comparison with the data. Although the theory shows variations that are possibly observed in the data due to scatter, theory and experiment are generally in good agreement.

8.1.4 Mass Transfer Results

Although the design of the experimental apparatus was intended to allow for accurate collection and metering of the deluge water operating difficulties resulted in uncontrolled water loss, especially at high angles and high deluge flow rates. As a consequence accurate measurements of the deluge water evaporation rates were not obtained. However, an approximate measure of the evaporation rate was determined for each test by subtraction of the average inlet and outlet humidities. The results of computations derived from these measurements and the corresponding predictions are presented in Figures 21-25.

Figure 21 presents measured and predicted values of the overall mass transfer coefficient for each test. The solid line is the prediction based on constant values of ξ_m and h_d^*. The experimental data are seen to scatter widely due presumably to difficulties with sampling and averaging the outlet air humidity and temperature. Disregarding a few of the lowest data points the analysis would appear to overpredict Σ_m^* by about 20%.

There appears to be little if any dependence of Σ_m^* on Γ but the uncertainty in the data are too great to be conclusive.

The results in Figure 22 show that Σ_m^* increases with increasing G_o analogous to the variation of U_o^*. The deluge model agrees reasonably well with the data at high G_o but overpredicts Σ_m^* at low velocity.

The mass transfer extension of the deluge model employs a resistance transformation parameter ξ_m that is analogous to ξ. Values of ξ_m were computed using the deluge model and these results are presented in Figure 23 as the ratio ξ_m/ξ where the ξ values used are those given in Figure 17. It can be seen that ξ_m is approximately equal to ξ to within $\pm$ 10% for the range of ambient conditions used in the experiments. However, whereas ξ was shown to be essentially independent of operating conditions (i.e., see Figure 17), it is apparent that ξ_m decreases with increasing Γ and thus may not in general be assumed constant.

Figures 24 and 25 compare measured and predicted values of the effectivenesses based on temperature, humidity and enthalpy as functions of G_o and Γ. The agreement of theory with experiment was good for ϕ^*, fair for ϕ_m^* and poor for ϕ. In all cases, predicted trends agreed with the data but the predicted outlet humidity $H_{\infty 2}$ was consistently high and the resulting outlet temperature was too low. It must be pointed out that determination of $T_{\infty 2}$ from the set ($i_{\infty 2}$, $H_{\infty 2}$) is extremely sensitive to changes in the values used. In addition, the uncertainty in measured outlet values of $T_{\infty 2}$ and $i_{\infty 2}$ has already been noted. Therefore, it is not possible at this time to determine to what extent the disagreement is attributable to deficiencies in the model or in the data. Additional tests are required to better evaluate this aspect of the deluge model.

Figure 26 shows that the proportion of the heat load rejected as latent heat increases with increasing values of Γ. The data correlate well with Γ and the predicted correlation is in excellent agreement with the data. It can be seen that for operating conditions corresponding to high values of Γ, the latent heat component can exceed that rejected by the core. In this case, the air would actually be cooled upon passing through the heat exchanger. Although this would not necessarily be bad, it may not represent the best use of available water.

8.2 SUMMARY OF PERFORMANCE COMPARISONS

In Section 7 a number of comparisons were made of performance characteristics of a number of heat exchangers tested in the present and preceding experiments.

Figures 27 and 28 compare the present data on pressure drop and heat transfer through the Trane core with that measured previously on the HOTERV core. The mass velocity at the face is the independent variable. The HOTERV core exhibits lower pressure drop at relatively low velocity but higher pressure drop at all values of $G_o > 1700$ lb/hr ft^2. The f_o value for HOTERV is nearly constant, indicating that form drag predominates. At low

air flow the form drag is greatly reduced, consequently, the total pressure drop is less at low flows. In the deluged-mode, the Trane core has significantly lower pressure drop. The sine-wave nature of the Trane surface probably provides less holdup of liquid and consequently more free area for air flow than the HOTERV surface at the same deluge rate.

A more meaningful comparison of performance in the all-dry mode of operation is the value of $A/\Delta T_i$ per unit frontal area, as a function of fan power. A plot of this type is shown in Figure 29a. This comparison incorporates the influence of air flow rate on the log-mean temperature driving force. One may, in addition, choose to include the volumetric efficiency of the heat exchanger by dividing through by the length of air travel through the heat exchanger. Figure 29b is such a plot. It shows that on the basis of a volumetric efficiency, the Curtiss-Wright heat exchanger, being built for the ACT facility, is more effective than those tested in the WATA loop and reported in reference 3. The Trane surface is shown to be volumetrically more effective than the HOTERV heat exchanger. However, on the basis of frontal area alone, as shown in Figure 29a, the HOTERV heat exchanger is slightly superior to the Trane unit at relatively low fan power but less efficient at high fan power. At design conditions for each surface, the Trane surface is about 4 percent more effective on a frontal area basis and about 35 percent more effective on a volumetric basis. Neither surface is quite as effective as the Curtiss-Wright surface ordered for ACT. The Trane is volumetrically more effective than either Curtiss-Wright surface tested in the WATA facility, but is slightly less effective on the basis of frontal area.

A conventional helical fin, wound on 1/2 in. tubes at 11 fins/in. and arranged in five rows of close-pack staggered configuration is also shown to be an effective heat exchanger on a volumetric basis. On the basis of frontal area, the five-row heat exchanger is slightly inferior to the HOTERV exchanger. Another basis of comparison, that of the heat transfer capability per unit of total surface area, obtained by dividing the ordinate of Figure 29b by the specific surface area, would show that the helical fin tube arrangement was the most effective on this basis. These results indicate that the cost effectiveness of the Trane and Curtiss-Wright surfaces do not result primarily from their superior heat transfer performance per square foot of exposed surface, but rather from the lower cost projections for a completely assembled heat exchanger bundle.

The heat transfer capability increases with approximately the 0.3 power of the fan power. Consequently, higher power of the fan will not greatly increase the heat rejection capability. Figure 30 shows this relationship on a linear graph which brings out the resulting "knee" effect; i.e., the greater impact of the detrimental effect of reduced power in comparison to improved performance with higher power. Experimental data obtained in the WATA loop are superimposed on the analytical projection of performance to show the fit between these data and the derived expression.

Figure 31 shows a comparison of the enhancement factor Q_w/Q_d for the HOTERV and Trane cores. Both actual and predicted values are shown for

the test conditions used in the respective experiments. These operating conditions were not the same, however, so the results are not directly comparable. Thus a second computation was made for the Trane core at conditions equivalent to those used in the HOTERV tests. These results are presented as the second and somewhat lower curve for the Trane core. The results show that at comparable operating conditions, Q_w/Q_d for the Trane core is about 20% higher than for the HOTERV core at the same air flow rates. This is largely due to the greater frictional loss of the HOTERV core at a given air flow rate.

Figure 32 shows comparisons of experimental and computed values of U_o* for the HOTERV and Trane cores. For comparable conditions at low air flow rates the computed U_o* for the Trane core is higher than the HOTERV data. However, at the higher air flow rates where both are likely to be used, the predicted performance of the Trane core is about equal to the HOTERV data. Thus, disregarding the effects of friction, the two cores will have similar heat rejection capabilities at the same air flow rate. This is also illustrated in another way in Figure 33 which plots Q/ITD for the two cores. The effect of the high pressure drop of the HOTERV core is to change the dry heat transfer rate against which comparison is made so that Q_w/Q_d is higher in Figure 31 at all conditions for the Trane core.

SECTION 9

REFERENCES

1. Johnson, B. M., R. T. Alleman, D. W. Faletti, B. C. Fryer and F. R. Zaloudek. 1976. Dry Cooling of Power Generating Stations: A Summary of the Economic Evaluation of Several Advanced Concepts Via a Design Optimization Study and a Conceptual Design and Cost Estimate. BNWL-2120, Pacific Northwest Laboratory, Richland, WA.

2. Braun, D. J., R. D. Tokarz, B. M. Johnson, R. T. Alleman, D. W. Faletti, L. J. MacGowan, H. L. Parry, Jr., G. C. Smith and F. R. Zaloudek. 1978. Comparative Cost Study of Four Wet/Dry Cooling Concepts That Use Ammonia as the Intermediate Heat Exchanger Fluid. PNL-2661, Pacific Northwest Laboratory, Richland, WA.

3. Parry, H. L., Jr., L. J. MacGowan, D. K. Kreid, L. E. Wiles, D. W. Faletti and B. M. Johnson. 1979. Augmented Dry Cooling Surface Test Program: Analysis and Experimental Results. PNL-2746, Pacific Northwest Laboratory, Richland, WA.

4. Kreid, D. K., B. M. Johnson and D. W. Faletti. 1978. "Approximate Analysis of Evaporative Heat Transfer from a Finned Surface." ASME Paper No. 78-HT-26, presented at the AIIAA/ASME Joint Thermophysics and Heat Transfer Conference May 25-26, 1978. Palo Alto, CA.

5. Kreid, D. K., H. L. Parry, Jr., and L. J. MacGowan. 1979. "Performance of a Plate Fin Air Cooled Heat Exchanger with Deluged Water Augmentation." ASME Paper 79-WA/Ener-1, presented at the ASME Winter Annual Meeting, December 2-7, 1979. New York, NY.

6. Kals, W. 1972. "Wet Surface Air Coolers: Characteristics and Usefulness." ASME Paper No. 72-HT-28.

7. Kline, S. J., and F. A. McClintock. 1953. "Describing Uncertainties in Single Sample Experiments." Mechanical Engineering.

8. Gebhart, Benjamin. 1971. Heat Transfer. 2nd ed., McGraw-Hill, New York, NY, p. 260.

9. ASHRAE Handbook, 1977, American Society of Heating, Refrigerating, and Air-Conditioning Engineers, Inc., New York, NY.

10. Keenan, J. H., F. G. Keyes, P. G. Hill and J. G. Moore. 1969. Steam Tables: Thermodynamic Properties of Water Including Vapor, Liquid and Solid Phases. John Wiley and Sons, New York, NY.

11. Cox, B., and P. A. Jallouk. 1972. "Methods for Evaluating the Performances of Compact Heat Transfer Surfaces." ASME Paper No. 72-WA/HT-56, presented at the ASME Winter Annual Meeting.

12. Kern, D. G., 1950. Process Heat Transfer. 1st ed., McGraw-Hill, New York, NY, p. 607.

APPENDIX A

DEVELOPMENT OF THE DELUGE MODEL

APPENDIX A

DEVELOPMENT OF THE DELUGE MODEL

DERIVATION OF THE MASS/HEAT TRANSFER ANALOGY

The flow configuration and geometry employed in development of the Equations for the surface mass/heat transfer analogy are illustrated in Figure A-1a. The wetted heat transfer surface is oriented in the x-z plane with a thin, uniform film of deluge water flowing in the (-z) direction. Air is assumed to flow normal to the deluge water stream in the (+x) direction as shown. A control volume with cross-sectional area A_s extends from the air-water interface to an assumed adiabatic, material surface (i.e. a symmetry plane) at a distance δ from the water surface. For a boundary layer flow, δ might be chosen so that the control volume extends just beyond the boundary layer. For an internal flow, as in the case of flow between fins as illustrated in Figure A-1b, δ may be taken as half the free fin gap diameter, $\delta = g_d/2$. It is then apparent that the analysis performed for the control volume in Figure A-1a is equally valid for that in Figure A-1b.

The mass/energy balances that follow employ a number of assumptions. The principal assumptions will be summarized here and will be referred to by number in the subsequent analysis.

1. All processes are assumed to be steady-state, steady-flow quasi-equilibrium processes

2. The mass flux of air is assumed uniform over all planes normal to the airflow (i.e. V_o is uniform in any given x-y plane)

3. The deluge water film is assumed to be uniform and of constant thickness (i.e. shrinkage of film due to evaporation is neglected)

4. The heat transfer coefficient h_s and mass transfer coefficient σ_s will be assumed spatially uniform at all locations on the surface.

5. The air at the air/water interface is assumed to be saturated at the surface Temperature T_s

6. The rate of evaporation at the air-water interface is assumed to be "diffusion limited" governed by Ficks law

7. The energy content of the make-up delugate water that is provided to maintain steady-state operation is assumed negligible compared to the heat transfer from the surface.

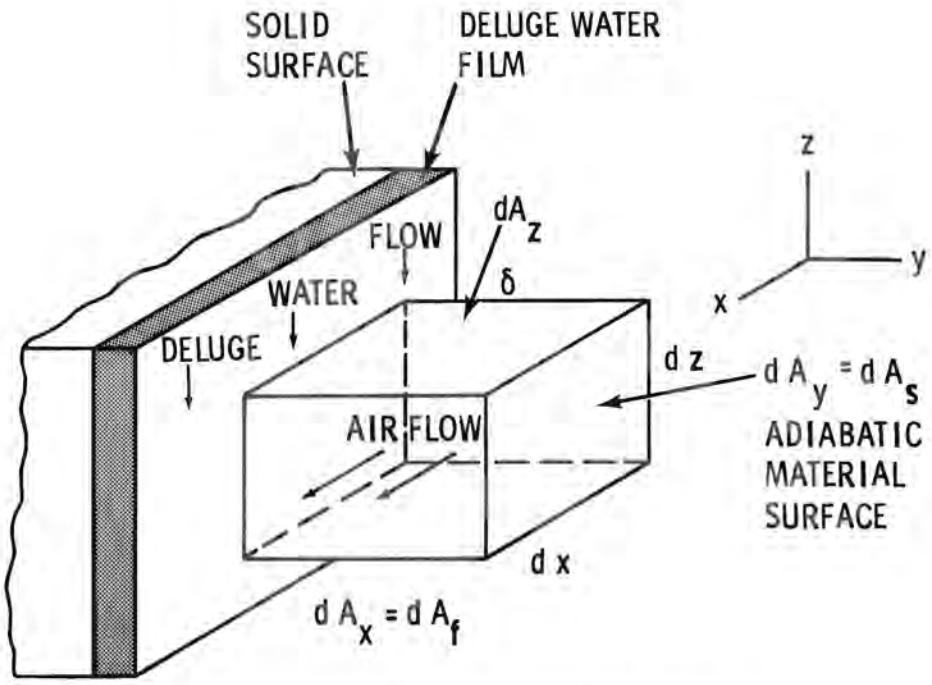

A. CONTROL VOLUME, GENERAL BOUNDARY LAYER

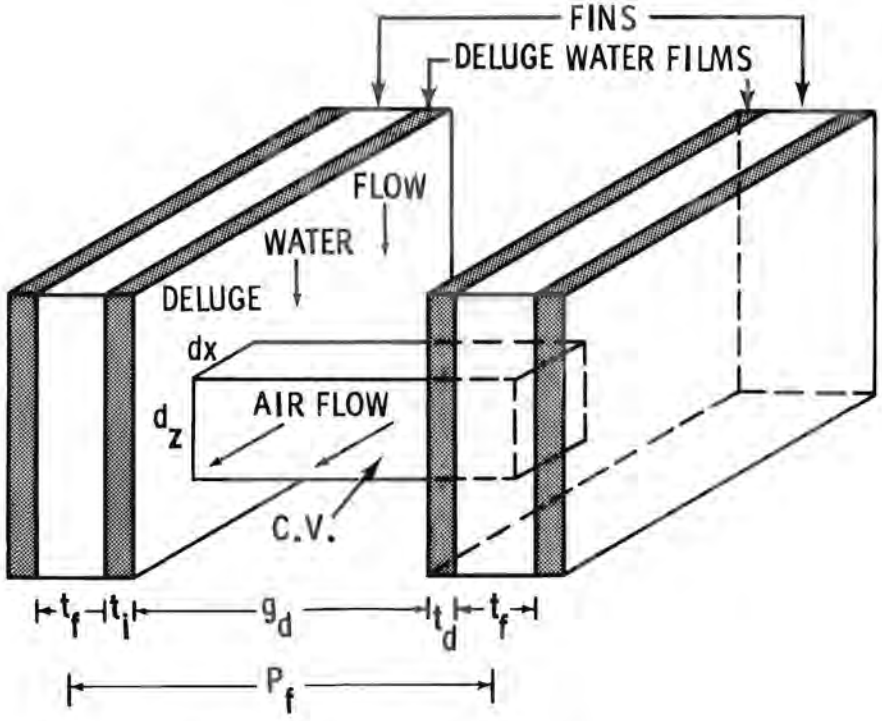

B. CONTROL VOLUME, FINNED SURFACE

Figure A-1. Illustration of control volume used for heat/mass balance.

MASS CONSERVATION

The law of conservation of mass of water for the control volume shown in Figure A-1a for steady-state, steady-flow conditions may be given by

$$d\dot{m}_a dH_\infty = d\dot{m}_v \tag{A-1}$$

This simply states that the water vapor gained by the air must be equal to the liquid water that is evaporated and lost from the deluge water film. Then, $d\dot{m}_v$ can be given by Ficks law in the form

$$d\dot{m}_v = \sigma_s(H'_s - H_\infty)dA_s \tag{A-2}$$

where H'_s is the moisture content of saturated air at T_s and σ_s in the surface mass transfer coefficient.

Equation A-2 may now be substituted into Equation A-1. Using $dm_a = G_a dA_x$, $dA_x = \delta dz$ and $dA_s = dxdz$ then yields

$$G_a(\delta dz)dH_\infty = \sigma_s(H'_s - H_\infty)(dxdz) \tag{A-3}$$

$$\frac{dH_\infty}{H'_s - H_\infty} = \left(\frac{\sigma_s}{G_a \delta}\right)dx \tag{A-4}$$

$$= \left(\frac{\sigma_s D}{G_a \delta}\right)dX \tag{A-5}$$

where D is a characteristic length and $X = x/D$ is the nondimensional distance in the airflow direction (D will subsequently be taken as the heat exchanger depth). In general, integration of Equation A-5 would require explicit functions for $\delta(x)$ and $H_s(x)$. For a pair of parallel surfaces as in Figure A-1b, $\delta = gd/2$ = constant. In this case the dimensionless parameter in Equation A-5 is constant, but, $H'_s(x)$ must still be specified to perform the integration to determine H_∞.

ENERGY CONSERVATION

The law of conservation of energy for the control volume in Figure A-1a for steady-state, steady-flow processes, may be given as follows,

$$dQ_{cv} + d\dot{m}_a i_\infty + d\dot{m}_d i_d = d\dot{m}_a(i_\infty + di_\infty) + (d\dot{m}_d - d\dot{m}_v)i_d \tag{A-6}$$

$$d\dot{m}_a di_\infty = d\dot{Q}_{cv} + d\dot{m}_v i_d \tag{A-7}$$

Thus, the energy gain of the air stream is equal to the rate of heat transfer from the cooled surface plus the energy content of the liquid make-up water that must be provided to maintain steady state. The latter term is normally small and will be neglected.

The heat transferred into the control volume may be separated into changes in the sensible and latent heat contents of the air as follows;

$$dQ_{cv} = d\dot{Q}_{as} + d\dot{Q}_{av} \tag{A-8}$$

It is assumed that the transfer of sensible energy and the evaporation/transport of water vapor at the surface are separable, independent processes. It is further assumed that the transfer of sensible heat may be given by the normal Equation for convective heat transfer, namely

$$dQ_{as} = h_s(T_s - T_\infty)dA_s \tag{A-9}$$

where h_s on the wet surface is assumed to be equal to the value determined for a dry surface at the same airflow conditions. This is one of the fundamental assumptions employed in the analysis.

The transfer of latent heat at the surface, using Equation A-2 may be computed as follows,

$$dQ_{av} = \lambda_s d\dot{m}_v \tag{A-10}$$

$$= \lambda_s \sigma_s (H'_s - H_\infty)dA_s \tag{A-11}$$

where λ_s is the heat of vaporization at the surface conditions. Substituting Equations A-9 and A-11 into A-8 yields

$$dQ_{cv} = h_s(T_s - T_\infty)dA_s + \lambda_s\sigma_s(H'_s - H_\infty)dA_s \tag{A-12}$$

$$= \sigma_s\left[C_a(T_s - T_\infty)\left(\frac{h_s}{C_a\sigma_s}\right) + \lambda_s(H'_s - H_\infty)\right]dA_s \tag{A-13}$$

The dimensionless parameter in Equation A-13 is a turbulent or convective Lewis number

$$Le = \frac{h_s}{C_a\sigma_s} \simeq 1 \tag{A-14}$$

For air/water vapor systems it has been shown[12] that the heat/mass transfer analogy is approximately valid and that Le may be assumed equal to one. With this fundamental assumption, the term in brackets is very nearly equal to the difference in the enthalpy of moist air evaluated between the surface and the free stream conditions

$$C_a(T_a - T_s) + \lambda_s(H'_s - H_\infty) \simeq (i'_s - i_\infty) \tag{A-15}$$

The accuracy of this approximation has been shown[4] to be quite good for most applications.

With the above approximations, Equation A-13 for wet heat transfer may be given by the following

$$dQ_{cv} \simeq \sigma_s(i'_s - i_\infty)dA_s \tag{A-16}$$

By using the assumption Le ≈ 1 we obtain an equivalent alternative Equation

$$dQ_s \simeq h_s\left(\frac{i'_s - i_\infty}{C_a}\right) dA_s \tag{A-17}$$

Equations A-16 and A-17 are completely analogous to Equation A-9. The only difference is that for a wet surface the driving potential for heat transfer is taken to be the enthalpy difference instead of the temperature difference. The "pseudo" temperature difference $(i'_s - i_\infty)/C_a$ incorporates the dual driving potentials due to temperature and humidity differences. These Equations form the "deluge" model for prediction of heat/mass transfer from a wet surface.

Again using $dA_x = \delta dz$ and $dA_z = dxdz$, Equation A-16 may be substituted for dQ_s in Equation A-7 (neglecting make-up water) to obtain a differential Equation for i_∞. The result is

$$\dot{dm}_a di_\infty = \sigma_s(i'_s - i_\infty)dA_s \tag{A-18}$$

Separation of variables then gives

$$G_a(\delta dy)di_\infty = \sigma_s(i'_s - i_\infty)(dxdy) \tag{A-19}$$

$$\frac{di_\infty}{(i'_s - i_\infty)} = \left(\frac{\sigma_s D}{G_a \delta}\right) dx \tag{A-20}$$

The alternate, equivalent expression obtained by using Le = 1 is

$$\frac{di_{\infty}}{(i_s' - i_{\infty})} = \left(\frac{h_s D}{C_a G_a \delta}\right) dX \qquad \text{(A-21)}$$

Equations A-20 and A-21 are functionally identical to Equation A-5. Thus, the nondimensional solutions to Equation A-5 for H_{∞} and Equation A-21 for i_{∞} should be identical if the mass/heat transfer analogy is valid as assumed.

EXTENSION OF THE HEAT/MASS TRANSFER ANALOGY TO PREDICTION OF WET HEAT EXCHANGER PERFORMANCE

The principal results of the analysis to this point are summarized by Equations A-5 and A-21. in principle, these Equations could be used to predict the mass and heat transfer from any element of wetted surface dA_s upon which h_s, σ_s, T_s, H_s, T_{∞} and H_{∞} may each be assumed known and spatially uniform. However, for all but the simplest heat exchangers, many of the above parameters would not be known nor would they be spatially uniform. In particular, the air/water interface conditions T_s and H_s' will normally vary significantly due to the radial temperature distribution in the fins and due also to the change in the air conditions in the direction of airflow. These surface conditions would not generally be known at any location nor could they be predicted by any practical means. Consequently, the results in Equations A-5 and A-21 are of little practical value in their present form.

To convert Equations A-5 and A-21 to a more useful form we introduce the concepts of fin efficiency and the overall heat/mass transfer coefficients. To do so requires several additional assumptions and simplifications that must be briefly discussed. The principal considerations as related to heat transfer are as follows:

- It is accepted practice in heat exchanger analysis to assume that h_s is spatially uniform, even through this is generally acknowledged to be an oversimplification in most cases. However, in keeping with this convention it will be assumed that h_s is spatially uniform and that it may be computed from correlations derived from dry performance measurements (σ_s can then be calculated by using Le = 1)

- The analysis is restricted to the case where the primary fluid temperature T_p is assumed constant (as in a condensor).

- The air is assumed to enter the core at uniform temperature $T_{\infty 1}$ humidity $H_{\infty 1}$ and velocity V_{∞}. The air velocity is assumed to be uniform in all planes normal to the airflow although variations in V_{∞} are allowed in the direction of flow.

- As a consequence of the above assumptions, the free stream conditions T_∞, H_∞ may be assumed to vary in the axial (airflow) direction only.

- The surface conditions T_s, H'_s are assumed to vary locally due to variable thermal resistance of the fins. This effect is accounted for by use of the fin efficiency concept wherein a fin root temperature T_r is defined. As a result of preceding assumptions, T_r may then be assumed to vary in the airflow direction only.

Although these assumptions are stated primarily in terms of the heat transfer parameters, they are also assumed valid when related to the analogous mass transfer phenomena. A more general analysis allowing for spatial non-uniformity in the x-y plane could be performed but the resultant complexity would preclude the possibility of obtaining closed form solutions.

Definition of Fin Efficiency for a Wet Heat/Mass Transfer Surface

The fin efficiencies for mass transfer and heat transfer can be defined in a manner analogous to the technique used to compute the efficiency of a finned surface for normal (dry) operation. Computations will be made for a representative section of a finned tube assembly as illustrated in Figure A-2.

The heat transferred through the tube wall Q_o is equal to the sum of the heat liberated from the bare (unfinned) tube surface Q_t plus the heat that enters the fin root and is ultimately disipated from the fin surface Q_f.

$$Q_o = Q_t + Q_f \tag{A-22}$$

The air/water interface on the tube is assumed to be at temperature T_r. Thus Q_t from Equation A-21 may be given by

$$Q_t = h_s A_{st}\left(\frac{i'_r - i_\infty}{C_a}\right) \tag{A-23}$$

$$Q_f = \int_{A_{sf}} h_s\left(\frac{i'_s - i_\infty}{C_a}\right) dA \tag{A-24}$$

$$= h_s A_{sf}\left[\frac{1}{A_{sf}} \int_{A_{sf}}\left(\frac{i'_s - i_\infty}{i'_r - i_\infty}\right) dA\right]\left(\frac{i'_r - i_\infty}{C_a}\right) \tag{A-25}$$

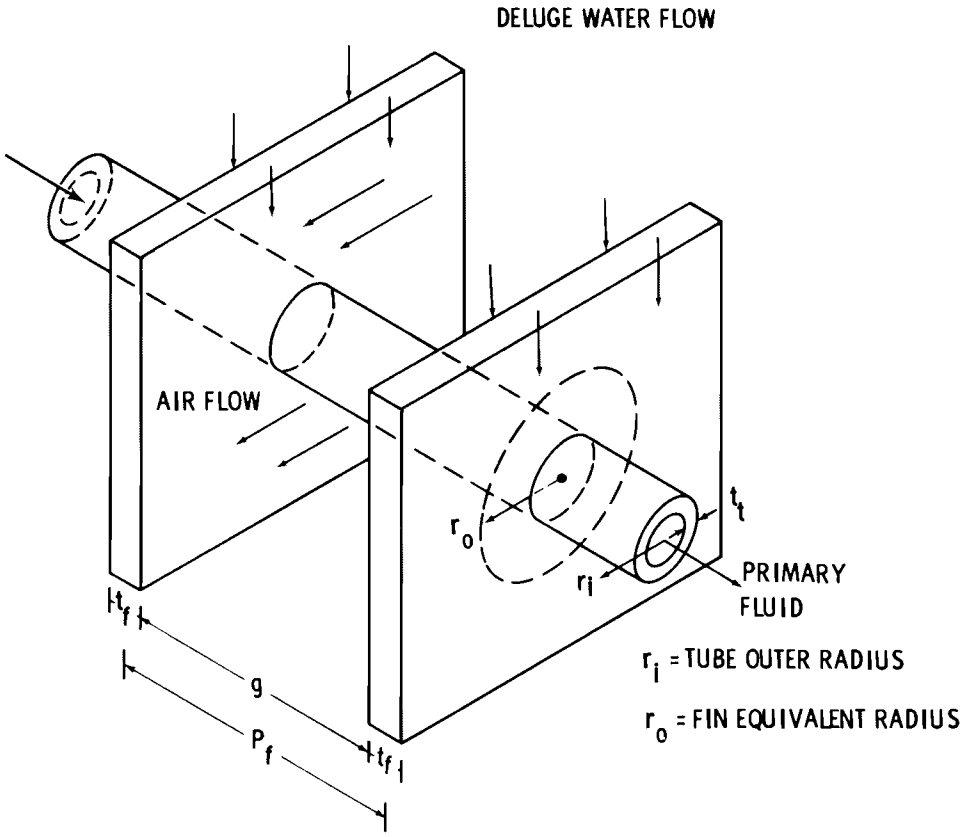

Figure A-2. Representative segment of a plate fin assembly.

$$= h_s A_{sf} \eta_f^* \left(\frac{i'_r - i_\infty}{C_a} \right) \tag{A-26}$$

Where the efficiency η_f^* is defined by

$$\eta_f^* = \frac{1}{A_{sf}} \int_{A_{sf}} \left(\frac{i'_s - i_\infty}{i'_r - i_\infty} \right) dA \tag{A-27}$$

Equation A-22 may now be given as follows

$$Q_o = h_s A_{st} \left(\frac{i'_r - i_\infty}{C_a} \right) + h_s A_{sf} \eta_f^* \left(\frac{i'_r - i_\infty}{C_a} \right) \tag{A-28}$$

$$= h_s A_s^* \left(\frac{i'_r - i_\infty}{C_a} \right) \tag{A-29}$$

Where the effective area A_s^* is given by

$$A_s^* = A_{st} + \eta_f^* A_{sf} \tag{A-30}$$

$$A_s^* = \frac{A_s^*}{A_s} \tag{A-31}$$

$$= \frac{A_{st} + \eta_f^* A_{sf}}{A_{st} + A_{sf}} \tag{A-32}$$

An analogous expression for the efficiency for mass transfer η_m^* may be derived in a similar manner. Explicit expressions for calculating η_f^* and η_m^* will be developed whereby the Equation (or graph) of η_f for dry heat transfer is transformed to a form suitable for wet mass/heat transfer by use of a simple transformation of variables. First, however, we must develop an expression for the overall heat transfer coefficient U_o^* wherein we develop the necessary transformation parameter.

Development of the Overall Heat Transfer Coefficient

The above results can now be used to compute the overall heat transfer coefficient for a segment of finned tube as illustrated in Figure A-2. to do so it is assumed that the enthalpy potential formulation for heat transfer at the surface, Equation A-17, may be extended in a form analogous to the expression used for conventional, dry heat transfer. The assumed expression is,

$$dQ = U_o^* A_s \left(\frac{i'_p - i_\infty}{C_a} \right) dX \tag{A-33}$$

where i'_p is the saturated air enthalpy at the primary or tube side temperature T_p. The next step is to determine an appropriate expression for U_o^* in terms of known parameters.

To derive an expression for U_o^* we note first that the driving potential in Equation A-33 can be separated into that across the inside thermal resistances plus that across the wetted surface.

$$\frac{dQ_{cv}}{U_o^* A_s} = \left[\left(\frac{i'_p - i'_r}{C_a} \right) + \left(\frac{i'_r - i_\infty}{C_a} \right) \right] dX \tag{A-34}$$

We then note from Equation A-29 that the surface enthalpy difference may be given by

$$\frac{dQ_{cv}}{h_s A_s^*} = \left(\frac{i_r' - i_\infty}{C_a}\right) dX \tag{A-35}$$

Since the same heat flux passes through each thermal resistance in series, dQ_{cv} may also be given in terms of the net inside thermal resistance and temperature difference as follows,

$$dQ_{cv} = \frac{(T_p - T_r)dX}{\left(\frac{1}{h_p A_p} + \frac{t}{kA_t} + \frac{1}{h_d A_s^*}\right)} = U_{pr} A_s (T_p - T_r) dX \tag{A-36}$$

Where h_d^* is the effective heat transfer coefficient in the deluge water film. This parameter contains effects due to the fin efficiency and nonuniform wetting. Means for determining h_d^* from experimental data are discussed in a subsequent analysis. The inside series resistance U_{pr} is defined by

$$U_{pr} = \left(\frac{1}{h_p a_p} + \frac{t}{k a_t} + \frac{1}{h_d^*}\right) \tag{A-37}$$

We now solve Equation A-36 for the temperature difference

$$\frac{dQ_{cv}}{U_{pr} h_s} = \left(T_p - T_r\right) dX \tag{A-38}$$

Transforming $(T_p - T_r)$ to an equivalent enthalpy difference yields

$$(T_p - T_r) = \left[\frac{C_a (T_p - T_r)}{i_p' - i_r'}\right] \left(\frac{i_p' - i_r'}{C_a}\right) \tag{A-39}$$

$$= \frac{1}{\xi} \left(\frac{(i_p' - i_r')}{C_a}\right) \tag{A-40}$$

where the transformation parameter ξ is defined by

$$\xi = \frac{(i_p' - i_r')}{C_a (T_p - T_r)} \tag{A-41}$$

From Equations A-38 and A-40 we then obtain an expression for the equivalent internal enthalpy difference as follows

$$\left(\frac{i'_p - i'_r}{C_a}\right) dX = \frac{\xi d\dot{Q}_{cv}}{U_{pr}A_s} \tag{A-42}$$

Substituting Equations A-35 and A-42 into Equation A-34 and clearing we obtain an expression for U_o^* as follows

$$\frac{dQ_{cv}}{U_o^* A_s} = \frac{d\dot{Q}_{cv}}{h_s A_s^*} + \frac{\xi d\dot{Q}_{cv}}{U_{pr}A_s} \tag{A-43}$$

$$U_o^* = \left(\frac{\xi}{U_{pr}} + \frac{1}{h_s a_s^*}\right)^{-1} \tag{A-44}$$

$$= \left[\xi\left(\frac{1}{h_p a_p} + \frac{t}{k a_t} + \frac{1}{h_d^*}\right) + \frac{1}{h_s a_s^*}\right]^{-1} \tag{A-45}$$

Equations for the local heat transfer rate and enthalpy gradient analogous to Equations A-17 and A-21 may now be written in terms of the overall heat transfer coefficient U_o^*. The results are

$$dQ_{cv} = U_o^* A_s \left(\frac{i'_p - i_\infty}{C_a}\right) dX \tag{A-46}$$

$$\frac{di_\infty}{(i'_p - i_\infty)} = \left(\frac{U_o^* A_s}{C_a \dot{m}_a}\right) dX \tag{A-47}$$

$$= N^* dX \tag{A-48}$$

where the heat exchanger NTU is defined by

$$N^* = \frac{U_o^* A_s}{\dot{m}_a C_a} \tag{A-49}$$

and the dimensionless axial coordinate is given by $X = x/D$. Equations A-46 and A-48 may now be integrated to obtain the total heat transfer and the air enthalpy profile in the heat exchanger. In addition, these results may be

extended by analogy to the equivalent results for the surface mass transfer (evaporation) rate and air humidity profile.

Extension to the Mass Transfer Analogy

The analogy between heat and mass transfer may be used to directly convert the above heat transfer Equations to analogous expressions for mass transfer. By analogy to Equation A-29, the total surface evaporation rate for an element of finned surface is assumed to be given by

$$\dot{m}_{cv} = \sigma_s(H'_r - H_\infty)(A_{st} + \eta_m^* A_{sf})dx \qquad \text{(A-50)}$$

where the fin efficiency for mass transfer is defined by analogy to Equation A-27

$$\eta_m^* = \frac{1}{A_{sf}} \int_{A_{sf}} \left(\frac{H'_s - H_\infty}{H'_r - H_\infty}\right) dA \qquad \text{(A-51)}$$

This function may be evaluated approximately using the expression for η_f (dry) and a simple transformation of variables. The evaluation of η_f^* and η_m^* is dealt with in a subsequent analysis. By using Le = 1, Equation A-50 may also be given in the following alternative form,

$$\dot{m}_{cv} = h_s A_m^* \left(\frac{H'_r - H_\infty}{C_a}\right) dx \qquad \text{(A-52)}$$

We then assume by analogy that an overall mass transfer coefficient Σ_m^* may be used with an overall driving potential $(H'_p - H_\infty)$ to compute the surface evaporation by analogy to Equation A-33

$$\dot{m}_{cv} = \Sigma_m^* A_s (H'_p - H_\infty)dx \qquad \text{(A-53)}$$

Proceeding as in the heat transfer analysis, it is assumed that $(H_p - H_\infty)$ can be separated into driving potential across the resistances to mass transfer on the inside (fictitious) and the outside. We thus obtain from Equation A-53

$$\frac{\dot{m}_{cv}}{\Sigma_m A_s} = \left[(H'_p - H'_r) + (H'_r - H_\infty)\right] dx \qquad \text{(A-54)}$$

The outside driving potential may be obtained from Equation A-52

$$\frac{\dot{dm}_{cv}}{\sigma_s A^*_m} = (H'_r - H_\infty)dX \tag{A-55}$$

Unlike the heat transfer process, there is no mass transfer across the internal resistances, there is only evaporation at the surface. However, it is the heat transfer that drives the evaporation so that the two processes are closely coupled. This is the basis of the mass/heat transfer analogy. We thus seek to derive an "effective" resistance to mass transfer such that the ratio of the available driving potential (H_p-H_r) to the resistance is equal to the surface evaporation rate. Furthermore, we seek to define this resistance in terms of the actual thermal resistance by a transformation of variables analogous to that used in the heat transfer analogy. We thus assume that $\dot{dm}_{cv}$ can be given by an expression analogous to Equation A-42,

$$\dot{dm}_{cv} = \frac{U_{pr} A_s}{\xi_m} \left(\frac{H'_p - H'_r}{C_a} \right) dX \tag{A-56}$$

An expression for determining the resistance transformation parameter ξ_m will be derived in a subsequent section.

Solving Equation A-56 for (H'_p-H'_r) and substituting this result and Equation A-55 into Equation A-54 then gives an expression for Σ^*_m. The result is

$$\frac{\dot{dm}_{cv}}{\Sigma^*_m A_s} = \frac{\dot{dm}_{cv}}{\sigma_s A^*_m} + \frac{\dot{dm}_{cv} C_a}{\xi_m U_{pr}} \tag{A-57}$$

$$\Sigma^*_m = \left(\frac{1}{\sigma_s a^*_m} + \frac{\xi_m C_a}{U_{pr}} \right)^{-1} \tag{A-58}$$

$$C_a \Sigma^*_m = \left(\frac{1}{h_s a^*_m} + \frac{\xi_m}{U_{pr}} \right)^{-1} \tag{A-59}$$

The latter result was obtained by use of the assumed identity, Le = 1. Note that the expression for $C_a\Sigma^*_m$ in Equation A-59 is exactly analogous to the result for U^*_o in Equation A-44 except for the substitution of ξ_m for ξ and A^*_m for A^*_s.

The results for the local evaporation rate and humidity profile may now be given by analogy to Equations A-46 and A-47. The results are

$$d\dot{m}_{cv} = \Sigma^*_m A_s (H'_p - H_\infty) dX \tag{A-60}$$

$$\frac{dH_\infty}{(H'_p - H_\infty)} = N^*_m dX \tag{A-61}$$

where the NTU for mass transfer is defined by

$$N^*_m = \frac{\Sigma^*_m A_s}{\dot{m}_a} \tag{A-62}$$

these expressions may now be integrated to obtain the total rate of evaporation in the heat exchanger and the profile of humidity ratio in the air.

Computation of the Performance of a Deluged Air Cooled Condensor

The dimensionless differential Equations for the airstream humidity and enthalpy are given by Equations A-61 and A-48. These will be repeated here for convenience

$$\frac{dH_\infty}{(H'_p - H_\infty)} = N^*_m dX \tag{A-61}$$

$$\frac{di_\infty}{(i'_p - i_\infty)} = N^* dX \tag{A-48}$$

Given the dependence of T_p, T_∞, H_∞, N^*_m and N^* upon x, these expressions could be integrated to obtain profiles of H_∞ and i_∞ in the heat exchanger. From these profiles and air property data the profile of T_∞ may also be established. A second integration can then be performed to obtain the total rate of evaporation and heat transfer in the heat exchanger. To perform these integrations, some additional assumptions and approximations are required.

- Both N^*_m and N^* are assumed to be constant, evaluated at suitable average conditions.
- The core temperature is assumed to be constant as in a condensor.
- All properties are assumed to be uniform in the plane normal to the direction of flow

With these assumptions, integrations of Equations A-61 and A-48 are straight forward. The results are

$$\left(\frac{H'_p - H_\infty(x)}{H'_p - H_{\infty 1}}\right) = e^{-N^*_m \chi} \tag{A-63}$$

$$\left(\frac{i'_p - i_\infty(x)}{i'_p - i_{\infty 1}}\right) = e^{-N^* \chi} \tag{A-64}$$

where properties with subscript "1" denote air inlet conditions. These results are exactly analogous to the expression for the temperature profile in a dry heat exchanger.

The total rates of heat and mass transfer in the heat exchanger can now be determined by integration of Equations A-63 and A-64. The computations are as follows

$$Q_o = \int_V U^*_o A_s (i'_{p1} - i_\infty) d\chi \tag{A-65}$$

$$= U^*_o A_s (i'_{p1} - i_{\infty 1}) \int_{\chi=0}^{1} e^{-N^* \chi} d\chi \tag{A-66}$$

Integrating and clearing yields

$$Q_o = \dot{m}_a (i'_{p1} - i_{\infty 1})(1 - e^{-N^*}) \tag{A-67}$$

An overall energy balance yields the following alternative expression for Q_o

$$Q_o = \dot{m}_a (i_{\infty 2} - i_{\infty 1}) \tag{A-68}$$

Defining a wet fin effectiveness analogous to the definition of effectiveness for a dry system yields

$$\phi^* = \frac{i_{\infty 2} - i_{\infty 1}}{i'_{p1} - i_{\infty 1}} \tag{A-69}$$

$$Q = \dot{m}_a \phi^* (i'_p - i_\infty) \tag{A-70}$$

From Equation A-67, the effectiveness can then be given by

$$\phi^* = 1 - e^{-N^*} \tag{A-71}$$

The Equations for evaporation in the core may be integrated in an analogous manner. The results are as follows,

$$\dot{m}_o = \dot{m}_a (H'_{p1} - H_{\infty 1}) \phi^*_m \tag{A-72}$$

where the effectiveness for mass transfer is given by

$$\phi^*_m = \frac{H_{\infty 2} - H_{\infty 1}}{H'_{p1} - H_{\infty 1}} \tag{A-73}$$

$$= 1 - e^{-N^*_m} \tag{A-74}$$

The above results are exactly analogous to the corresponding Equations for heat transfer in a dry heat exchanger for similar conditions. The analogous Equations for the dry heat exchanger are

$$\frac{T_p - T_\infty}{T_p - T_{\infty 1}} = e^{-NX} \tag{A-75}$$

$$Q_o = \dot{m}_a C_a \phi (T_p - T_{\infty 1}) \tag{A-76}$$

$$\phi = \frac{T_{\infty 2} - T_{\infty 1}}{T_p - T_{\infty 1}} \tag{A-77}$$

$$= 1 - e^{-N} \tag{A-78}$$

Thus, given means for calculating ξ, ξ_m and h_d, the wet performance of a heat exchanger may be completely characterized on the basis of dry performance data.

An alternative technique may be used to compute the mass/heat transfer using analogies to the log mean temperature difference. For heat transfer we may write

$$Q = U_o^* A_s \, \Delta i_{lm/Ca} \tag{A-79}$$

where the log mean enthalpy difference is defined by

$$\Delta i_{lm} = \frac{(i'_{p1} - i_{\infty 1}) - (i'_{p2} - i_{\infty 2})}{\ln \left| \frac{i'_{p1} - i_{\infty 1}}{i'_{p2} - i_{\infty 2}} \right|} \tag{A-80}$$

Similarly the deluge water evaporation rate may be given by

$$\dot{m}_o = \Sigma_m^* A_s \Delta H_{lm} \tag{A-81}$$

$$\Delta H_{lm} = \frac{(H'_{p1} - H_{\infty 1}) - (H'_{p2} - H_{\infty 2})}{\ln \left| \frac{H'_{p1} - H_{\infty 1}}{H'_{p2} - H_{\infty 2}} \right|} \tag{A-82}$$

EVALUATION OF IMPORTANT PARAMETERS

Determination of the Root Temperature, Resistance Transformation Parameter and Deluge Film Coefficient

The fin root temperature T_r and deluge film coefficient h_d (or h_d^*) must be known to completely characterize the performance of a wetted heat exchanger using the deluge model. This is in addition to the requirement that all other thermal resistances in the system must be known. The geometry and material properties of the system may be assumed to be known. The inside coefficient h_p is modeled using a standard correlation from the literature and h_s is modeled with a correlation obtained from measurements of heat transfer for the system operated dry. However, because of the complex geometry and the spatial nonuniformity of air flowrate, deluge water flowrate and surface wetting, no comparable means for modeling h_d has been identified. Thus, the only available means for determining this parameter is empirically from experimental data.

A technique for determining h_d from experimental data can be derived by requiring that the formulation for heat transfer from the primary side to the air/water interface must give the same result as the Equation for heat transfer from the surface to the air. Equation A-36 can be used to compute

the total rate of heat transfer to the surface if the temperature (T_p-T_r) is interpreted to be an "appropriate" average value. Thus we may write

$$Q_o = U_{pr}A_s(T_p - T_r) \tag{A-83}$$

$$= \left[\frac{1}{U_{pt}} + \frac{1}{h_d^*}\right]^{-1} A_s(T_p - T_r) \tag{A-84}$$

Solving for h_d^* yields

$$h_d^* = \left[\frac{A_s(T_p - T_r)}{\dot{Q}_o} - \frac{1}{U_{pt}}\right]^{-1} \tag{A-85}$$

This expression is not sufficient to compute h_d^* unless an experimental value for (T_p-T_r) can be obtained. After considerable analysis and evaluation of results, no acceptable independent means for determining T_r or h_d^* has been identified.

It was originally suspected that for wet operation, the average temperature of the deluge water that falls from the bottom of the heat exchanger might be expected to approximate the fin root temperature. If this was true, Equation A-85 could be used to compute h_d^* and Equation A-41 could be used to compute ξ with $T_r = T_d$. This approach was attempted, however, with little success. With $T_r = T_d$, the predicted values of U_o were found to be higher than the data by 20-30%. In addition, experimental uncertainty in measurement of T_d was relatively large resulting in large uncertainty in the values of h_d^*. This approach was thus abandoned and the following empirical technique for determining h_d was developed.

The overall heat transfer to the air can be given by Equation A-70. Thus, using Equation A-71 for ϕ^*, the overall heat transfer coefficient may be computed from the data as follows,

$$U_o^* = -\frac{\dot{m}_a C_a}{A_s}\left(\ln\left|1 - \frac{\dot{Q}_o}{\dot{m}_a(i'_p - i_\infty)_1}\right|\right) \tag{A-86}$$

From Equation A-45 U_o^* may also be given in terms of the series thermal resistances by Equation A-44

$$\frac{1}{U_o^*} = \frac{\xi}{U_{pt}} + \frac{\xi}{h_d^*} + \frac{1}{h_s a_s^*} \tag{A-87}$$

Solving for h_d^* then yields a second expression for h_d^*

$$h_d^* = \left[\frac{1}{\xi}\left(\frac{1}{U_o^*} - \frac{1}{h_s a_s^*}\right) - \frac{1}{U_{pt}}\right]^{-1} \tag{A-88}$$

In Equation A-88, U_o^* is the experimental value determined in Equation A-86 and h_s is the experimental value for dry heat transfer.

Equation A-85 is explicitly dependent on T_r and Equation A-88 depends on T_r through ξ and A_s^*. All other parameters in both Equations are known for a given operating condition. Thus, Equations A-85 and A-88 constitute a set of two Equations in two unknowns that can be solved simultaneously to yield unique values of h_d^* and T_r that satisfy both Equations. Because of the complex interrelationships of these parameters, the most accurate means of solution is by iteration. This was done by a series of successive approximations with T_r as the iterative variable. The results of these calculations for the present experiments are given in the text.

The above development indicates how experimental data can be used to derive empirical values of h_d and ξ. A similar iterative procedure could be used to calculate values of ξ (and therefore of U_o^*, ϕ^*, Q, etc.) for other operating conditions using the values of h_d determined from the experiments. However, using Equations A-84 and A-88 for this procedure is tedious and not readily amenable to hand calculation. Thus, an alternative, approximate procedure has been devised.

In a subsequent Section of this appendix, it is shown that the primary to root temperature difference may be given by (Equation A-128),

$$\frac{(T_p - T_r)}{(T_p - T_\infty)_1} = \left[\frac{C_a \dot{m}_a \phi^*}{U_{pr} A_s}\right]^{\Gamma} \tag{A-89}$$

Solving for T_r gives

$$T_r = T_p - (T_p - T_\infty)_1 \left[\frac{C_a \dot{m}_a \phi^*}{U_{pr} A_s}\right]^{\Gamma} \tag{A-90}$$

where for brevity a new variable α is defined by

$$\alpha = \frac{C_a \dot{m}_a \phi^*}{U_{pr} A_s} \tag{A-91}$$

To solve the expression for T_r, it is necessary to first estimate the quantity denoted α. To do so, a value of ξ is first estimated (note that this is equivalent to estimating T_r). Using this ξ value and the known (or estimated) value of h_d, the deluge model can be used to calculate ϕ^* and U_{pr}. Equation A-89 may then be solved for T_r and a new ξ value (calculated from Equation A-41). The procedure can be repeated iteratively until the starting and ending values of ξ are the same. Usually only one or two iterations are needed to obtain acceptable accuracy.

This procedure has been used to calculate the root conditions and associated ξ values for a range of operating conditions of interest in the present study. In computing T_r and ξ a constant average value of α was used for each core temperature. In addition T_r, H'_r and i'_r were rounded to values for the closest whole degree. The approximations are valid because ξ depends primarily on T_p. The other data and assumptions employed in making these and other calculations that follow are summarized in Table A-1.

The results of the calculations for ξ are presented in Figure A-3. It can be seen that ξ depends most significantly on T_p. For moderate values of T_p and ITD, ξ may be effectively assumed constant. These results for $T_p = 120^oF$ are verified by the experimental results presented in the text.

Another useful expression can be devised that defines the relationship between the root conditions and the operating conditions. The local rate of heat transfer from the primary fluid to the fin root may be given by Equation A-83

$$Q = U_{pr}(T_p - T_r)A_s \tag{A-92}$$

Similarly, the heat transfer from the surface to the air may be given by Equation A-29

$$Q = h_s\left(\frac{i'_r - i_\infty}{C_a}\right)A_s^* \tag{A-93}$$

Since the same heat flux passes through both resistances in series, the above Equations for Q must be equal. Thus we obtain

$$h_s\left(\frac{i'_r - i_\infty}{C_a}\right)A_s^* = U_{pr}(T_p - T_r)A_s \tag{A-94}$$

$$= U_{pr}\frac{1}{\xi}\left(\frac{i'_p - i'_r}{C_a}\right)A_s \tag{A-95}$$

TABLE A-1. DESIGN, OPERATION DATA AND ASSUMPTIONS USED IN EXAMPLE COMPUTATIONS WITH THE DELUGE MODEL

Description of Parameter	Symbol	Units	Assumed Fixed Value	Core Temperatures T_p(°F) 110	120	130
Surface Area	A_s	ft^2	974	--	--	--
Air Specific Heat	C_a	(Btu/lb-°F)	0.25	--	--	--
Air Flowrate	$\dot{m}_a$	(lb/hr)	13,800	--	--	--
Air Frontal Velocity	V_o	(ft/sec)	4.5	--	--	--
Deluge Water	$\dot{m}_d$	gpm	3.0	--	--	--
Surface H.X. coef.	h_s	(Btu/ft^2-hr-°F)	9.2	--	--	--
Internal H.X. coef.	U_{pt}	(Btu/ft^2-hr-°F)	86.1	--	--	--
Deluge H.X. coef.	h_d^*	(Btu/ft^2-hr-°F)	26	--	--	--
Res. Transformation	ξ			7.5	9.5	11.5
Eff. Area Ratio	a_s^*			0.60	0.65	0.70
Overall H.X. coef.	U_o^*	(Btu/ft^2-hr-°)F		1.80	1.56	1.37
NTU Parameter	N*			0.508	0.440	0.381
Effectiveness	ϕ^*			0.398	0.356	0.317
	α			0.071	0.062	0.056
	κ			0.518	0.590	0.638

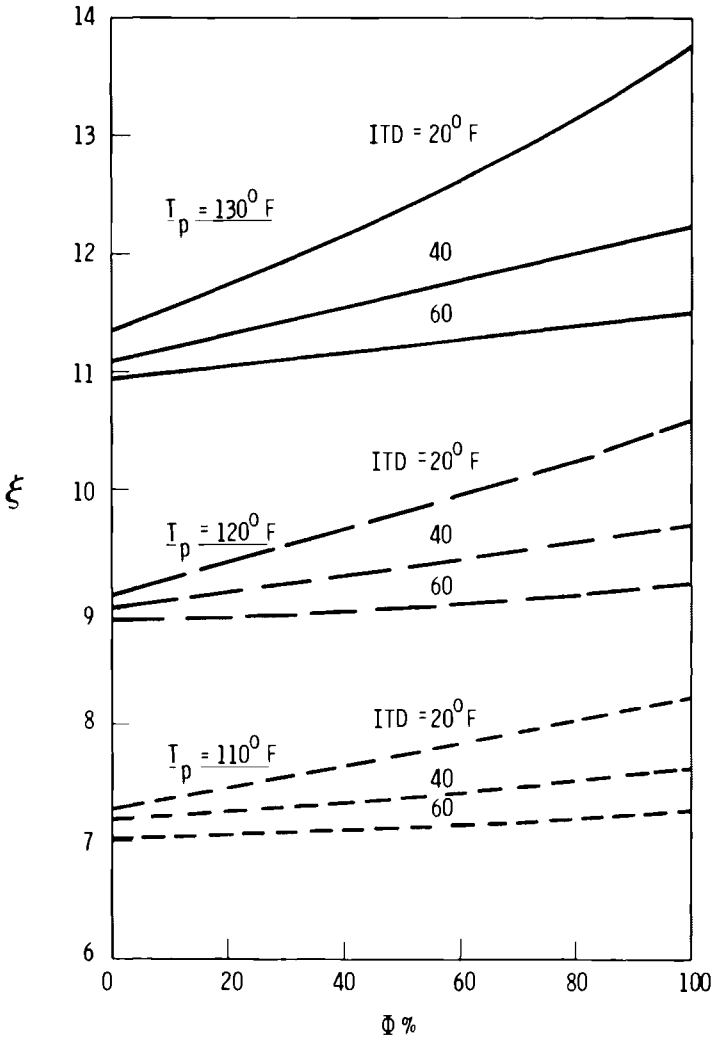

Figure A-3. Computation of ξ as a function of conditions for the trane core for data and assumptions summarized in Table A-1 . . .

Solving for i'_r then yields

$$i'_r = \frac{\left(h_s a^* i_\infty + \frac{U_{pr}}{\xi} i'_p\right)}{\left(h_s a^*_s + \frac{U_{pr}}{\xi}\right)} \qquad \text{(A-96)}$$

where $a^*_s = A^*_s / A_s$. Rearranging the above expression for i'_r then yields

$$i'_r = \left(\frac{U^*_o}{h_s a^*_s}\right) i'_p + \left(\frac{\xi U^*_o}{U_{pr}}\right) i_\infty \qquad \text{(A-97)}$$

Unfortunately, Equation A-97 cannot be solved explicitly for i'_r because of the complex inter-relationships among the parameters. This expression is useful, however, in that it illustrates the dependence of the root conditions on the fundamental heat exchanger design and operating parameters.

Development of an Expression for ξ_m

From Equation A-42, the heat transfer across the internal thermal resistances may be given by

$$dQ_{cv} = \frac{U_{pr} A_s}{\xi} \left(\frac{i'_p - i'_r}{C_a} \right) dX \qquad \text{(A-98)}$$

Then, from Equation A-56, the mass transfer is assumed to be given by

$$d\dot{m}_{cv} = \frac{U_{pr} A_s}{\xi_m} \left(\frac{H'_p - H'_r}{C_a} \right) dX \qquad \text{(A-99)}$$

Taking the ratio of these expressions gives

$$\frac{dQ_{cv}}{d\dot{m}_{cv}} = \frac{\xi_m}{\xi} \left(\frac{i'_p - i'_r}{H'_p - H'_r} \right) \qquad \text{(A-100)}$$

The ratio dQ_{cv}/dm_{cv} may also be given in terms of the effectivenesses and inlet driving potentials by

$$\frac{dQ_{cv}}{d\dot{m}_{cv}} = \frac{\dot{m}_a \phi^* (i'_p - i_\infty)_1}{\dot{m}_a \phi^*_m (H'_p - H_\infty)_1} \qquad \text{(A-101)}$$

$$= \frac{\phi^*}{\phi^*_m} \frac{(i'_p - i_\infty)_1}{(H'_p - H_\infty)_1} \qquad \text{(A-102)}$$

Equating Equations A-100 and A-101 and clearing then yields

$$\delta = \frac{\xi_m \phi^*_m}{\xi \phi^*} \qquad \text{(A-103)}$$

$$= \frac{\left(\frac{H'_p - H'_r}{i'_p - i'_r}\right)}{\left(\frac{H'_p - H_\infty}{i'_p - i_\infty}\right)_1} \qquad \text{(A-104)}$$

This is the relationship that should exist between ξ, ξ_m, ϕ^* and ϕ^*_m according to the deluge model.

Equation A-104 may be used to calculate δ using empirically determined or calculated root conditions. The root conditions derived in extracting h_d values from the data were used in this way to compute "experimental" values of δ. These results are reported in the text.

Calculated values of δ have also been determined for the same conditions and assumptions used to compute ξ (see Table A-1). These results are presented in Figure A-4, plotted as a function of (T_p, ITD, Φ_∞) similar to the plot of ξ in Figure A-3.

It is shown in section A-4 that a number of important parameters used to characterize the performance of a wetted heat exchanger (including δ) may be correlated with the driving potential ratio Γ, defined as follows

$$\Gamma = \frac{(i'_p - i_\infty)_1}{C_a(T_p - T_\infty)_1} \qquad \text{(A-105)}$$

This parameter is the ratio of the effective inlet driving potential for heat transfer $(i'_p - i_\infty)/C_a$ to the actual inlet temperature difference $(T_p - T_\infty)$. Values of Γ are plotted in Figure A-5 as a function of conditions (T_p, ITD, Φ_∞) for the range of interest in the present study.

Computed values of δ are plotted in Figure A-6 as a function of Γ for fixed values of T_p. The correlation in Figure A-6 is not exact; however, individual computed values of δ differ from the values given by the lines by less than $\pm 2\%$ for the range of conditions considered.

To determine ξ_m and ϕ^*_m from the values for δ, an iterative solution can be used, employing the experimental or calculated values of δ. This can be done by an iterative procedure using the definition of ϕ^* developed in the deluge model. This was done for the experimental results and the results are reported in the text.

For most purposes, the above iterative procedure is very cumbersome and a closed form solution would be more useful. Thus, an approximate means for solving Equation A-103 for ξ_m and ϕ^*_m has been derived. The necessary development may be summarized as follows.

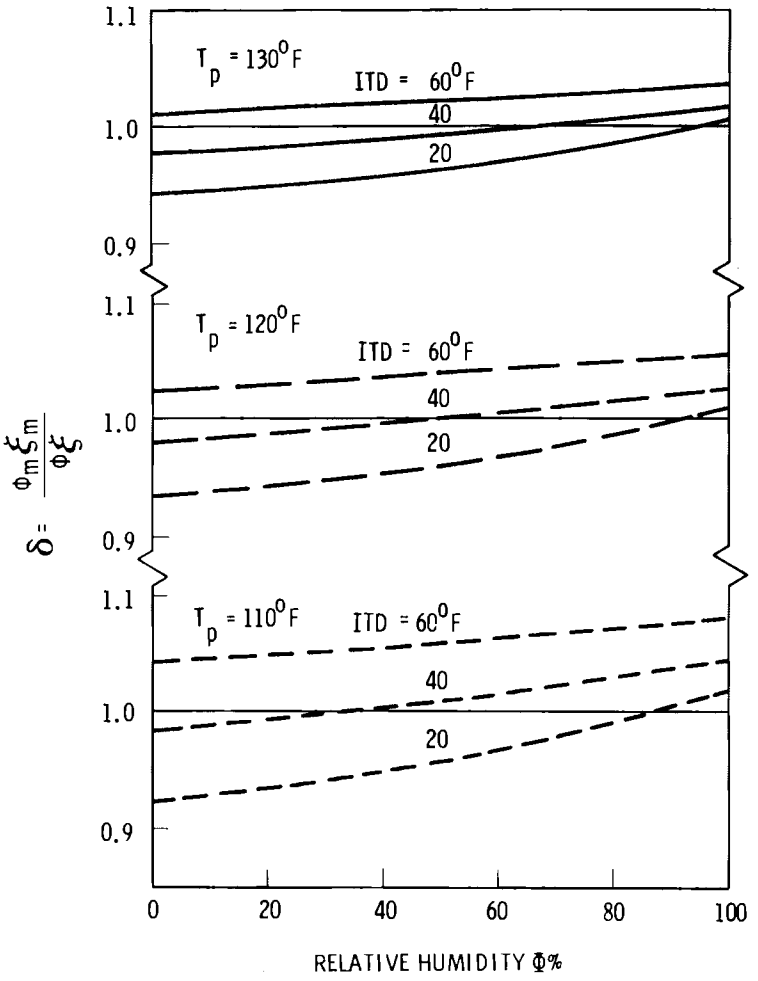

Figure A-4. Calculation of δ for representative conditions in Table A-1.

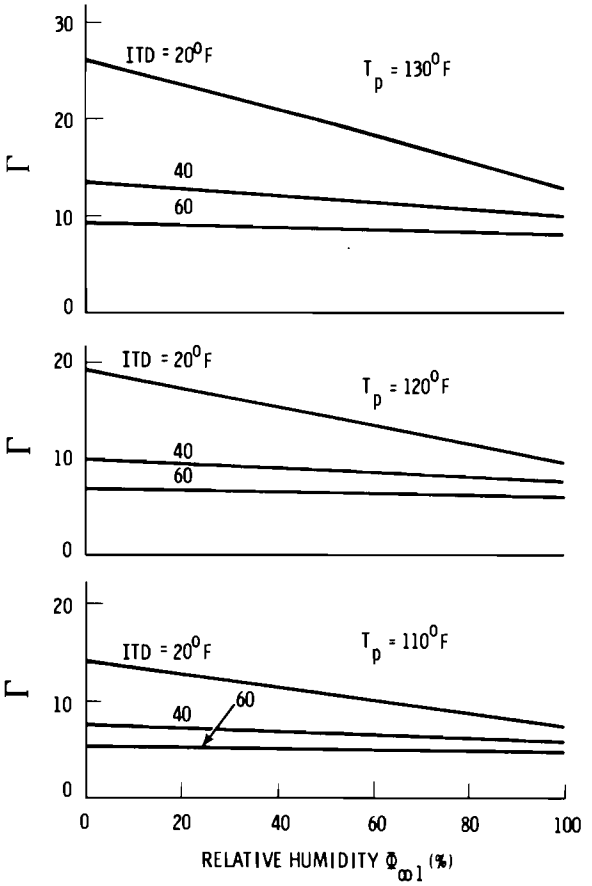

Figure A-5. Evaluation of the inlet driving potential ratio for representative conditions in Table A-1.

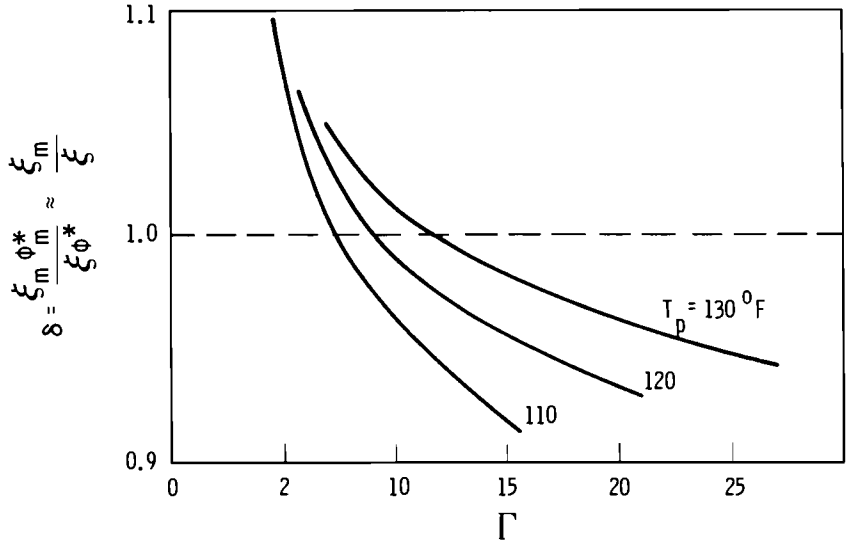

Figure A-6. Approximate prediction of δ for trane core at conditions specified in Table A-1.

For most operating conditions, it can be assumed that $\delta \approx 1$ to within about ±5%. For these conditions, the result in Equation A-103 can be solved by a series of approximation to obtain closed form approximations for ξ_m/ξ and ϕ^*_m/ϕ^* as functions of δ.

From Equations A-71 and A-74, the ratio of effectivenesses may be given by

$$\frac{\phi^*_m}{\phi^*} = \frac{1 - e^{-N^*_m}}{1 - e^{-N^*}} \tag{A-106}$$

$$= \frac{1 - e^{-N^*}\left[e^{(N^* - N^*_m)}\right]}{1 - e^{-N^*}} \tag{A-107}$$

$$\simeq \frac{1 - e^{-N^*}\left[1 + (N^* - N^*_m) - \ldots\right]}{1 - e^{-N^*}} \tag{A-108}$$

the latter result follows from a Taylor expansion assuming $|N^*-N^*_m| \ll 1$. Rearranging and using the definitions of N^*_m and N^* then yields

$$\frac{\phi^*_m}{\phi^*} \approx 1 - U^*_m\left(\frac{1}{U^*_m} - \frac{1}{U^*_o}\right)\left(\frac{N^* e^{-N^*}}{1 - e^{-N^*}}\right) \tag{A-109}$$

Equations A-59 and A-44 may be used for U^*_m and U^*_o with the additional assumptions that $a^*_m \approx a^*_s$, and $U_{pr} \approx$ constant, Equation A-109 may be written as follows:

$$\frac{\phi^*_m}{\phi^*} \approx 1 - K\left(1 - \frac{\xi}{\xi_m}\right) \tag{A-110}$$

where K is defined by

$$K = \left(\frac{\xi_m U^*_m}{U_{pr}}\right)\left(\frac{N^* e^{-N^*}}{1 - e^{-N^*}}\right) \tag{A-111}$$

Solving Equations A-103 and A-110 for ξ_m/ξ and ϕ^*_m/ϕ^* then yields

$$\left(\frac{\xi_m}{\xi} - 1\right) \approx \left(\frac{\delta - 1}{1 - K}\right) \tag{A-112}$$

$$\left(\frac{\phi^*_m}{\phi^*} - 1\right) \approx \frac{K(1 - \delta)}{(\delta - K)} \tag{A-113}$$

Equations A-112 and A-113 have been used to calculate ξ_m/ξ and ϕ_m^*/ϕ^* for the set of conditions and assumptions summarized in Table A-1. The results for ξ_m/ξ are presented in Figure A-7. Comparisons performed in the text of this report for $T_p = 120^oF$ show that these computations are in excellent agreement with the experiments.

For conditions typically employed in the present experiments, calculations give $K \approx 0.59$, $(\delta-1) \lesssim \pm 0.05$. The corresponding variations in ξ_m/ξ and ϕ_m^*/ϕ are then,

$$\left(\frac{\xi_m}{\xi} - 1\right) \lesssim \pm 0.12$$

$$\left(\frac{\phi_m^*}{\phi_m} - 1\right) \lesssim \pm 0.07$$

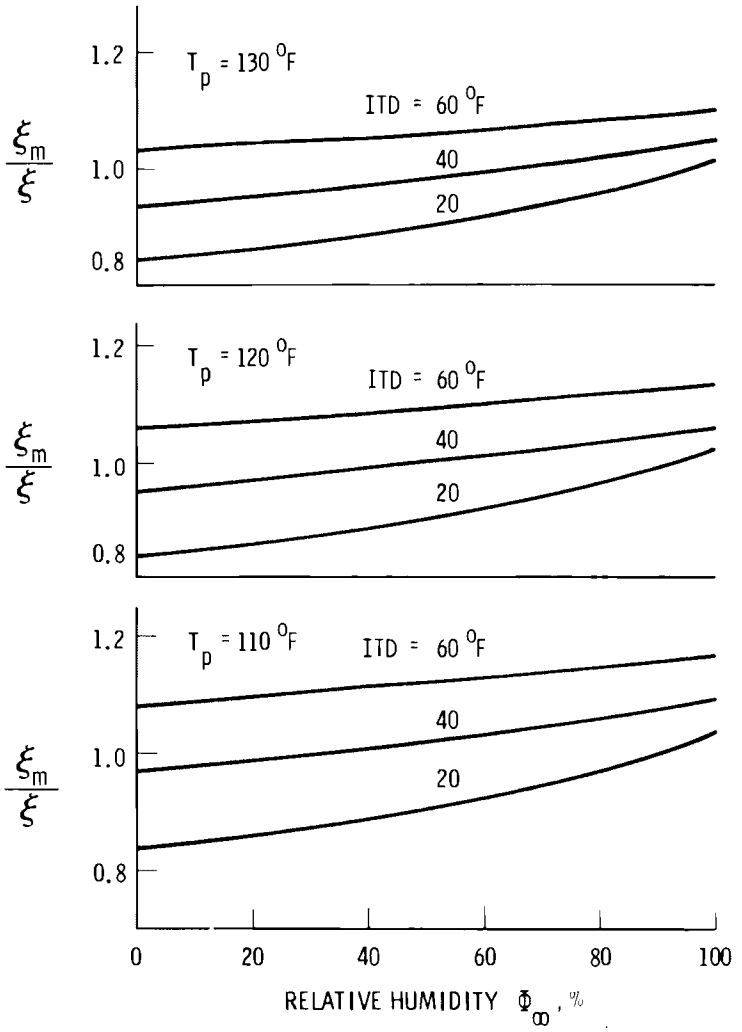

Figure A-7. Computation of ξ_m/ξ for the trane core for conditions summarized in Table A-1.

Thus, for most conditions of interest in the present study, it may be assumed that $\delta_m \approx \delta$ to within $\pm 12\%$ and $\phi_m^* \approx \phi^*$ to within $\pm 7\%$. These results are also in good agreement with the results of the experiments.

3.3 Calculation of the Fin Efficiencies for Wet Heat/Mass Transfer

Previous analysis[3] has shown that the wet surface efficiency η_f^* can be calculated from an Equation or graph of the dry surface efficiency for the given heat exchanger by use of a simple transformation of variables. For brevity, the derivation will not be repeated here. For a dry surface, η_f will assume to be given by a function of the form valid for a cylindrical fin (see Figure 2 in the main discussion of this document),

$$\eta_f = f\left(\frac{r_o}{r_i}, \sqrt{Bi_f}\right) \tag{A-114}$$

where r_o/r_i is the ratio of the fin outer radius (actual or equivalent) to the fin inner or root radius. If the fins are not cylindrical, r_o may be taken as the equivalent cylindrical fin radius that would give the same fin area as the actual configuration. The parameter Bi_f is a Biot modulus for the fin

$$Bi_f = \frac{l_f^2 h_s}{k y_b} \tag{A-115}$$

where $l_f = (r_o - r_i)$ and $y_b = t/2$

For a wet heat exchanger, the function η_f may be used to compute η_f^* by using an "effective" value of the surface heat transfer coefficient h_e^* that incorporates the net effective thermal resistance of the deluge water film and the surface. The definition of h_e^* is

$$h_e^* = \left[\frac{1}{h_d} + \frac{1}{\xi h_s}\right]^{-1} \tag{A-116}$$

where h_d is the average deluge film coefficient ($h_d^* = h_d a_s^*$) and ξ is the thermal resistance transformation parameter. η_f may now be given by

$$\eta_f^* = f\left(\frac{r_o}{r_i}, \sqrt{Bi_f^*}\right) \tag{A-117}$$

where Bi_f^* is the wet surface Biot modulus

$$Bi_f^* = \frac{l_f^2 h_e^*}{k y_b} \tag{A-118}$$

By analogy, the efficiency for mass transfer may also be computed from the dry fin efficiency by an analogous transformation of variables. The results may be summarized as follows,

$$\eta_m^* = f\left(\frac{r_o}{r_i}, \sqrt{Bi_m^*}\right) \tag{A-119}$$

where

$$h_m^* = \left[\frac{1}{h_d} + \frac{1}{\xi_m h_s}\right]^{-1} \tag{A-120}$$

$$Bi_m^* = \frac{l_f^2 h_m^*}{k y_b} \tag{A-121}$$

Expressions for the resistance transformation parameters ξ and ξ_m and the deluge film coefficient h_d have been developed in the preceding analysis. It is also shown in the preceding analysis that ξ and ξ_m are essentially equal for most conditions. In this case, the efficiencies for heat and mass transfer may be assumed equal because of the relatively weak dependence of η_f^* on ξ.

3.4 Prediction of Heat Transfer Correlations

There are a number of ways that can be used to correlate and present heat transfer data. The problem of presenting wet heat transfer data is more complicated than for dry heat transfer because several additional variables must be accounted for. After some analysis and a considerable amount of experimentation with the data, a number of means were devised for handling and presenting the data that are unique to the case of wetted heat exchangers. The theoretical basis for some of these correlations will now be provided.

One of the standard quantities used in characterizing heat exchanger performance is the heat transfer per unit ITD. This parameter may be computed using the deluge model to obtain a simple correlation in terms of the normalized driving potential for heat transfer.

From Equation A-70, the heat transfer rate may be given by

$$Q = \dot{m}_a \phi^* (i'_p - i_\infty)_1 \tag{A-122}$$

dividing by the inlet temperature difference (ITD) and clearing gives

$$\frac{Q}{(T_p - T_\infty)_1} = (\dot{m}_a \phi^* C_a)\left[\frac{(i'_p - i_\infty)_1}{C_a(T_p - T_\infty)_1}\right] \tag{A-123}$$

$$= (\dot{m}_a \phi^* C_a)\Gamma \tag{A-124}$$

where the normalized inlet driving potential for heat transfer Γ is defined by

$$\Gamma = \frac{(i'_{p1} - i_{\infty 1})}{C_a(T_{p1} - T_{\infty 1})} \tag{A-125}$$

This term incorporates the combined effects of the driving potentials for sensible and latent heat transfer. It is a purely thermodynamic variable that depends only on the inlet conditions (T_p, ITD, Φ). Values of Γ as a function of conditions for a range of variables of interest in this study are presented in Figure A-5. This variable also arose in analysis concerning the computation of δ in section A-2.

From Equation A-124 it can be seen that for constant values of the product $(\dot{m}_a \phi^* C_a)$, the heat transfer per unit of ITD should be linearly dependent upon Γ. (For a fixed air flowrate, $(\dot{m}_a \phi^* C_a)$ should be effectively constant). Furthermore, the slope of a graph of (Q/ITD) vs Γ must be equal to the product $\dot{m} C_a \phi^*$. As shown in the text, this prediction is in excellent agreement with the data.

Another similar correlation can be derived using the primary to fin root temperature difference. From Equation A-36

$$(T_p - T_r) = \frac{Q}{U_{pr} A_s} \tag{A-126}$$

dividing by $(T_p - T_{\infty 1})$, then yields

$$\frac{(T_p - T_r)}{(T_p - T_{\infty 1})} = \frac{1}{U_{pr} A_s}\left(\frac{\dot{Q}}{(T_p - T_\infty)_1}\right) \tag{A-127}$$

$$= \left(\frac{C_a \dot{m}_a \phi^*}{U_{pr} A_s}\right)\Gamma \tag{A-128}$$

where the latter result follows from Equation A-124. Thus, for fixed flow conditions (where the coefficient in Equation A-128 may be assumed constant), the given temperature ratio should be linearly dependent on Γ. In this case, the slope of the line will be equal to the coefficient of Γ in Equation A-128. As shown in the text, this prediction is also in excellent agreement with the data.

There are a number of potential comparisons between wet and dry heat transfer that could be made to assess the enhancement due to deluge. One of the most useful comparisons has been found to be the ratio of wet to dry heat transfer for the same core temperature and inlet air conditions at the same air-side pressure drop. This particular comparison was chosen because in a wetted cooling tower adjacent sections of heat exchanger will operate wet and dry with the same overall Δp. This will result in a substantially reduced air velocity in the wet portion of the tower due to increased friction caused by the deluge water. Thus, comparison on the basis of equal airflow would not be reasonable.

Prediction of Q_w/Q_d according to the above definition is quite simple. From Equation A-70 and A-76 we obtain,

$$\frac{Q_w}{Q_d} = \frac{\dot{m}_a^* \phi^* (i_p - i_\infty)_1}{\dot{m}_a \phi C_a (T_p - T_\infty)_1} \tag{A-129}$$

$$= \left(\frac{\dot{m}_a^*}{\dot{m}_a}\right)\left(\frac{\phi^*}{\phi}\right)\Gamma \tag{A-130}$$

Thus, Q_w/Q_d may also be expected to correlate with the parameter Γ.

For a given T_p, $\dot{m}_d$ and $\dot{m}_a^*$, the core Δp and effectiveness ϕ^* are determined. The corresponding dry airflow $\dot{m}_a$ is determined by Δp which then also fixes ϕ. Thus, for given wet operating conditions (T_p, $\dot{m}_d$, $\dot{m}_a^*$), Equation A-130 predicts that Q_w/Q_d should be linearly dependent upon Γ. Experimental data have been found to be in excellent agreement with this prediction.

The heat rejected by a wetted heat exchanger can be given as the sum of the heat required to evaporate the water (the latent heat) and that which raises the temperature of the moist air (the sensible heat). The ratio of the latent heat to the total heat transfer Q_v/Q_o can be a useful quantity in characterizing the performance of a wetted heat exchanger. An estimate of Q_v/Q_o can be obtained from the deluge model.

From a simple energy balance, the ratio of the latent heat to total heat transfer rates may be given by

$$\frac{Q_v}{Q_o} = \frac{\lambda_s \dot{m}_a \phi_m^* (H_p' - H_\infty)_1}{\dot{m}_a \phi^* (i_p' - i_\infty)_1} \tag{A-131}$$

$$= \left(\frac{\phi_m^*}{\phi^*}\right) \Gamma_m \tag{A-132}$$

where Γ_m is defined by

$$\Gamma_m = \frac{\lambda_s (H_p' - H_\infty)}{(i_p' - i_\infty)} \tag{A-133}$$

The parameter Γ_m is the ratio of the driving potential for mass transfer to the driving potential for heat transfer on a wet surface. This parameter is analogous to Γ and has been evaluated in a similar manner. The results are plotted in Figure A-8 as a function of (T_p,ITD, Φ_∞) in a manner similar to the results for Γ in Figure A-5. However, for the range of variables considered, Γ_m may also be plotted as a function of Γ as shown in Figure A-9. Although the correlation shown in Figure A-9 is not exact, the calculated points differ from the line by less than $\pm$1% over the range of variables considered.

For conditions where $\delta \approx 1$, so that $\phi_m^*/\phi^* \approx 1$, the results of Equation A-113 may be used in Equation A-132. The result is

$$\frac{Q_v}{Q_o} = 1 - \left(\frac{K(\delta - 1)}{(\delta - K)}\right) \Gamma_m \tag{A-134}$$

Values for Q_v/Q_o have been computed using Equation A-131 for conditions representative of the present experiments. These results are presented in Figure A-9. For fixed values of T_p, these results have also been found to correlate approximately with Γ. Comparisons of experimental and predicted values of Q_v/Q_o vs Γ are presented in the text which show excellent agreement between theory and experiment.

The only other parameter that was found to correlate will with Γ was the parameter δ (see Section 3.2 of this appendix). The transformation parameter (ξ) depends on the core and inlet conditions but not in a manner than correlates well with Γ.

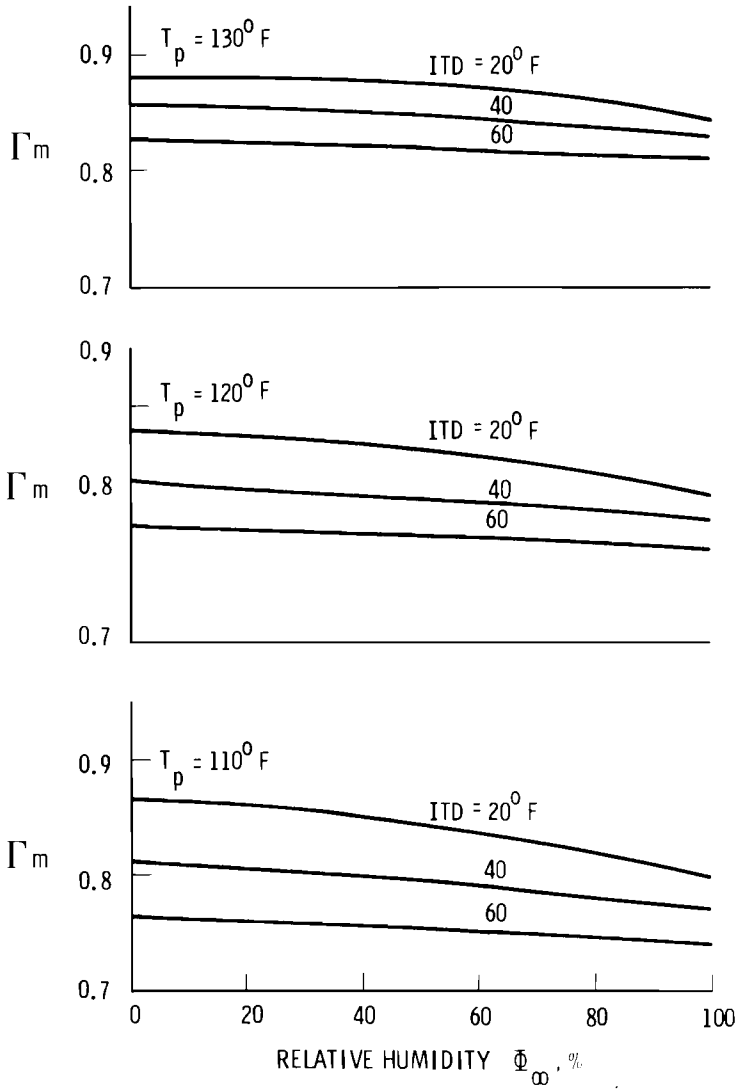

Figure A-8. Calculation of Γ_m as a function of operating conditions.

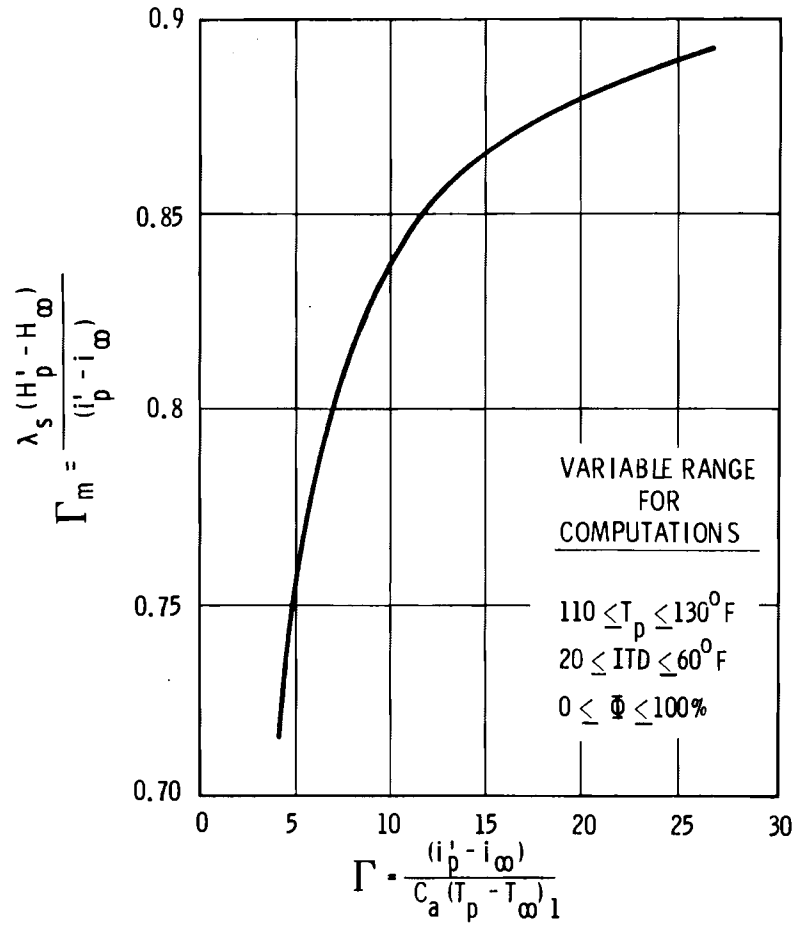

Figure A-9. Approximate correlation of Γ_m with Γ for conditions of the experiments.

APPENDIX B

SAMPLE CALCULATIONS

APPENDIX B

SAMPLE CALCULATIONS

The following calculations are an example of the reduction of the pressure drop data to friction factor, f, and effective friction factor or loss coefficient, f_o.

The equation given by Trane Company (Ref. 2) is used to calculate f.

$$f = \frac{2g_c\rho_m \Delta P A_{min}^3}{\dot{m}_{air}^2 A_s} - \frac{\sigma^2 A_{min} N'E}{A_s}$$

The second term is an estimate of expansion and contraction losses where

$$E = \frac{1.75}{\sigma_f^2} - \frac{2.75}{\sigma_f} + 1.0$$

$$\sigma_f = 1.0\text{–FPI} \times T_f$$

$\sigma = 0.5340$ ft^2 of free area/ft^2 of face area

$A_{min} = 6.4075$ ft^2

$A_s = 974.14$ ft^2

$N' = 3$ (number of coils)

FPI = 10 fins/in.

$T_f = 0.0085$ in.

$$\sigma_f = 1.0 - (10)(0.0085) = 0.9150$$

$$E = \frac{1.75}{(0.915)^2} - \frac{2.75}{0.915} + 1.0 = 0.0848$$

The second term in the equation becomes

$$\sigma^2 \frac{A_{min}}{A_s} N'E = \frac{(0.5340)^2 \times 6.4075 \times 3 \times 0.0848}{974.14}$$

$$= 4.77 \times 10^{-4}$$

To complete the calculation of f data from dry test #1 is used.

ΔP over core = 0.09 in. H_2O

T_{air} in = 85.88°F

T_{air} out = 120.86°F

ΔP over annubar = 0.25 in. H_2O

$$\dot{m}_{air} = 90326 \sqrt{\rho_{ann}} \sqrt{\Delta P_{ann}}$$

$$\rho_{ann} = 0.069 \ (lb/ft^3)$$

$$\dot{m}_{air} = 90326 \sqrt{0.069} \sqrt{0.25}$$

$$= 11{,}863 \ lb/hr$$

$$\rho_m = 0.071 \ lb/ft^3$$

Therefore,

$$f_o = \frac{(6.4075)^3}{974.14} \times 2 \times 4.173 \times 10^8 \times \frac{0.071 \times 0.09(5.198)}{(11863)^2}$$

$$= \frac{[ft^2]^3 \ [ft/hr^2] \ [lb/ft^3] \ [in.\ H_2O]}{ft^2 \ [lb/hr]^2} \left[\frac{lb/ft^2}{in.\ H_2O}\right]$$

$$= 0.0532$$

and $$f = 0.0532 - 4.77 \times 10^{-4}$$

$$= 0.0527$$

Note that the expansion and contraction losses are less than 1% of the total loss.

DRY HEAT TRANSFER CALCULATIONS

As an example of the dry heat transfer calculations, Test #1 is shown below:

$$T_{air\ in} = t_1 = 85.88^{o}F$$

$$T_{air\ out} = t_2 = 120.86^{o}F$$

$$T_{water\ in} = T_1 = 125.41^{o}F$$

$$\Delta T_{core} = \frac{14.5\ \mu V}{24\ \mu V/^{o}F} = 0.60^{o}F$$

$$T_{water\ out} = T_2 = T_{water\ in} - \Delta T_{core}$$

$$= 125.41 - 0.60$$

$$= 124.81^{o}F$$

$$LMTD = \frac{(T_1 - t_2) - (T_2 - t_1)}{\ln \frac{(T_1 - t_2)}{(T_2 - t_1)}} = 16.02^{o}F$$

The amount of heat transferred from the water to the air is calculated as follows:

$$Q_{REJ} = Q_{heater} + Q_{PERIPHERAL}$$

$$Q_{heater} = \dot{m}_h\ C_p\ \Delta T_h$$

$$\dot{m}_h = 34.5 \times 61.56 \times .1337 \times 60$$

$$[gpm]\ [lb/ft^3]\ [ft^3/gal]\ [min/hr]$$

$$= 17037\ lb/hr$$

$$Cp = 1.00\ Btu/lb_m{}^{o}F$$

$$\Delta T_h = \frac{122}{24} \frac{[\mu V]}{[\mu V/^{o}F]} = 5.08^{o}F$$

$$Q_{heater} = 17037 \times 1.00 \times 5.08$$

$$[lb/hr]\ [Btu/lb_m{}^{o}F]\ [^{o}F]$$

$$= 8654.9\ Btu/hr$$

$$Q_{PERIPHERAL} = 17{,}700\ Btu/hr\ (from\ graph)$$

$$Q_{REJ} = 86549 + 17700$$

$$= 104249\ Btu/hr$$

Overall heat transfer coefficient U is then calculated

$$U = \frac{Q_{REJ}}{A_s \times LMTD} = \frac{104249}{974.14} \times 16.02$$

$$\frac{[Btu/hr]}{[ft^2]\,[^{o}F]}$$

$$= 6.680\ \frac{Btu}{hr\text{-}ft^{2o}F}$$

The face velocity, V_o, is calculated

$$V_o = \frac{\dot{m}_a}{\rho_{air} \cdot A_f}$$

$\dot{m}_a$ = 11863 lb/hr (see previous section)

ρ_{air} = 0.0742 lb/ft^3 (@85^{o}F)

A_f = 12.0 ft^2

$$V_o = \frac{11863}{0.0742 \times 12.0 \times 3600}$$

$$\frac{[lb/hr]}{[lb/ft^3]\ [ft^2]\ [sec/hr]}$$

$$= 3.70\ fps$$

The inside heat transfer coefficient is calculated from the DiHus-Boelter equation:

$$h_p = 0.023 \frac{K_{water}}{D_H} Re_d^{0.8} Pr^{0.3}$$

$$K_{water} = \frac{0.365 \text{ Btu}}{\text{hr-ft}^{\circ}\text{F}}$$

$$D_H = \frac{(0.625 - 2 \times 0.049)}{12}$$

$$= 0.0439 \text{ ft}$$

$$Pr_{water} = 3.62 \ (@125^{\circ}\text{F})$$

$$Re_d = \frac{V \cdot D_H}{\nu}$$

$$V = \frac{\dot{V}}{A_{flow}}$$

$$\dot{V} = \frac{346 \times .1337}{60}$$

$$\frac{[\text{gpm}]\ [\text{ft}^3/\text{gal}]}{[\text{sec/min}]}$$

$$= 0.7710 \text{ ft}^3/\text{sec}$$

$$A_{flow} = 48 \times \pi \times \frac{(.625 - 2 \times .049)^2}{4 \times 144}$$

$$\frac{[\#\text{ of tubes}]\ [\text{in.}^2]}{[\text{in.}^2/\text{ft}^2]}$$

$$= 0.0727 \text{ ft}^2$$

$$\therefore \quad V = \frac{0.7710}{0.0727} \frac{[\text{ft}^3/\text{sec}]}{[\text{ft}^2]}$$

$$= 10.60 \text{ fps}$$

$$\nu = 0.605 \times 10^{-5} \text{ ft}^2/\text{sec} \ (@125^{o}\text{F})$$

$$Re_d = \frac{10.60 \times 0.0439}{0.605 \times 10^{-5}}$$

$$\frac{[\text{fps}]\ [\text{ft}]}{[\text{ft}^2/\text{sec}]}$$

$$= 76944$$

$$\therefore \ hp = \frac{0.023 \times 0.365}{0.0439} \times (76944)^{0.8} \ (3.62)^{0.3}$$

$$\frac{[\text{Btu/hr-ft}^{o}\text{F}]}{[\text{ft}]}$$

$$= \frac{2281 \text{ Btu}}{\text{hr-ft}^{2o}\text{F}}$$

The outside heat transfer coefficient which includes the fin efficiency is given by the following equation:

$$h_o = \left[\frac{1}{U} - \frac{A_s}{h_p A_i} - \frac{A_s t_t}{A_{io} k_f}\right]^{-1}$$

$$k_f = 111.7 \text{ Btu/hr-ft}^{o}\text{F}$$

$$t_f = 0.0041 \text{ ft}$$

$$A_i = 39.74 \text{ ft}^2$$

$$A_{io} = 41.44 \text{ ft}^2$$

$$\therefore \ h_o = \left[\frac{1}{6.68} - \frac{974.14}{2281 \times 39.74} - \frac{974.14 \times 0.0041}{41.44 \times 111.7}\right]^{-1}$$

$$= 7.242 \text{ Btu/hr-ft}^{2o}\text{F}$$

If we extract the fin efficiency, we obtain the air side surface heat transfer coefficient, h_s:

$$h_s = \left(\frac{A_s}{A_{st} + \eta_f A_{sf}}\right) h_o$$

$$A_{st} = 43.14 \text{ ft}^2$$

$$A_{sf} = 931.0 \text{ ft}^2$$

The fin efficiency is a function of both $r_e r_b$ and $Bi^{\frac{1}{2}}$, where

$$Bi^{\frac{1}{2}} = l_f \left(\frac{h_s}{k y_b} \right)^{\frac{1}{2}} \quad \text{[see Figure 8]}$$

$$r_b = 0.3125 \text{ in.}$$

$$k = 128 \text{ Btu/hr-ft}^{\circ}\text{F}$$

$$y_b = 0.00425 \text{ in.}$$

r_e is the outside radius, a circular fin which would have the same total surface area as the Trane surface. r_e is calculated as follows:

$$A_{sf} = 144 \times 239 \times [2\pi(r_e^2 - 0.3125^2) + 2\pi r_e \times 0.0085]$$

$$= 931.0 \text{ ft}^2 = 134064 \text{ in.}^2$$

Simplifying

$$r_e^2 + 0.0085\, r_e - 0.7176 = 0$$

solving for r_e gives

$$r_e = 0.8429 \text{ in.}$$

therefore $\frac{r_e}{r_b} = 2.697$

$$l_f = r_c - r_b = 0.5304 \text{ in.}$$

Since $Bi^{\frac{1}{2}}$ depends on h_s; $Bi^{\frac{1}{2}}$, h_s, and η_f must be determined by iteration. Assume that $\eta_f = 1.0$ or $h_s = h_o$, then:

$$Bi^{\frac{1}{2}} = \frac{0.5304}{12}\left(\frac{7.242 \times 12}{128 \times 0.00425}\right)^{\frac{1}{2}} \frac{[\text{in.}]}{[\text{in./ft}]}\left(\frac{[\text{Btu/hr-ft}^{2\text{o}}\text{F}]\,[\text{in./ft}]}{[\text{Btu/hr-ft}^{\text{o}}\text{F}]\,[\text{in.}]}\right)^{\frac{1}{2}}$$

$$= 0.5587$$

$$\eta_f = 0.85$$

After several more iterations the final answers are

$$\eta_f = 0.83$$

$$h_s = 8.65 \text{ Btu/hr-ft}^{2\text{o}}\text{F}$$

The heat transfer is also defined by a Colburn factor j_o defined as follows:

$$jo = \frac{h_s}{GCp} Pr^{2/3}$$

where $$G = \frac{\dot{m}_{air}}{A_{min}}$$

$$Pr = 0.70$$

$$Cp = 0.240 \text{ Btu/lb}_m{}^{\text{o}}\text{F}$$

$$G = \frac{11863}{6.4075} \frac{[\text{lb/hr}]}{[\text{ft}^2]}$$

$$= 1851.4 \text{ lb/hr} \cdot \text{ft}^2$$

$$j_o = \frac{8.65}{1851.4 \times 0.24}(0.7)^{2/3} \frac{[\text{Btu/hr-ft}^{2\text{o}}\text{F}]}{[\text{lb/hr-ft}^2]\,[\text{Btu/lb} \cdot {}^{\text{o}}\text{F}]}$$

$$= 0.0153$$

WET HEAT TRANSFER

A sample of all wet heat transfer calculations follows. All calculations were performed on the computer. Data from Test #5A is used in the sample calculations.

Note that each input temperature has four values which are recorded at one-minute intervals. An average of these four numbers is used for calculations.

Air Temperatures

Inlet dry bulb temperatures are averaged over six locations. Outlet d.b. temperatures are averaged over five locations. The sixth is interfered with by the deluge inlet water.

$$T_{\infty 1} = 90.44^{o}F \qquad \begin{bmatrix} 1 = \text{inlet} \\ 2 = \text{outlet} \end{bmatrix}$$

$$T_{\infty 2} = 106.33^{o}F$$

The dew point temperatures are

$$Td_{p1} = 69.30^{o}F$$

$$Td_{p2} = 94.65^{o}F$$

The calculation of air properties follows the outline given in Reference 1. The saturation pressures for the above four temperature are calculated using the Keenan-Keyes formula

$$\log_{10}\left(\frac{P_{ws}}{218.167}\right) = -\frac{\beta}{T}\left(\frac{a + b\beta + c\beta^{3}}{1 + d\beta}\right)$$

where P_{ws} = saturation pressure, atm.

β = 647.27 - T

T = absolute temp. K^{o}

a = 3.2437814

b = 5.86826×10^{-3}

c = 1.1702379×10^{-8}

d = 2.1878462×10^{-3}

The saturation pressures must be calculated for all four temperatures given above.

$$P_{ws}(T_{\infty 1}) = 0.04820 \text{ atm}$$

$$P_{ws}(T_{\infty 2}) = 0.07799 \text{ atm}$$

$$P_{ws}(Td_{p1}) = 0.02414 \text{ atm}$$

$$P_{ws}(Td_{p2}) = 0.05492 \text{ atm}$$

The barometric pressure (P) is 29.66 in. Hg.

$$= 0.99127 \text{ atm.}$$

The humidity ratios may be calculated

$$H = 0.62198 \frac{P_{ws}}{P - P_{ws}}$$

$$H(T_{\infty 1}) = 0.03179$$

$$H(T_{\infty 2}) = 0.05312$$

$$H(Td_{p1}) = 0.01552$$

$$H(Td_{p2}) = 0.03648$$

The relative humidities are calculated.

$$\phi_1 = \frac{P_{ws}(Td_{p1})}{P_{ws}(T_{\infty 1})} \times 100$$

$$\phi_2 = \frac{P_{ws}(Td_{p2})}{P_{ws}(T_{\infty 2})} \times 100$$

$$\phi_1 = 50.07\%$$

$$\phi_2 = 70.41\%$$

The specific volumes are calculated.

$$\nu = \frac{R_a T_\infty}{P} (1 + 1.6078\ H(Td_p))$$

where $R_a = 53.352\ \frac{ft\ lb_f}{lb_m\ ^oR}$

$T_\infty = T_\infty(^oF) + 459.7$

$P = P(\text{in. Hg}) \times 70.73,\ lb_f/ft^2$

$V_1 = 14.34\ ft^3/lb_m$

$V_2 = 15.24\ ft^3/lb_m$

Calculated heat capacity C_a:

$$C_a = .240 + \frac{.444}{2} (H(Td_{p1}) + H(Td_{p2}))$$

$$= .240 + \frac{.444}{2}(.01556 + .03650)$$

$$= 0.252\ Btu/lb_m\ ^oF$$

The enthalpies are calculated

$$i(x) = 0.240\ T_\infty + H(x)(1061 + 0.444\ T_\infty)$$

$\therefore$ $i(T_{\infty 1}) = 0.240(90.4458) + 0.031769(1061 + 0.444 \times 90.4458)$

$= 56.71$ Btu/lb dry air

likewise $i(T_{\infty 2}) = 84.38$

$i(Td_{p1}) = 38.80$

$i(Td_{p2}) = 65.95$

The air flow rate is calculated from the pressure drop across the annubar (ΔP_{am}).

$$\dot{m}_a = 90326 \sqrt{\Delta P_{ann}} \sqrt{1/V_2}$$

$$= 90326 \sqrt{.35} \sqrt{1/15.270}$$

$$= 13688.7 \text{ lb/hr}$$

The air frontal velocity is calculated.

$$V_o = \frac{\dot{m}_a \times V_1}{A_c \times 3600}$$

A_f = frontal area, 12 ft^2

$$V_o = \frac{13688.7 \times 14.3403}{12.0 \times 3600}$$

$$V_o = 4.544 \text{ fps}$$

Heat change in air

$$Q = \dot{m}_a(i(Td_{p2}) - i(Td_{p1}))$$

$$= 13688.7(65.945 - 38.800)$$

$$= 371579.8 \text{ Btu/hr}$$

The mass flow rates of water must be calculated at three different places: 1) deluge water inlet, 2) core water inlet, 3) heater inlet. The temperatures involved are as follows:

deluge inlet -- 100.675^oF
deluge outlet -- 105.575^oF
core inlet -- 120.1375^oF
core outlet -- 117.721^oF

The core outlet temperature is calculated by subtracting the core temperature drop from the inlet temperature. The temperature for the heater inlet is assumed to be the same as the core outlet temperature.

The masses of the water at the three different temperatures are

WW1) = 8.2783 lb/gal
WW2) = 8.2424 lb/gal
WW3) = 8.2473 lb/gal

The mass flow rates in the three different streams become

$$\dot{m}_w ① = 60 \times 8.2783 \times 3.0 = 1490.1 \text{ lb/hr}$$

$$\dot{m}_w ② = 60 \times 8.2429 \times 347.0 = 171606.8 \text{ lb/hr}$$

$$\dot{m}_w ③ = 60 \times 8.2473 \times 34.1 = 16874.0 \text{ lb/hr}$$

The heat input to the deluge water is

$$Q_d = \dot{m}① \times T(\text{del out}) - T(\text{del in})$$

$$= 1490.1 \times (105.575 - 100.675)$$

$$= 7301.49 \text{ Btu/hr}$$

The heat loss across the core is

$$Q_{loss} = \dot{m}② \times (T \text{ core in} - T \text{ core out})$$

$$= 171606.8 \ (120.1375 - 117.721)$$

$$= 414{,}716.4 \text{ Btu/hr}$$

The heat input to the heaters is

$$Q_h = \dot{m}③ C_p \Delta T_h$$

$$= 16874.0 \times 1.0 \times \frac{550}{24} \qquad \frac{[\text{lb/hr}][\text{Btu/lb}_m{}^{o}\text{F}][\mu\text{V}]}{[\mu\text{V}/{}^{o}\text{F}]}$$

$$= 386695.8 \text{ Btu/hr}$$

The actual heat transferred from the primary to the secondary side of the core is

$$Q_{heaters} + Q_{pump} - Q_{deluge} - Q_{surrounding}$$

The combination of $Q_{pump} - Q_{surrounding}$ was measured experimentally and is given by the following equation:

$$Q_{pump} - Q_{surrounding} = 25600 - 187.5 \ (T_{core} - T_{ambient})$$

For this case $T_{ambient} = 87.15^{o}F$

$T_{core} = 120.1375^{o}F$

$Q_{pump} - Q_{surrounding} = 19414.8$ Btu/hr

Therefore, the total heat transferred is

$Q_T = 386695.8 + 19414.8 - 7301.49$

$= 398809.2$ Btu/hr

The properties of saturated air are also calculated at the two primary side temperatures.

$T_{p1} = 120.1375^{o}F$ $\qquad$ $T_{p2} = 117.721^{o}F$

$P_{ws}(T_{p1}) = 0.11566$ atm

$P_{ws}(T_{p2}) = 0.10812$ atm

$H(T_{p1}) = 0.08216$

$H(T_{p2}) = 0.07615$

$i(T_{p1}) = 120.39$ Btu/lb$_m$

$i(T_{p2}) = 113.02$ Btu/lb$_m$

The overall wet heat transfer coefficient can be calculated from experimental values three different ways:

$$U_{o1}^{*} = \frac{C_a Q}{A_s} \quad \frac{\ln \frac{i(T_{p1}) - i(Td_{p1})}{i(T_{p2}) - i(Td_{p2})}}{i(T_{p1}) - i(Td_{p1}) - i(T_{p2})} + i(Td_{p2})$$

$$U_{o2}^{*} = -\frac{\dot{m}_a C_a}{A_s} \quad \ln \left| 1 - \frac{Q}{\dot{m}_a (i(T_{p1}) - i(Td_{p1}))} \right|$$

$$U_{o3}^{*} = -\frac{\dot{m}_a C_a}{A_s} \ln\left|1 - \frac{i(Td_{p2}) - i(Td_{p1})}{i(T_{p1}) - i(Td_{p1})}\right|$$

$$U_{o1}^{*} = \frac{.25154 \times 398809.2}{974.14} \frac{\ln \frac{120.385 - 38.80}{113.024 - 65.945}}{120.385 - 38.80 - 113.024 + 65.945}$$

$$= 1.641 \text{ Btu/hr-ft}^{2o}\text{F}$$

$$U_{o2}^{*} = -\frac{13688.7 \times .2515}{974.14} \ln\left|1 - \frac{398809.2}{13688.7(120.385 - 38.80)}\right|$$

$$= 1.558 \text{ Btu/hr-ft}^{2o}\text{F}$$

$$U_{o3}^{*} = -\frac{13688.7 \times .2515}{974.14} \ln\left|1 - \frac{65.945 - 38.80}{120.385 - 38.80}\right|$$

$$= 1.430 \text{ Btu/hr-ft}^{2o}\text{F}$$

The calculation of Reynolds number is as follows:

$$\text{Re} = \frac{\text{Air Mass Velocity x Hydraulic Diameter}}{\text{Viscosity}}$$

$$\text{Viscosity} = 0.0461 \text{ lb/ft} \cdot \text{hr}$$

$$\text{Air Mass Velocity} = \frac{\dot{m}_a}{A_{min}}$$

$$= \frac{13688.7}{6.41} = 2136.4 \frac{\text{lb}}{\text{hr-ft}^2}$$

Hydraulic Diameter = 0.00972 ft (given by Trane)

$$\text{Re} = \frac{0.00972 \times 2136.4}{0.0461} \frac{[\text{ft}][\text{lb/hr}]}{[\text{lb/ft} \cdot \text{hr}][\text{ft}^2]}$$

$$= 450.35$$

The primary side heat transfer coefficient is calculated using the Dittus-Boelter equation and is the same as calculated for dry heat transfer.

The amount of deluge water evaporated is:

$$\dot{m}_w = \dot{m}_a [H(Td_{p2}) - H(Td_{p1})]$$

$$= 13688.7[0.03648 - 0.01552]$$

$$= 286.86 \text{ lb/hr}$$

The overall mass transfer coefficients are:

$$\Sigma_o^{①} = \frac{\dot{m}_w}{A_s \Delta H_{lm}}$$

$$= \frac{286.86}{974.14} \frac{\ln \left| \frac{0.082158 - 0.01552}{0.076146 - 0.03648} \right|}{(0.082158 - 0.01552 - 0.076146 + 0.03648)}$$

$$= 5.664 \frac{lb_m}{hr\text{-}ft^2}$$

$$\Sigma_o^{②} = - \frac{\dot{m}_a}{A_s} N_m^*$$

$$= \frac{-13688.7}{974.14} \times \ln \left| 1 - 0.3145 \right|$$

$$= 5.306 \frac{lb_m}{hr\text{-}ft^2}$$

Additional calculations:

$$\Gamma = \frac{i(T_{p1}) - i(T_{\infty 1})}{C_a [T_{p1} - T_{\infty 1}]}$$

$$= \frac{120.385 - 38.80}{0.252 \ (120.14 - 90.44)}$$

$$= 10.90$$

Predicted Calculations

As discussed in Section 4 of the text and also in Appendix A, the following equations must be solved simultaneously to determine h_d^*, ξ, and T_r.

$$\xi = \frac{i(T_{pl}) - i(T_r)}{C_a(T_{pl} - T_r)}$$

$$h_d^* = \left(\frac{1}{\xi U_o^*} - \frac{1}{h_s a_s^* \xi} - \frac{1}{U_{pt}}\right)^{-1}$$

$$T_r = T_{pl} - \frac{Q_{rej}}{A_s}\left(\frac{1}{h_d^*} + \frac{1}{U_{pt}}\right)$$

These equations must be solved by iteration. Since $T_r \sim T_d$, the initial assumption will be that $T_r = T_d$.

$$T_r = T_d = 105.6^oF$$

Using the same procedure for calculating air properties as was already presented, the saturation pressure is found.

$$P_{ws}(T_r) = 0.07647 \text{ atm}$$

$$H(T_r) = 0.05199$$

$$i(T_r) = 82.95 \text{ Btu/lb}_m$$

$$\xi = \frac{120.39 - 82.95}{0.252(120.14 - 105.6)}$$

$$= 10.22$$

$$h_e = \left(\frac{1}{h_d} + \frac{1}{\xi h_s}\right)^{-1}$$

$$h_d = \frac{h_d^*}{a_s^*}$$

The value of a_s^* must also be determined by iteration.

Assume $a_s^* = 0.6$

$$h_d^* = \left(\frac{1}{10.22 \cdot 1.56} - \frac{1}{8.72 \cdot 10.22 \cdot 0.6} - 0.01161\right)^{-1}$$

$$= 30.85 \text{ Btu/hr-ft}^{2o}\text{F}$$

$$h_d = \frac{30.85}{0.6} = 51.42 \text{ Btu/hr-ft}^{2o}\text{F}$$

$$h_e = \left(\frac{1}{51.42} + \frac{1}{10.22 \cdot 8.72}\right)^{-1} = 32.61 \text{ Btu/hr-ft}^{2o}\text{F}$$

$$Bi^{\frac{1}{2}*} = 0.0442 \left(\frac{32.61 \cdot 12}{128 \cdot 0.00425}\right)^{\frac{1}{2}}$$

$$= 1.185$$

$$\eta_f^* = 0.602 \quad \text{(From Figure)}$$

$$a_s^* = \frac{43.14 + 0.602 \cdot 931.0}{974.14}$$

$$= 0.619$$

The next value of h_d^* may be calculated.

$$h_d^* = \left(\frac{1}{10.22 \cdot 1.56} - \frac{1}{8.72 \cdot 10.22 \cdot .619} - 0.01161\right)^{-1}$$

$$= 30.31 \text{ Btu/hr-ft}^{2o}\text{F}$$

Using this value of h_d^* a new T_r is calculated.

$$T_r = 120.14 - \frac{398809}{974.14}\left(\frac{1}{30.31} + \frac{1}{86.1}\right)$$

$$= 101.88^{o}\text{F}$$

A new value of ξ is calculated and the process is repeated until the exact values are converged upon. They are

$$T_r = 99.82^oF$$

$$\xi = 9.55$$

$$h_d^* = 26.94 \text{ Btu/hr-ft}^{2o}F$$

$$a_s^* = 0.654$$

To determine the predicted values for Σ_o^* a similar procedure is followed to determine ξ_m and a_m^*. They are

$$\xi_m = 9.09$$

$$a_m^* = 0.657$$

$$\Sigma_o^* = 6.44 \text{ lb/hr-ft}^2$$

Using the predicted values of Σ_o^* and the measured values of U_o^*, the outlet dry bulb temperature is predicted.

$$\phi^* = 1 - e^{-\frac{U_o^* A_s}{C_a \dot{m}_a}}$$

$$= 1 - e^{-\frac{1.56 \cdot 974.14}{.252 \cdot 13689}}$$

$$= 0.356$$

$$\phi_m^* = 1 - e^{-\frac{\Sigma_o^* A_s}{\dot{m}_a}}$$

$$= 1 - e^{-\frac{6.44 \cdot 974.14}{13689}}$$

$$= 0.368$$

$$i(T_{dp2}) = \phi^*[i(T_{p1}) - i(T_{dp1})] + i(T_{dp1})$$

$$= 0.356\ [120.385 - 38.80] + 38.80$$

$$= 67.84 \text{ Btu/lb}_m$$

$$H(T_{dp2}) = \phi_m * [H(T_{p1}) - H(T_{dp1})] + H(T_{dp1})$$

$$= 0.368 [0.08216 - 0.01552] + 0.01552$$

$$= 0.04004$$

$$T_{\infty 2} = \frac{i(T_{dp2}) - 1061\ H(T_{dp2})}{0.240 + 0.444\ H(T_{dp2})}$$

$$= \frac{67.84 - 1061(0.04004)}{0.240 + 0.444(0.04004)}$$

$$= 98.39^{o}F$$

The following is a calculation of Q_{wet}/Q_{dry}. Q_{wet} was already determined:

$$Q_{wet} = 398809 \text{ Btu/hr}$$

Q_{dry} is the estimated heat transferred under dry operation at the same pressure drop as under wet operation. An empirical equation was developed for the dry heat transfer coefficient with fin efficiency excluded.

$$h_s = 21.8338\ \Delta P^{0.4}$$

$$h_s = 21.8338\ (.16)^{0.4}$$

$$= 10.49 \text{ Btu/hr-ft}^{2o}F$$

The overall heat transfer coefficient can be calculated:

$$U = \left[\frac{A_s}{h_s(A_{st} + \eta_f A_{sf})} + \frac{A_s}{h_p A_i} + \frac{A_s t_t}{A_{io} k_f}\right]^{-1}$$

where $\eta_f = 0.79$

$$= \left[\frac{974.14}{10.49(43.14 + 0.79 \times 931.0)} + \frac{974.14}{2281 \times 39.74} + \frac{974.14 \times 0.0041}{41.44 \times 111.7}\right]^{-1}$$

$$= 7.63 \text{ Btu/hr-ft}^{2o}F$$

The NTU rating is:

$$NTU = \frac{UA_s}{\dot{m}_a C_a}$$

The mass flow rate is different from wet conditions and is found from the empirical equation

$$\dot{m}_a = 56611\ \Delta P_{core}^{0.6196}$$

$$= 56611\ (.16)^{0.6196}$$

$$= 18187.5\ \text{lb/hr}$$

$$\therefore \quad NTU = \frac{7.63 \times 974.14}{18187.5 \times .240} \qquad \frac{[\text{Btu/hr-ft}^2{}^{o}\text{F}][\text{ft}^2]}{[\text{lb/hr}][\text{Btu/lb}_m{}^{o}\text{F}]}$$

$$= 1.703$$

The surface effectiveness is:

$$\phi = 1 - e^{-NTU}$$

$$= 1 - e^{-1.622} = 0.818$$

The dry heat transfer is:

$$Q_{dry} = \phi \dot{m}_a C_a (T_{p1} - T_{\infty 1})$$

$$= 0.818 \times 18187.5 \times .240 \times (120.14 - 90.44)$$

$$= 106023\ \text{Btu/hr}$$

Therefore, the enhancement ratio is:

$$\frac{Q_{wet}}{Q_{dry}} = \frac{398809}{106023}$$

$$= 3.76$$

APPENDIX C

UNCERTAINTY ANALYSIS

APPENDIX C

UNCERTAINTY ANALYSIS

All of the following uncertainty calculations follow the method outlined in Section 5.

Dry Heat Transfer:

The main parameter of interest in the dry heat transfer measurements is the overall heat transfer coefficient, U_o. U_o is calculated by the following equation:

$$U_o = \frac{Q_{Rej}}{A_s \Delta T_{\ell m}}$$

From this equation the uncertainty of U_o can be written

$$\frac{\delta U_o}{U_o} = \left[\left(\frac{\delta Q_{Rej}}{Q_{Rej}}\right)^2 + \left(\frac{\delta A_s}{A_s}\right)^2 + \left(\frac{\delta(\Delta T_{\ell m})}{\Delta T_{\ell m}}\right)^2\right]^{1/2}$$

The uncertainty in A_s is estimated as:

$$\frac{\delta A_s}{A_s} = \frac{10}{974.14} = 0.010$$

The formula for Q_{Rej} is (See section 3):

$$Q_{Rej} = Q_{in} + Q_{Peripheral} + \Delta Q$$

where ΔQ is included to account for the variation from equilibrium conditions. The uncertainty in Q_{Rej} becomes:

$$\delta Q_{Rej} = (\delta Q_{in}^2 + \delta Q_{Peripheral}^2 + \delta \Delta Q^2)^{1/2}$$

$$Q_{in} = \dot{m}_h C_p \Delta T_h$$

$$\frac{\delta Q_{in}}{Q_{in}} = \left[\left(\frac{\delta \dot{m}_h}{\dot{m}_h}\right)^2 + \left(\frac{\delta C_p}{C_p}\right)^2 + \left(\frac{\delta \Delta T_h}{\Delta T_h}\right)^2\right]^{1/2}$$

All the calculations done for dry heat transfer will use Test #1 (see Appendix B).

$$\dot{m}_h = 34.5 \times 61.56 \times .1337 \times 60 = 17037 \text{ lbm/hr}$$

[gpm] [lb/ft^3] [ft^3/gal] [min/hr]

$$\frac{\delta \dot{m}_h}{\dot{m}_h} = \left[\left(\frac{0.5}{34.5}\right)^2 + \left(\frac{0.5}{61.56}\right)^2\right]^{1/2}$$

$$= 0.017$$

$$\frac{\delta C_p}{C_p} = \frac{0.01}{1.00} = 0.010$$

$$\frac{\delta \Delta T_h}{\Delta T_h} = \frac{0.5}{5.08} = 0.098$$

Therefore:

$$\frac{\delta Q_{in}}{Q_{in}} = \left[(.017)^2 + (.01)^2 + (.098)^2\right]^{1/2}$$

$$= 0.100$$

Since Q_{in} = 86549 Btu/hr

$$\delta Q_{in} = 8655 \text{ Btu/hr}$$

$\delta Q_{Peripheral}$ is estimated at 500 Btu/hr.

$\delta \Delta Q$ is an estimate of the observed variation from equilibrium in the system. Typically the temperature of the water in the main loop varied less than 0.5°F in 30 minutes. Therefore:

$$\delta \Delta Q = \frac{0.5}{1/2} \times 4670 \times 1.0$$

[°F/hr] [lb] [Btu/lb °F]

$$= 4670 \text{ Btu/hr}$$

The total uncertainty in Q_{rej} becomes:

$$\delta Q_{Rej} = (8655^2 + 500^2 + 4670^2)^{1/2}$$

$$= 9847 \text{ Btu/hr}$$

and $$\frac{\delta Q_{Rej}}{Q_{Rej}} = \frac{9847}{104249} = 0.094$$

The equation for $\Delta T_{\ell m}$ is:

$$\Delta T_{\ell m} = \frac{(T_1-t_1) - (T_2-t_2)}{\ell n \left(\frac{T_1-t_1}{T_2-t_2}\right)}$$

Assign:

$$u = (T_1-t_1) - (T_2-t_2) = \Delta T_1 - \Delta T_2$$

$$v = \ell n \frac{(T_1-t_1)}{(T_2-t_2)} = \ell n \frac{\Delta T_1}{\Delta T_2}$$

$$\delta \Delta T_{\ell m} = \left[\left(\frac{\partial \Delta T_{\ell m}}{\partial \Delta T_1}\right)^2 \delta \Delta T_1^{\,2} + \left(\frac{\partial \Delta T_{\ell m}}{\partial \Delta T_2}\right)^2 \delta \Delta T_2^{\,2}\right]^{1/2}$$

$$\frac{\partial \Delta T_{\ell m}}{\partial \Delta T_1} = \frac{v \frac{\partial u}{\partial \Delta T_1} - u \frac{\partial v}{\partial \Delta T_1}}{v^2}$$

$$\frac{\partial u}{\partial \Delta T_1} = 1 \qquad \frac{\partial u}{\partial \Delta T_2} = -1$$

$$\frac{\partial v}{\partial \Delta T_1} = \frac{1}{\Delta T_1} \qquad \frac{\partial v}{\partial \Delta T_2} = \frac{-1}{\Delta T_2}$$

Therefore;

$$\frac{\partial \Delta T_{\ell m}}{\partial \Delta T_1} = \frac{\ell n \frac{\Delta T_1}{\Delta T_2} - \frac{(\Delta T_1 - \Delta T_2)}{\Delta T_1}}{\ell n \left(\frac{\Delta T_1}{\Delta T_2}\right)^2} = \frac{1 - \frac{\Delta T_{\ell m}}{\Delta T_1}}{\ln \frac{\Delta T_1}{\Delta T_2}}$$

Likewise:

$$\frac{\partial \Delta T_{\ell m}}{\partial \Delta T_2} = \frac{\frac{\Delta T_{\ell m}}{\Delta T_2} - 1}{\Delta \ln \frac{\Delta T_1}{\Delta T_2}}$$

Finally

$$\frac{\delta \Delta T_{\ell m}}{\Delta T_{\ell m}} = \left[\left(\frac{1-\Delta T_{\ell m}/\Delta T_1}{\Delta T_1 - \Delta T_2} \right)^2 \delta \Delta T_1^{\ 2} + \left(\frac{\Delta T_{\ell m}/\Delta T_2 - 1}{\Delta T_1 - \Delta T_2} \right)^2 \delta \Delta T_2^{\ 2} \right]^{1/2}$$

For test #1

$T_1 = 125.41\ ^\circ F$ $\qquad$ $\Delta T_1 = 4.55$

$t_1 = 120.86\ ^\circ F$ $\qquad$ $\Delta T_2 = 38.93$

$T_2 - 124.81\ ^\circ F$ $\qquad$ $\Delta T_{\ell m} = 16.02\ ^\circ F$

$t_2 = 85.88\ ^\circ F$

$$\frac{\delta \Delta T_{\ell m}}{\Delta T_{\ell m}} = \left[\left(\frac{1-(16.02/4.55)}{4.55-38.93} \right)^2 \delta \Delta T_1^2 + \left(\frac{(16.02/38.93-1)}{4.55-38.93} \right) \delta \Delta T_2^{\ 2} \right]^{1/2}$$

$$= \left[0.00538\ \delta \Delta T_1^2 + 0.00029\ \delta \Delta T_2^{\ 2} \right]^{1/2}$$

Estimate $\delta \Delta T_1 = 1.0\ ^\circ F$

$\delta \Delta T_2 = 1.0\ ^\circ F$

$$\frac{\delta \Delta T_{\ell m}}{\Delta T_{\ell m}} = \left[0.00538\ (1.0)^2 + 0.00029\ (1.0)^2 \right]^{1/2}$$

$$= 0.075$$

The uncertainty in U_o can now be calculated:

$$\frac{U_o}{U_o} = \left[(0.094)^2 + (0.010)^2 + (0.075)^2 \right]^{1/2}$$

$$= 0.12$$

Wet heat transfer:

Two major parameters are of interest in wet heat transfer namely h_d* and U_o*. Uncertainty analysis will be done for U_{o2}* since it was used to demonstrate the variations in U_o* in Section 6.

$$U_{o2}^* = \frac{\dot{m}_a\ C_a}{A_s}\ \ln\left|1 - \frac{Q_{rej}}{\dot{m}_a\left|i_{\infty 1} - i'_{p1}\right|}\right|$$

Define $\quad X = \dfrac{\dot{m}_a\ C_a}{A_s} \qquad y = \dfrac{Q_{rej}}{\dot{m}_a\left|i_{\infty 1} - i'_{p1}\right|}$

$$U_{o2}^* = X \ln\left|1-y\right|$$

$$\delta U_{o2}^* = \left[\left(\frac{\partial U_{o2}^*}{\partial x}\right)^2 \partial x^2 + \left(\frac{\partial U_{o2}^*}{\partial y}\right)^2 \delta y^2\right]^{1/2}$$

$$\frac{\partial U_{o2}}{\partial x} = \ln\left|1-y\right| \qquad \frac{\partial U_{o2}}{\partial y} = -\frac{x}{1-y}$$

$$\delta U_{o2}^* = \left[(\ln|1-y|)^2\ \delta x^2 + \left(\frac{x}{1-y}\right)^2 \delta y^2\right]^{1/2}$$

$$\frac{\delta U_{o2}^*}{U_{o2}^*} = \left[\left(\frac{\delta x}{X}\right)^2 + \left(\frac{\delta y}{(1-y)\ln|1-y|}\right)^2\right]^{1/2}$$

$$\frac{\delta x}{X} = \left[\left(\frac{\delta \dot{m}_a}{\dot{m}_a}\right)^2 + \left(\frac{\delta C_a}{C_a}\right)^2 + \left(\frac{\delta A_s}{A_s}\right)^2\right]^{1/2}$$

All calculations are done for test #5-A.

$$\frac{\delta A_s}{A_s} = 0.010$$

$$\frac{\delta C_a}{C_a} = \frac{0.005}{0.252} = 0.020$$

$$\frac{\delta \dot{m}_a}{\dot{m}a} = 0.10$$

The value of $\delta\dot{m}_a/\dot{m}_a$ will vary with the magnitude of the manometer reading. All things considered, 0.10 seemed to be a reasonable value.

$$\frac{\delta x}{X} = [(0.05)^2 + (0.02)^2 + (0.10)^2]^{1/2}$$

$$= 0.11$$

$$\frac{\delta y}{y} = \left[\left(\frac{\delta Q_{rej}}{Q_{rej}}\right)^2 + \left(\frac{\delta\dot{m}_a}{\dot{m}_a}\right)^2 + \left(\frac{\delta(i_{\infty 1} - i'_{p1})}{(i_{\infty 1} - i'_{p1})}\right)^2\right]^{1/2}$$

From previous calculations

$$\frac{\delta Q_{rej}}{Q_{rej}} = 0.094$$

$$\frac{\delta\dot{m}_a}{\dot{m}_a} = 0.10$$

$$\delta(i_{\infty 1}-i'_{p1}) = [\delta_{i\infty 1}{}^2 + \delta i_{pi}{}^2]^{1/2}$$

$$\delta i_{\infty 1} = \delta i'_{p1} = 2.0 \text{ [from Psychometric chart]}$$

$$\delta(i_{\infty 1}-i'_{p1}) = 2.83$$

From Appendix C

$$i_{\infty 1} = 38.80 \text{ Btu/lb}$$

$$i'_{p1} = 120.39 \text{ Btu/lb}$$

Therefore:

$$\frac{\delta y}{y} = \left[(0.094)^2 + (0.10)^2 + \left(\frac{2.83}{120.39-38.80}\right)^2\right]^{1/2}$$

$$= 0.14$$

$$y = \frac{Q_{rej}}{m_a(i_{\infty 1}-i_{pi})} = \frac{398809}{13688.7(120.39-38.80)}$$

$$= 0.3571$$

$$\delta y = 0.051$$

Finally:

$$\frac{\delta U^*_{o2}}{U^*_{o2}} = \left[(0.11)^2 + \left(\frac{0.051}{(1-0.3571)\ \ln\ (1-0.3571)} \right)^2 \right]^{1/2}$$

$$\frac{\delta U^*_{o2}}{U^*_{o2}} = 0.21$$

The uncertainty in the deluge coefficient h_d^* can be calculated as follows:

$$h_d^* = \left[\frac{1}{\xi U_o^*} - \frac{1}{\xi h_s a_s^*} - \frac{1}{U_{pt}} \right]^{-1}$$

$$= \left[x - y - z \right]^{-1}$$

$$\delta h_d^* = \left[\left(\frac{\partial h_d^*}{\partial x} \right)^2 \delta x^2 + \left(\frac{\partial h_d^*}{\partial y} \right)^2 \delta y^2 + \left(\frac{\partial h_d^*}{\partial z} \right)^2 \delta z^2 \right]^{1/2}$$

$$\frac{\partial h_d^*}{\partial x} = \frac{-\partial h_d^*}{\partial y} = \frac{-\partial h_d^*}{\partial z} = \frac{-1}{(x - y - z)^2}$$

$$\frac{\delta h_d^*}{h_d^*} = \left[\frac{\delta x^2 + \delta y^2 + \delta z^2}{(x - y - z)^2} \right]^{1/2}$$

$$\delta x^2 = \frac{1}{\xi^2 U_o^{*2}} \left(\frac{\delta \xi^2}{\xi^2} + \frac{\delta U_o^{*2}}{U_o^{*2}} \right)$$

$$\xi = \frac{i_{pl}' - i_r'}{C_a (T_{pl} - T_r)}$$

$$\delta \xi^2 = \xi^2 \left(\frac{\delta i_{pl}'^2 + \delta i_r'^2}{(i_{pl}' - i_r')^2} + \frac{\delta C_a^{\ 2}}{C_a^{\ 2}} + \frac{\delta T_p^{\ 2} + \delta T_r^{\ 2}}{(T_p - T_r)^2} \right)$$

From Test #5-A:

$i_{pl}' = 120.4$ Btu/lb$_m$ $\qquad \delta i_{pl}' = 2.0$

$i_r' = 71.5$ Btu/lb$_m$ $\qquad \delta i_r' = 2.0$

$C_a = 0.252$ Btu/lb$_m$ ^oF $\qquad \delta C_a = 0.005$

$T_{pl} = 120.1^oF$ $\qquad \delta T_{pl} = 1.0$

$T_r = 99.8^oF$ $\qquad \delta T_r = 3.0$

$\xi = 9.55$

$$\delta\xi^2 = 9.55^2\left(\frac{2.0^2 + 2.0^2}{(120.4 - 71.5)^2} + \frac{0.005}{.252}^2 + \frac{1.0^2 + 3.0^2}{(120.1 - 99.8)^2}\right)$$

$$= 2.55$$

From previous calculations:

$$\frac{\delta U_o^*}{U_o^*} = 0.21 \qquad U_o^* = 1.56$$

$$\therefore \quad \delta x^2 = \frac{1}{(9.55)^2(1.56)^2}\left(\frac{2.55}{(9.55)^2} + (0.21)^2\right)$$

$$= 3.25 \times 10^{-4}$$

$$\delta y^2 = \frac{1}{\xi^2 h_s^2 a_s^{*2}}\left(\frac{\delta\xi^2}{\xi^2} + \frac{\delta h_s^2}{h_s} + \frac{\delta a_s^{*2}}{a_s^*}\right)$$

Assume: $\dfrac{\delta h_s}{h_s} = 0.10$

$$\frac{\delta a_s^*}{a_s^*} = 0.10$$

From previous calculations:

$h_s = 8.72$ Btu/hr-ft^{2o}F $\qquad a_s^* = 0.654$

$$\delta y^2 = \frac{1}{(9.55)^2(8.72)^2(.654)^2}\left((0.17)^2 + (0.10)^2 + (0.10)^2\right)$$

$$= 1.65 \times 10^{-5}$$

$$\delta z^2 = \frac{\delta U_{pt}^{\ 2}}{U_{pt}^{\ 4}}$$

From previous calculations:

$$\frac{\delta U_{pt}}{U_{pt}} = 0.10 \qquad U_{pt} = 86.1 \text{ Btu/hr-ft}^{2o}\text{F}$$

$$\delta z^2 = \frac{(0.10)^2}{(86.1)^2} = 1.35 \times 10^{-6}$$

$$x = \frac{1}{\xi U_o^*} = \frac{1}{(9.55)(1.56)} = 0.0671$$

$$y = \frac{1}{\xi h_s a_s^*} = \frac{1}{(9.55)(8.72)(.654)} = 0.0184$$

$$z = \frac{1}{U_{pt}} = \frac{1}{86.1} = 0.0116$$

Finally:

$$\frac{\delta h_d^*}{h_d^*} = \left[\frac{3.25 \times 10^{-4} + 1.65 \times 10^{-5} + 1.35 \times 10^{-6}}{(0.0671 - 0.0184 - 0.0116)^2}\right]^{1/2}$$

$$= 0.50$$

APPENDIX D

LISTING OF DATA ANALYSIS PROGRAM

APPENDIX D

LISTING OF DATA ANALYSIS PROGRAM

```
      DIMENSION DATE(3),TIME(3),CORE(3),IRUN(3)
      DIMENSION ARAYA(4)
      DIMENSION ARRAY(4,2)
      DIMENSION ARRAY1(4,6)
      DIMENSION ARRAY2(4,6)
      DIMENSION ARRAY3(4)
      DIMENSION ARRAY4(4)
      DIMENSION ARRAY6(4,2)
      DIMENSION ARRAY8(4)
      DIMENSION ARRAY9(4)
      DIMENSION ARAY10(4,2)
      DIMENSION ARAY11(4)
C
C     READ IN NUMBER OF TEST CASES
C
      ICONT2 = 0
      READ(5,50) ICOUNT
50    FORMAT(I10)
25    CONTINUE
      ICONT2 = ICONT2 + 1
C
C     READ    -     DATE,TIME,CORE,RUN
C
      READ(5,100) DATE,TIME,CORE,IRUN
100   FORMAT(4(2A4,A2))
C
C     READ    -     AIR FLOW RATE AND BAROMETRIC PRESSURE
C
      READ(5,200) ANDLP,P
200   FORMAT(2E10.0)
C
C
C     READ DELTA T'S   (HEATER AND CORE)   AND DELTA P
C
      READ(5,20) DTMVH,DTMVC,DELTA
20    FORMAT(3E10.0)
C
C     READ WATER FLOW RATES ,MAIN, HAEATER, AND DEKUGE
C
      READ(5,30)WMLG,WHLG,WDLG
30    FORMAT(3E10.0)
C
C     READ MEASURED HUMIDITIES
C
      READ(5,40) TMEA1,TMEA2
40    FORMAT(2F10.0)
C
C     READ AIR TEMPERATURES - INSIDE AMBIENT
C
      READ(5,300)  (ARAYA(I),I=1,4)
C
C     READ AIR TEMPERATURES - AMBIENT AND ANNULAR
C
      READ(5,300)((ARRAY(I,J),I=1,4),J=1,2)
300   FORMAT(4E10.0)
C
C     READ AIR TEMPERATURES - CORE INLET
C
      READ(5,400)((ARRAY1(I,J),I=1,4),J=1,6)
400   FORMAT(4E10.0)
```

```
C
C     READ AIR TEMPERATURES - CORE OUTLET
C
      READ(5,500)((ARRAY2(I,J),I=1,4),J=1,6)
500   FORMAT(4E10.0)
C
C     READ DEW POINT TEMPERATURES - CORE INLET AND CORE OUTLET
C
      READ(5,600)(ARRAY3(I),I=1,4)
600   FORMAT(4E10.0)
      READ(5,600) (ARRAY4(I),I=1,4)
C
C     CALCULATE AVERAGE OF AIR TEMPERATURE - INSIDE AMBIENT
      TAIR=0.
      DO 700 I = 1,4
      TAIR = ARAYA(I) + TAIR
700   CONTINUE
      TAIR = TAIR/4.
C
C     CALCULATE AVERAGE OF AIR TEMPERATURE - CORE INLET
C
      T1 = 0.
      DO 2000 J=1,6
      DO 2000 I=1,4
      T1=ARRAY1(I,J)+T1
2000  CONTINUE
      T1=T1/24.
      TAI = T1
C
C     CALCULATE AVERAGE OF AIR TEMPERATURE - CORE OUTLET
C
      T2 = 0.
      DO 2100 J = 2,6
      DO 2100 I=1,4
      T2=ARRAY2(I,J)+T2
2100  CONTINUE
      T2 = T2/20.
C
C     CALCULATE AVERAGE OF DEW POINT TEMPERATURE - CORE INLET
C
      T3 = 0.
      DO 2200 I=1,4
      T3 = ARRAY3(I)+T3
2200  CONTINUE
      T3 = T3/4.
C
C     CALCULATE AVERAGE OF DEW POINT TEMPERATURE - CORE OUTLET
C
      T4 = 0.
      DO 2300 I=1,4
      PB = P
      T4 = ARRAY4(I)+T4
2300  CONTINUE
      T4 = T4/4.
C
```

```
C
C       CALCULATE PARTIAL PRESSURE
C
        A = 3.2437814
        B = 5.86826*10.E-4
        C=1.1702379*10.E-9
        D=2.1878462*10.E-4
        T = (T3-32)/1.8+273.17
        BETA = 647.27-T
        PW = -(BETA/T*((A+B*BETA+C*BETA**3)/(1.0+D*BETA)))
        PW1=10**PW*218.167
C
C       SECOND PARTIAL PRESSURE
C
        A = 3.2437814
        B = 5.86826*10.E-4
        C=1.1702379*10.E-9
        D=2.1878462*10.E-4
        T = (T4-32)/1.8+273.17
        BETA = 647.27-T
        PW = -(BETA/T*((A+B*BETA+C*BETA**3)/(1.0+D*BETA)))
        PW2 = 10**PW*218.167
C
C       THIRD PARTIAL PRESSURE
C
        A = 3.2437814
        B = 5.86826*10.E-4
        C=1.1702379*10.E-9
        D=2.1878462*10.E-4
        T = (T1-32.)/1.8+273.17
        BETA=647.27-T
        PW = -(BETA/T*((A+B*BETA+C*BETA**3)/(1.0+D*BETA)))
        PWS1 = 10**PW*218.167
C
C       FOURTH PARTIAL PRESSURE
C
        A = 3.2437814
        B = 5.86826*10.E-4
        C=1.1702379*10.E-9
        D=2.1878462*10.E-4
        T = (T2-32.)/1.8+273.17
        BETA = 647.27-T
        PW = -(BETA/T*((A+B*BETA+C*BETA**3)/(1.0+D*BETA)))
        PWS2 = 10**PW*218.167
C
C       CALCULATE HUMIDITY RATIOS
C
        P = P * .033421
        W1 = 0.62198 * PW1/(P-PW1)
        W2 = 0.62198 * PW2/(P-PW2)
        WS1=0.62198*PWS1/(P-PWS1 )
        WS2=0.62198*PWS2/(P-PWS2)
C
C       CALCULATE RELATIVE HUMIDITY
C
        PHI1 = (PW1/PWS1) * 100.
        PHI2 = (PW2/PWS2) * 100.
```

```
C
C     CONVERT TO ABSOLUTE TEMPERATURE  INLET AND OUTLET DRY BULBS
C
      TVA1 = T1+459.7
      TVA2 = T2+459.7
C
      P1 = P*2116.22
C     CALCULATE SPECIFIC VOLUMES
C
      VA1 = 53.352 * TVA1*(1.0+1.6078*W1)/P1
      VA2 = 53.352*TVA2*(1.0+1.6078*W2)/P1
C
C     CALCULATE MOIST HEAT CAPACITY
C
      W10 = (W1+W2)/2.
      CA = 0.240+0.444*W10
      CA1=0.240 + 0.444*W1
C
C     CALCULATE ENTHALPYS
C
      H1 = 0.240*T1+W1*(1061.+0.444*T1)
      H2 = 0.240*T2+W2*(1061.+0.444*T2)
      HS1 = 0.240*T1+WS1*(1061.+0.444*T1)
      HS2 = 0.240*T2+WS2*(1061.+0.444*T2)
C
C     CALCULATE AIR FLOW RATE - LB/HR (AMFR)
C
      AMFR = 90326*SQRT(ANDLP)*SQRT(1.0/VA2)
C
C     CALCULATE AIR FLOW RATE - FPS (AV)
C
      AC = 12.0
      AV=AMFR*VA1/(3600.*AC)
C
C
C     COMPUTE DELTA T'S TO (F)
C
      DTFH  =DTMVH/.024
      DTFC = DTMVC/.024
C
C     CALCULATE FIRST HEAT OUTPUT,  AIR
C
      HTOUT = AMFR * (H2-H1)
C
C
C     WRITE IT ALL OUT
C
      WRITE(6,5000)
5000  FORMAT(1H1,52X,'WATA HEAT TRANSFER TESTS'///)
C
      WRITE(6,5010) DATE,TIME,CORE,IRUN
5010  FORMAT(26X,'DATE-',2A4,A2,8X,'TIME-',2A4,A2,8X,'CORE-',
     1     2A4,A2,8X,'RUN-',2A4,A2//)
C
      WRITE(6,5020) ANDLP,AMFR,AV
5020  FORMAT(23X,'AIR FLOW RATE',2X,F3.2, 2X,'IN. H20',7X,F7.0,
     1     2X,'LB/HR',7X,F4.2,2X,'FPS'//)
```

```
C
      WRITE(6,5050)
5050  FORMAT(1X,'AIR TEMPERATURES-'//)
      WRITE(6,5055) ARAYA
5055  FORMAT(7X,'INSIDE AMBIENT (  )',2X,4(F5.1,2X),'DEGREES F',/)
C
      WRITE(6,5060) (ARRAY(I,1),I=1,4),H1
5060  FORMAT(6X,'OUTSIDE AMBIENT (31)',2X,4(F5.1,2X),'DEGREES F',/
     1     89X,'ENTHALPY(1)',9X,F5.2 ,2X,'BTU/LB'/)
C
      WRITE(6,5070)(ARRAY(I,2),I=1,4),W1
5070  FORMAT(14X,'ANNUBAR (25)',2X,4(F5.1,2X),'DEGREES F',/
     1     89X,'HUMIDITY RATIO',6X, F5.4 ,2X,'LB/LB')
C
      WRITE(6,5080) (ARRAY1(I,1),I=1,4),TMEA1,PHI1
5080  FORMAT(11X,'POSITION 1 (  )  ',4(F5.1,2X),'DEGREES F',10X,
     1     'MEASURED',/,78X,F5.2,6X,'RELATIVE HUMIDITY(1)',F5.2  ,2X,'PER
     2CENT'/)
C
      WRITE(6,5090)(ARRAY1(I,2),I=1,4),H2
5090  FORMAT(11X,'POSITION 2 ( 8)  ',4(F5.1,2X),'DEGREES F',/89X,
     1     'ENTHALPY(2)',9X,F5.2  ,2X,'BTU/LB'/)
      WRITE(6,5100)(ARRAY1(I,3),I=1,4),T1,W2
5100  FORMAT(4X,'CORE   POSITION 3 ( 9)  ',4(F5.1,2X),'DEGREES F',
     1      4X,'T = ',F5.1,/, 4X,'INLET',80X,'HUMIDITY RATIO(2)',3X,
     2      F5.4  ,2X,'LB/LB'/)
C
      WRITE(6,5110)(ARRAY1(I,4),I=1,4),TMEA2,PHI2
5110  FORMAT(11X,'POSITION 4 (  )  ',4(F5.1,2X),'DEGREES F',10X,
     1     'MEASURED'/78X,F5.2,6X,'RELATIVE HUMIDITY(2)',F5.2  ,2X,
     2     'BTU/LB'/)
C
      WRITE(6,5120)(ARRAY1(I,5),I=1,4),VA1
5120  FORMAT(11X,'POSITION 5 (10)  ',4(F5.1,2X),'DEGREES F',/
     1      89X,'VOLUME(1)',11X,F5.2,2X,'FT3/LB'/)
      WRITE(6,5130)(ARRAY1(I,6),I=1,4)
5130  FORMAT(11X,'POSITION 6 (  )  ',4(F5.1,2X),'DEGREES F',///)
C
C     WRITE OUT AIR TEMPERATURES - CORE OUTLET
C
      WRITE(6,5140)(ARRAY2(I,1),I=1,4),HS1
5140  FORMAT(11X,'POSITION 1 (  )  ',4(F5.1,2X),'DEGREES F',/
C
     1     89X,'ENTHALPY(1)',9X,F5.2 ,2X,'BTU/LB'/)
C
      WRITE(6,5150)(ARRAY2(I,2),I=1,4),WS1
5150  FORMAT(11X,'POSITION 2 (21)  ',4(F5.1,2X),'DEGREES F',/
     1     89X,'HUMIDITY RATIO(1)',3X,F5.4 ,2X,'LB/LB'/)
C
      WRITE(6,5160)(ARRAY2(I,3),I=1,4),T2,HS2
5160  FORMAT(4X,'CORE',3X,'POSITION 3 ( 2)  ',4(F5.1,2X),
     1     'DEGREES F',4X,'T = ',F5.1,/4X,'OUTLET',79X,'ENTHALPY(2)',
     2      9X,F5.2  ,2X,'BTU/LB'/)
C
      WRITE(6,5170)(ARRAY2(I,4),I=1,4),WS2
5170  FORMAT(11X,'POSITION 4 (  )  ',4(F5.1,2X),'DEGREES F',/
     1     89X,'HUMIDITY RATIO(2)',3X,F5.4  ,2X,'LB/LB'/)
C
C
```

```
C
C
      WRITE(6,5180)(ARRAY2(I,5),I=1,4),VA2
5180  FORMAT(11X,'POSITION 5 ( 3)  ',4(F5.1,2X),'DEGREES F',/
     1      89X,'VOLUME(2)',11X,F5.2,2X,'FT3/LB'/)
C
      WRITE(6,5190) (ARRAY2(I,6),I=1,4)
5190  FORMAT(11X,'POSITION 6 ( 4)  ',4(F5.1,2X),'DEGREES F',/)
C
      WRITE(6,5200) CA,HTOUT
5200  FORMAT(74X,'HEAT CAPACITY',1X,F7.4,1X,'BTU/LBM F'/
     1      74X,'HEAT OUTPUT   ',F9.0,1X,'BTU/HR'//)
C
      WRITE(6,5210) (ARRAY3(I),I=1,4),T3
5210  FORMAT(4X,'DEW POINT TEMPERATURES-',/,11X,'CORE INLET (27)'
     1    2X,4(F5.1,2X),'DEGREES F',4X,'AVE INLET',3X,F5.1,/)
      WRITE(6,5230) (ARRAY4(I),I=1,4),T4
5230  FORMAT(
     2    10X,'CORE OUTLET (26)  ',4(F5.1,2X),'DEGREES F',4X,
     3    'AVE OUTLET',2X,F5.1///)
C
C
C
C
C     READ WATER TEMPERATURES (CORE INLET)
C
      READ(5,5500)((ARRAY6(I,J),I=1,4),J=1,2)
5500  FORMAT(4E10.0)
C
C     READ DELUGE INLET TEMPERATURES
C
      READ(5,5520)(ARRAY8(I),I=1,4)
5520  FORMAT(4E10.0)
C
C     READ DELUGE OUTLET TEMPERATURES
C
      READ(5,5530)(ARRAY9(I),I=1,4)
5530  FORMAT(4E10.0)
C
C     READ DELUGE STORAGE TEMPERATURES
C
      READ(5,5540)((ARAY10(I,J),I=1,4),J=1,2)
5540  FORMAT(4E10.0)
      READ(5,5545) (ARAY11(I),I=1,4)
5545  FORMAT(4E10.0)
C
C     CALCULATE AVERAGE OF CORE WATER INLET POSITIONS
C
      T1 = 0.
      DO 5550 J=1,2
      DO 5550 I=1,4
      T1=ARRAY6(I,J)+T1
5550  CONTINUE
      T1=T1/8.
C
```

```
C     CALCULATE AVERAGE CORE OUTLET TEMPERATURE
C
      T2 = T1 - DTFC
C
C     CALCULATE AVERAGE OF DELUGE INLET TEMPERATURES
      T5 = 0.
      DO 5560 I = 1,4
      T5 = ARRAY8(I)+T5
5560  CONTINUE
      T5 = T5/4.
C
C     CALCULATE AVERAGE OF DELUGE OUTLET TEMPERATURES
C
      T3=0.
      DO 5570 I=1,4
      T3=ARRAY9(I)+T3
5570  CONTINUE
      T3 = T3/4.
C
C     COMPUTE WATER FLOW RATES,  GPM TO LB/HR
C
      TA = (T1-32.)/1.8
      TB = (T5-32.)/1.8
      TC = (T2-32.)/1.8
      A = -3.1538 * 10.E-6
      B = -5.7575 * 10.E-5
      C = 8.3462
      WW1 = A*TA**2+B*TA+C
      WW2 = A*TB**2+B*TB+C
      WW3 = A*TC**2+B*TC+C
      WMLP = 60.*WW1*WMLG
      WHLP = 60.*WW3*WHLG
      WDLP = 60.*WW2*WDLG
C
C
C     COMPUTE HEAT INPUT AND OUTPUT
C
      QD = WDLP*(T3-T5)
      Q = 25600. - 187.5 * (T1-TAIR)
      HTIN = DTFH*WHLP+Q-QD
C
      WRITE(6,5030) WMLG,WHLG,WDLG,WMLP,WHLP,WDLP
5030  FORMAT(22X,'WATER FLOW RATE-',2X,'MAIN',2X,F5.1,3X,'GPM',
     1    6X,'HEATER',2X,F4.1,4X,'GPM',8X,'DELUGE',2X,F3.1,2X,'GPM'//
     2    40X,'LOOP',2X,F7.0,1X,'LB/HR',4X,'LOOP',4X,F6.0,2X,
     3 'LB/HR',6X,'LOOP',1X,F7.0///)
C
      WRITE(6,5040) DTMVH,DTFH,HTIN,DTMVC,DTFC,QD
5040  FORMAT(22X,'HEATER IN/OUT DELTA T  ',F4.3,2X,'MV',
     1    2X,F5.2,1X,'F',11X,'HEAT INPUT-',2X,F7.0,2X,'BTU/HR'/
     $  22X,'CORE IN/OUT DELTA T',4X,
     2         F4.3,2X,'MV',2X,F5.2,1X,'F'
     3     11X,'CORE HEAT = ',F7.0//)
C
```

```
C     CALCULATE PARTIAL PRESSURE
C
      A = 3.2437814
      B = 5.86826*10.E-4
      C=1.1702379*10.E-9
      D=2.1878462*10.E-4
      T = (T1-32.)/1.8+273.17
      BETA=647.27-T
      PW = -(BETA/T*((A+B*BETA+C*BETA**3)/(1.0+D*BETA)))
      PW1=10**PW*218.167
C
C     SECOND PARTIAL PRESSURE
C
      A = 3.2437814
      B = 5.86826*10.E-4
      C=1.1702379*10.E-9
      D=2.1878462*10.E-4
      T = (T2-32.)/1.8+273.17
      BETA = 647.27-T
      PW = -(BETA/T*((A+B*BETA+C*BETA**3)/(1.0+D*BETA)))
      PW2=10**PW*218.167
C
C     THIRD PARTIAL PRESSURE
C
      A = 3.2437814
      B = 5.86826*10.E-4
      C=1.1702379*10.E-9
      D=2.1878462*10.E-4
      T = (T3-32.)/1.8+273.17
      BETA = 647.27-T
      PW = -(BETA/T*((A+B*BETA+C*BETA**3)/(1.0+D*BETA)))
      PWS1= 10**PW*218.167
C
C     CALCULATE HUMIDITY RATIOS -- PRIMARY SIDE
C
      W12 = 0.62198 * PW1/(P-PW1)
      W22 = 0.62198 * PW2/(P-PW2)
C
C     CALCULATE ENTHALPIES  -- PRIMARY SIDE
C
      H12 = 0.240*T1+W12*(1061.+0.444*T1)
      H22 = 0.240*T2+W22*(1061.+0.444*T2)
C
C     CALCULATE HEAT OUTPUT -- PRIMARY SIDE
C
      DTFC=DTMVC/.024
      HTOUT=DTFC*WMLP
C
C     WRITE IT ALL OUT
C
      WRITE(6,6000)
```

```
C
      WRITE(6,6020) (ARRAY6(I,2),I=1,4),W12
6020  FORMAT(10X,'POSITION   (  )  ',4(F5.1,2X),'DEGREES F',25X,
     1     'HUMIDITY RATIO(1)',3X,F5.4 ,2X,'LB/LB'//)
C
      WRITE(6,6030) T2,H22,W22
6030  FORMAT(4X,'CORE  POSITION   (  )  ',28X,'DEGREES F',
     1  5X,'T= ',F5.1,12X,'ENTHALPY',12X,F5.1  ,2X,'BTU/LB'/,4X
     2   ,'OUTLET',/89X,'HUMIDITY RATIO(1)',3X,F5.4  ,2X,'LB/LB'//)
C
      WRITE(6,6040)(ARRAY8(I),I=1,4),HTOUT
6040  FORMAT(3X,'DELUGE POSITION   (  )  ',4(F5.1,2X),'DEGREES F',25X,
     1    'HEAT OUTPUT ',1X,F7.0,1X,'BTU/HR'/3X,'INLET'//)
      WRITE(6,6050)(ARRAY9(I),I=1,4),T3
6050  FORMAT(3X,'DELUGE POSITION   (  )  ',4(F5.1,2X),
     1    'DEGREES F',5X,'T=',F5.1/3X,'OUTLET'//)
      WRITE(6,6060)((ARAY10(I,J),I=1,4),J=1,2)
6060  FORMAT(1X,'DELUGE WEIGH TANK   (  )  ',4(F5.1,2X) ,'DEGREES F'/
     11X, 'STORAGE AUX. TANK   (  )  ',4(F5.1,2X),'DEGREES F'//)
      WRITE(6,6080) (ARAY11(I),I=1,4)
6080  FORMAT(/ 1X,'CORE STORAGE TANK   (  )  ',4(F5.1,2X),'DEGREES F'/)
      WRITE(6,6070) PB
6070  FORMAT(1X,'AIR PRESSURES-',/20X,'BAROMETRIC ',F5.2,
     2     'IN. HG.')
C
C     ADDITIONAL CALCULATIONS
C     OVERALL HEAT TRANSFER COEFFICIENTS
C
      AS = 974.14
      DH1 = H12-H1
      DH2 = H22-H2
      DELH = (DH1-DH2)/ALOG(DH1/DH2)
      VO1 = CA*HTIN/(AS*DELH)
      DUMMY = ABS(1-(HTIN/(AMFR*DH1)))
      VO2 = -AMFR*CA/AS *ALOG (DUMMY)
      DUMMY = ABS(1-(H2-H1)/DH1)
      VO3 = -AMFR*CA/AS*ALOG (DUMMY)
      RE = 0.0329*AMFR
C
C
C
C     DELUGE COEFFICIENT
      HP = 21.180248 * WMLG**0.8
      AP = 39.74
      APT=41.44
      TT = 111.7
      THK = 0.0041
      X1 = AS/(HP*AP)
      X2 = AS*THK/(TT*APT)
      HD = 1.0/((T1-T3)*AS/HTIN-X1-X2)
C
C
```

```
C
C       WET HEAT TRANSFER/ DRY HEAT TRANSFER
        HA=21.8338 * DELTA**0.4
        X = 0.0442 * SQRT(HA*22.06)
        ETAF = -0.38 * X + 1.052
        Y = 974.14 / (43.14 + ETAF * 931.)
        U = 1.0 / (Y/HA + 0.0116)
        RENO = 1862.5 * DELTA**0.6196
        XNTU=133.54*U/RENO
        PHEE=1.-EXP(-XNTU)
        Q = PHEE*RENO*7.29*(T1-TAI)
        XXX = HTIN/Q
        WRITE(6,9999) V01,V02,V03,HD
9999    FORMAT(5X,'U01 = ',F5.2,5X,'U02 = ',F7.2,5X,
       1      'U03 = ',F5.2,5X,'HD = ',F7.2)
        WRITE(6,9898) RE,HP
9898    FORMAT(5X,'RE = ',F7.2,5X,'HP = ',F7.2/)
        WRITE(6,6666) DELTA
6666    FORMAT(5X,'CORE DELTA P - ',F4.2,  'IN. H20')
        WRITE(6,61234) XXX
61234   FORMAT ( 5X,'QWET/QDRY = ', F6.3)
C
C       ADDITIONAL CALCULATIONS
C
        XYZ=0.0008152
        PHIH = (H2-H1)/(H12-H1)
        PHIM = (W2-W1)/(W12-W1)
        G=(H12-H1)/(T1-TAI)
        GM=(W12-W1)/(T1-TAI)
        RXI=XYZ*PHIH*(H12-H1)/(PHIM*(W12-W1))
        XN =-ALOG(ABS(1.-PHIH))
        XNM =-ALOG(ABS(1.-PHIM))
C
C       CALCULATIONS OF MASS EVAPORATION AND MASS TRANSFER COEFFICIENT
C
        DME = AMFR*(W2-W1)
        SIG1 = DME*ALOG((W12-W1)/(W22-W2))/(AS*(W12-W1-W22+W2))
        SIG2=AMFR*XNM/AS
        HS = 0.168957*RE**0.6456
        ZET=11.6
        HDX = HD/0.6
8000    CONTINUE
C
C
C       CALCULATE THEORETICAL VALUES FOR HEAT TRANSFER
C
        HE = 1./(1./HDX+1./(ZET*HS))
        BX = 0.0442*SQRT(HE*22.06)
        ETAFX=-0.38*BX+1.052
        ASX = (43.14+ETAFX*931.0)/974.14
        HDX1 = HD/ASX
        IF(ABS((HDX1-HDX)/HDX).LE.0.0005) GO TO 8001
        HDX= (HDX1+HDX)/2.
        GO TO 8000
8001    CONTINUE
        VOX = 1./(ZET*(X1+X2+1./HD)+1./(HS*ASX))
        XN2 = VOX*AS/(AMFR*CA)
        PHIH2 = 1.-EXP(-XN2)
C
```

```
C      CALCULATE THEORETICAL VALUES FOR MASS TRANSFER
C
       ZETM = RXI * ZET
8002   CONTINUE
       HEM = 1./(1./HDX+1./(ZETM*HS))
       BXM = 0.0442*SQRT(HEM*22.06)
       ETAFM = -0.38*BXM + 1.052
       AMX = (43.14+ETAFM*931.0)/974.14
       SIG3 = 1./(CA*(ZETM*(X1+X2+1./HD)+1./(HS*AMX)))
       XNM2 = SIG3*AS/AMFR
       PHIM2 = 1.-EXP(-XNM2)
       ZETMX=ZET*XYZ*PHIH2*(H12-H1)/(PHIM2*(W12-W1))
       IF(ABS((ZETMX-ZETM)/ZETMX).LE.0.0005) GO TO 8003
       ZETM = ZETMX
       GO TO 8002
8003   CONTINUE
C
C
C
C      CALCULATE OUTLET AIR CONDITIONS
       W2X = PHIM2* (W12-W1)+W1
C
       H2X = PHIH2 * (H12-H1)+H1
       TDB2 = (H2X-W2X*1061.)/(0.240+W2X*0.444)
C
C
       WRITE(6,7000) PHIH,PHIM,G,GM,RXI,XN,XNM
7000   FORMAT('1',5X,'PHIH = ',F6.3,5X,'PHIM = ',F6.3,5X,'GAMMA =',F6.3
     $      ,5X,'GAMMA M = ',F6.5
     $       ,5X, 'RXI = ',F6.3,5X,' N = ',F6.3,5X,'NM = ',F6.3/)
       WRITE(6,7200) DME,SIG1,SIG2,ZET
7200   FORMAT(5X,'MW = ',F10.2,5X,'SIG1 = ',
     $      F6.2,5X,'SIG2 = ',F6.2,5X,'ZETA = ',F6.3,5X/)
       WRITE(6,7300) PHIH2,XN2,VOX,ASX,PHIM2,XNM2
7300   FORMAT(5X,'PHI2 = ',F6.3,5X, 'N2 = ',F6.3,
     $      5X,'UOX = ',F6.3,5X,'ASX = ',F6.4,5X,
     1      'PHIM2 = ',F6.3,5X,'NM2 = ',F6.3/)
       WRITE(6,7400)SIG3,AMX,ZETMX,H2X,W2X,TDB2
7400   FORMAT(5X,'SIG3 = ',F6.2,5X,'AMX = ',F6.4,5X,'ZETAM = ',F6.3,1X//,
     2      5X,'AIR ENTHALPY 2 = ',F6.2,5X,'AIR HUMIDITY 2 = ',F6.5,5X,
     3     'AIR DRY BULB 2 = ',F6.2,5X/)
C
C
```

```
C
C          THE FOLLOWING CALCULATES HDX AND TR TO MATCH HEAT TRANSFER
C         PATHS FROM INSIDE TO OUTSIDE SURFACES
C
      TR=T3
89    CONTINUE
      T=(TR-32.)/1.8+273.17
      BETA=647.27-T
      PW = -(BETA/T*((A+B*BETA+C*BETA**3)/(1.0+D*BETA)))
      PWSD=10**PW*218.167
      WD=0.62198*PWSD/(P-PWSD)
      HSD=0.240*TR+WD*(1061.+0.444*TR)
      ZT=(H12-HSD)/(CA*(T1-TR))
87    CONTINUE
      HD=1./(1./(ZT*V02)-1./(HS*ASX*ZT)-X1-X2)
      HDX=HD/ASX
      IF(ABS((HDX1-HDX)/HDX1).LE.0.0005) GO TO 88
      HE=1./(1./HDX+1./(ZT*HS))
      BX = 0.0442*SQRT(HE*22.06)
      ETAFX=-0.38*BX+1.052
      ASX = (43.14+ETAFX*931.0)/974.14
      HDX1=HDX
      GO TO 87
88    CONTINUE
      TRX=TR
      TX=(HTIN+QD)*(1./HD+X1+X2)/AS
      TR=T1-TX
      IF(ABS((TR-TRX)/TRX).GE.0.0005) GO TO 89
      WRITE(6,7500) ASX,HD,ZT,TR,TX
7500  FORMAT(5X,'ASX = ',F6.4//,5X,'HD = ',F6.2//,5X,'ZETA = ',F6.3//,
     $     5X,'TR = ',F6.2//,5X,'TP - TR = ',F6.2///)
C
C
C
C         MASS TRANSFER PARAMETERS ARE CALCULATED USING TR AND HDX
C         CALCULATED ABOVE
C
      PPIH=1.-EXP(-V02*AS/(CA*AMFR))
      XYZ=(W12-WD)/(H12-HSD)
      RXI=XYZ*PPIH*(H12-H1)/(PHIM*(W12-W1))
      ZTM=ZT*RXI
7501  CONTINUE
      HEM=1./(1./HDX+1./(ZTM*HS))
      BXM=0.0442*SQRT(HEM*22.06)
      ETAFM=-0.38*BXM+1.052
      AMX=(43.14+ETAFM*931.)/974.14
      SIGM=1./(CA*(ZTM*(X1+X2+1./HD)+1./(HS*AMX)))
      XMM=SIGM*AS/AMFR
      PHIM=1.-EXP(-XMM)
      ZTMX=ZT*XYZ*PPIH*(H12-H1)/(PHIM*(W12-W1))
      IF(ABS((ZTMX-ZTM)/ZTM).LE.0.0005) GO TO 7502
      ZTM=ZTMX
      GO TO 7501
7502  CONTINUE
      WRITE(6,7600) ZTM,AMX,SIGM
7600  FORMAT(5X,'ZETA M = ',F6.4//,5X,'AMX = ',F6.4//,5X,'SIG M = ',F6.3/,'1')
     $     /,'1')
1     CONTINUE
      IF(ICONT .NE. ICONT2) GO TO 25
      END
@MAP,L
IN DATRE.MAIN
@XQT
```

GLOSSARY FOR DATA ANALYSIS PROGRAM

AC - core frontal area, ft^2

AMFR - air mass flow rate, lb/hr

AMX - reduced surface area for mass transfer, air side

ANDLP - annubar pressure drop, in. H_2O

AP - reduced surface area, water side

APT - reduced mean tube wall area

AS - total surface area - airside, ft^2

ASX - reduced surface area for heat transfer, air side

AV - frontal air velocity, ft/s

BX - (Biof Number)$^{1/2}$ for heat transfer

BXM - (Biof number)$^{1/2}$ for mass transfer

CA - moist specific heat, Btu/lbm °F

DELH - log mean enthalpy difference, Btu/lbm

DELTA - core pressure drop, in. H_2O

DH1 - $i'_{p1} - i_{\infty 1}$

DH2 - $i'_{p2} - i_{\infty 2}$

DME - total mass of water evaporated, lb/hr

DTFC - temperature drop across core, °F

DTFH - temperature gain across heaters, °F

DTMVC - temperature drop across core, mV

DTMVH - temperature gain across heaters, mV

EPI - ε, inlet enthalpy ratio

EPIM - ε_m, inlet humidity ratio

ETAF - experimental fin efficiency for heat transfer

ETAFM - predicted fin efficiency for mass transfer

ETAFX - predicted fin efficiency for heat transfer

H1 - $i_{\infty 1}$ inlet air enthalpy, Btu/lbm

H2 - $i_{\infty 2}$ outlet air enthalpy, Btu/lbm

H12 - i'_{p1} saturated air enthalpy at inlet water temperature, Btu/lbm

H22 - i'_{p2} saturated air enthalpy at outlet water temperature, Btu/lbm

HZX - predicted air outlet enthalpy, Btu/lbm

HA - air side surface heat transfer coefficient at same pressure as wet test, Btu/hr ft^2 °F

HD - deluge coefficient, Btu/hr ft^2 °F

HDX - apparent surface heat transfer coefficient, Btu/hr ft^2 °F

HDX1 - predicted apparent surface heat transfer coefficient, Btu/hr ft^2 °F

HE - effective surface heat transfer coefficient, Btu/hr ft^2 °F

HEM - effective surface heat transfer coefficient for mass transfer, Btu/hr ft^2 °F

HP - primary side heat transfer coefficient, Btu/hr ft^2 °F

HS - surface heat transfer coefficient, air side, Btu/hr ft^2 °F

HS1 - saturation air enthalpy at inlet, Btu/lbm

HS2 - saturation air enthalpy at outlet, Btu/lbm

HTIN - total heat transferred from water to air, Btu/hr

HTOUT - heat lost from core water, Btu/hr

HTOUT - heat gain in air, Btu/hr

P - barometric pressure, in. Hg., atm.

P1 - barometric pressure, psf

PHEE - heat exchanger effectiveness

PHI1 - relative humidity, air inlet

PHI2 - relative humidity, air outlet

PHIH - experimental heat transfer effectiveness

PHIH2 - predicted heat transfer effectiveness

PHIM - experimental mass transfer effectiveness

PHIM2 - predicted mass transfer effectiveness

PW1 - partial pressure at $T_{\infty 1}$

PW1 - saturation pressure at T_{p1}

PW2 - partial pressure at $T_{\infty 2}$

PW2 - saturation pressure at T_{p2}

PWS1 - saturation pressure at $T_{\infty 1}$

PWS1 - saturation pressure at T_{d1}

PWS2 - saturation pressure at $T_{\infty 2}$

Q - pump heat input, Btu/hr

QD - deluge water heat input, Btu/hr

RE - Reynolds number

RENO - Reynolds number at same core pressure drop

RXI - ratio of ξ_m to ξ

S1G1 - experimental mass transfer coefficient using log mean difference, lb/hr

S1G2 - experimental mass transfer coefficient using effectiveness, lb/hr

S1G3 - predicted mass transfer coefficient, lb/hr

T1 - $T_{\infty 1}$ - air inlet temperature, °F

T1 - T_{p1} - core water inlet temperature, °F

T_2 - $T_{\infty 2}$ - air outlet temperature, °F

T_2 - T_{p2} - core water outlet temperature, °F

T_3 - air inlet dew point temperature, °F

T_3 - deluge outlet temperature, °F

T_4 - air outlet dew point temperature, °F

T_5 - deluge inlet temperature, °F

TA T_{p1}, core water inlet temperature, °C

TAI $T_{\infty 1}$, air inlet temperature, °F

TAIR - ambient room temperature, °F

TB - deluge inlet temperature, °C

TC - core water outlet temperature, °C

TDB2 - predicted outlet air temperature, °F

THK - tube wall thickness, ft

TMEA1 - measured relative humidity, inlet

TMEA2 - measured relative humidity, outlet

TT - tube wall thermal conductivity, Btu/hr ft °F

TVA1 - absolute inlet air temperature, °R

TVA2 - absolute outlet air temperature, °R

U - overall dry heat transfer coefficient, Btu/hr ft^2 °F

VA1 - specific volume of air at inlet, ft^3/lb

VA2 - specific volume of air at outlet, ft^3/lb

VO1 - overall wet heat transfer coefficient, Btu/hr ft^2 °F

VO2 - overall wet heat transfer coefficient, Btu/hr ft^2 °F

VO3 - overall wet heat transfer coefficient, Btu/hr ft^2 °F

VOX - predicted overall wet heat transfer coefficient, Btu/hr ft^2 °F

W1 - humidity ratio of inlet air, lb/lb

W12 - humidity ratio of air at T_{p1}, lb/lb

W2 - humidity ratio of outlet air, lb/lb

W22 - humidity ratio of air at T_{p2}, lb/lb

W2X - predicted humidity ratio of outlet air, lb/lb

WDLG - flow rate of deluge water - gpm

WDLP - flow rate of deluge water, lb/hr

WHLG - flow rate of heater loop water, gpm

WHLP - flow rate of heater loop water, lb/hr

WIO - average humidity ratio of air, lb/lb

WMLG - flow rate of main loop water, gpm

WMLP - flow rate of main loop water - lb/hr

WS1 - humidity ratio of saturated inlet air, lb/lb

WS2 - humidity ratio of saturated outlet air, lb/lb

WW1 - weight of water at T_{p1}, lb/gal

WW2 - weight of water at T_{d1}, lb/gal

WW3 - weight of water at T_{p2}, lb/gal

X - $(\text{Biof number})^{1/2}$, experimental

X1 - thermal resistance of core water, hr ft^2 °F/Btu

X2 - thermal resistance of tube wall, hr ft^2 °F/Btu

XN - experimental NTU for heat transfer

XN2 - experimental NTU for mass transfer

XNM - predicted NTU for heat transfer

XNM2 - predicted NTU for mass transfer

XNTU - experimental NTU for dry heat transfer

XXX - Q wet/Q dry

Y - fin effectiveness ratio

ZET - ξ

ZETM - ξ_m

ZETMX - predicted ξ_m

APPENDIX E

DEVELOPMENT OF HEAT EXCHANGER PERFORMANCE AS A FUNCTION OF FAN POWER

APPENDIX E

DEVELOPMENT OF HEAT EXCHANGER PERFORMANCE AS A FUNCTION OF FAN POWER

The equations for the rate of heat transfer and fan power are

$$Q = \phi G_o A_f C_a \Delta T_i \tag{E-1}$$

$$p = \frac{\sigma A_f v^2 G_o^{\ 3}}{2 g_c}\left(K + \frac{f A_s}{\sigma A_f}\right) \tag{E-2}$$

An expression for G_o as a function of fan power is obtained by using the following assumptions

$$K << \frac{f A_s}{\sigma A_f} \tag{E-3}$$

$$f = f_r\left(\frac{R_e}{1000}\right) \tag{E-4}$$

$$R_e = \frac{D_h G_o}{\mu} \tag{E-5}$$

$$A_s = s A_f L \tag{E-6}$$

The expression for G_o is then

$$G_o = \left[P\left(\frac{500\, g_c\, \mu}{\sigma L A_f v^2 f_r}\right)\left(\frac{D_h}{1000\, \mu}\right)^{(1+m)}\right]^{\left(\frac{1}{3-m}\right)} \tag{E-7}$$

The following substitutions and assumptions may then be used to develop an expression for $Q/\Delta T_i$ as a function of fan power. For the limiting case where

$$\left(\frac{T_{p2} - T_{p1}}{T_{\infty 2} - T_{\infty 1}}\right) \simeq 0 \qquad \text{(E-8)}$$

(as in a condensor, or as in the WATA tests where $\dot{m}_p$ is very high) the effectiveness may be given by

$$\phi = 1 - e^{-N} \qquad \text{(E-9)}$$

where N is defined by

$$N = \frac{U_o A_s}{\dot{m}_a C_a} = \frac{4 U_o L}{G_o D_h C_a} \qquad \text{(E-10)}$$

The Colburn factor is defined by

$$j_u = \frac{U_o}{C_a G_o} Pr^{2/3} \qquad \text{(E-11)}$$

where it is assumed that j_u is of the form

$$j_u = j_r\left(\frac{Re}{1000}\right)^{-n} \qquad \text{(E-12)}$$

then U_o can be given by

$$U_o = C_a Pr^{-2/3} j_r \left(\frac{1000\ \mu}{D_h}\right)^n G_o^{(1-n)} \qquad \text{(E-13)}$$

Using Equation E-13 for U_o, Equation E-9 and Equations E-9 and E-10 for ϕ, Equation E-1 may be given as follows,

$$Q = A_f G_o C_a \Delta T_i \left\{ 1 - \exp\left[-\left(\frac{4Lj_r}{\mu Pr^{2/3}} \right) \left(\frac{1000\ \mu}{D_h} \right) (1+n)^{G^{-n}} \right] \right\} \tag{E-14}$$

Combining Equation E-14 with Equation E-7 for G_o then gives

$$\frac{Q}{C_a \Delta T_i A_f} = C_1 P^{\left(\frac{1}{3-m}\right)} \left\{ 1 - \exp\left[-C_2 P^{\left(\frac{-n}{3-m}\right)} \right] \right\} \tag{E-15}$$

where the constants C_1 and C_2 are defined as follows:

$$C_1 = \sigma \left[\frac{1000\ \mu g_c}{2\sigma L A_f v^2 f_r} \left(\frac{D_h}{1000\ \mu} \right)^{1+m} \right]^{1/(3-m)} \tag{E-16}$$

$$C_2 = \left[\frac{C_1}{\sigma} \right]^{-n} \left[\frac{4j_r L Pr^{-2/3}}{1000\ \mu} \left(\frac{1000\ \mu}{D_h} \right)^{1+n} \right] \tag{E-17}$$

The expression for the effectiveness - Ntu relation for crossflow with both fluids unmixed involves an infinite series for which graphs are available. The expression for counterflow yield values of ϕ that are less than ten percent low for values of Ntu < 5. This expression is:

$$\phi = \frac{1 - \exp\left[-Ntu \left(1 - \frac{\beta_w}{\beta_a} \right) \right]}{1 - \frac{\beta_w}{\beta_a} \exp\left[-Ntu \left(1 - \frac{\beta_w}{\beta_a} \right) \right]} \quad \text{for } \beta_w < \beta_a \tag{E-18}$$

The resulting expression for Q as a function of P is:

$$\frac{Q}{\Delta T_i C_a A_f} = \frac{C_1 P^{1/(3-m)} \left\{ 1 - \exp - \left[C_2 P^{-n/(3-m)} (1 - C_3 P^{1/(3-m)}) \right] \right\}}{1 - C_3 P^{1/(3-m)} \exp\left\{ C_2 P^{-n/(3-m)} \left[1 - C_3 P^{1/(3-m)} \right] \right\}} \tag{E-19}$$

where C_3 is defined by

$$C_3 = \frac{C_1}{\dot{m}_p C_p} \tag{E-20}$$

This is identical with the use of the log mean temperature difference as the driving force for heat transfer. For crossflow heat exchangers, this, together with the crossflow correction factor F_T can be used to characterize the type of heat exchangers of interest here. Thus $Q/T_i C_a A_f$ can be calculated by including F_T in the expression for C_2; i.e.:

$$C_2 = \left[\frac{C_1}{\sigma}\right]^{-n} \left[\frac{4F_T j_r L Pr^{-2/3}}{1000\ \mu} \left(\frac{1000\ \mu}{D_h}\right)^{1+n}\right] \tag{E-21}$$

This requires an iterative procedure of: (1) assuming a value for F_T, (2) verifying this value following the calculation of Q and the resultant temperature rise of stream representing C_{min}, and (3) repeating the calculation as necessary.

PNL-3428
UC-12

DISTRIBUTION

No. of Copies

OFFSITE

U.S. Department of Energy
A. A. Churm
Chicago Patent Group
9800 South Cass Avenue
Argonne, IL 60439

U.S. Department of Energy
Office of Assistant General Counsel for Patents
Washington, DC 20545

27 DOE Technical Information Center

10 U.S. Department of Energy
I. Helms
Advanced Systems and Materials Production
Washington, DC 20545

U.S. Department of Energy
W. F. Savage
Chief, Advanced Systems Evaluation Section
Washington, DC 20545

U.S. Department of Energy
N. Goldenberg
Director, Division of Advanced Nuclear Systems and Projects
Washington, DC 20545

U.S. Department of Energy
C. Grua
Environmental Control Technology
Office of Environmental Compliance Overview
Washington, DC 20545

No. of Copies

U.S. Department of Energy
W. E. Mott
Director, Environmental Control Technology
Office of Environmental Compliance Overview
Washington, DC 20545

Allied Chemical Company
B. R. Dickey
550 2nd Street
Idaho Falls, ID 83401

Allis-Chalmers Power Systems, Inc.
J. S. Joyce
1135 South 70th Street
West Allis, WI 53214

Aluminum Company of America
E. T. Wanderer
Alcoa Technical Center
Alcoa Center, PA 15069

American Electric Power Service Corporation
H. J. Janzon
2 Broadway
New York, NY 10004

American Electric Power Service Corporation
C. Swenson
2 Broadway
New York, NY 10004

Aqua-Chem
R. M. Ahlgren
P.O. Box 421
Milwaukee, WI 53201

No. of
Copies

Arizona Public Service Co.
W. E. Campbell
P.O. Box 21666
Phoenix, AZ 85036

Arizona Public Service Co.
T. Woods
P.O. Box 21666
Phoenix, AZ 85036

Babcock & Wilcox
M. W. Peterson
Fossil Power Division
20 South Van Buren
Barberton, OH 44203

Baltimore Aircoil Co., Inc.
R. E. Cates
Manager, Advanced Engineering
P.O. Box 7322
Baltimore, MD 21227

Baltimore Gas & Electric Co.
G. D. Creel
Gas & Electric Building
Baltimore, MD 21203

Battelle-Geneva
J. P. Budliger
7 Route De Drizi
1227 Geneva, SWITZERLAND

Bechtel Corporation
P. Leung
P.O. Box 60860
Terminal Annex
Los Angeles, CA 90060

Bechtel Corporation
G. R. Reti
P.O. Box 3965
San Francisco, CA 94119

R. W. Beck and Associates
J. P. Rossie
400 Prudential Plaza
Denver, CO 80202

No. of
Copies

Betz Environmental Engineers
J. Soost
One Plymouth Meeting Mall
Plymouth Meeting, PA 19462

Black, Crow and Eidsness, Inc.
C. G. Thompson
807 South McDonough
Montogomery, AL 35104

Black Hills Power and Light
Company
B. Westre
P.O. Box 1400
Rapid City, SD 57701

Boeing Aerospace Division
D. Gilbert (M.S. 2R00)
P.O. Box 3999
Seattle, WA 98124

Bonneville Power Administration
E. H. Hall
1002 N.E. Holladay Street
Box 3621
Portland, OR 97208

Burns and Roe, Inc.
700 Kinder Kamack Rd.
Oradel, NY 07649

California Energy Commission
C. Webb
1111 Howe Avenue
Sacramento, CA 95825

California State Energy Resources
Conservation and Development
Commission
L. E. Stamets
1111 Howe Avenue
Sacramento, CA 95825

Carolina Power & Light Co.
J. Sell
336 Fayettesville Street
Raleigh, NC 27602

No. of
Copies

Catalytic Construction Corp.
J. Morse
P.O. Box 15232
Charlotte, NC 28210

Ceramic Cooling Tower Co.
P. A. Frohwerk
P.O. Box 425
Fort Worth, TX 76101

Chicago Bridge and Iron Company
M. Husain
800 Jovie Boulevard
Oak Park, IL 60521

Combustion Engineering Lummus
Engineering Company
R. J. Croke
1515 Broad St.
Bloomingfield, NJ 07003

Columbus and Southern Ohio
Electric Co.
L. W. Meridith
General Manager, Generation
Department
215 North Front Street
Columbus, OH 43215

Combustion Engineering
H. H. Osborn
Air Preheater Company
Wellsville, NY 14895

Commonwealth Edison
R. H. Holyoak
One First Plaza
P.O. Box 767
Chicago, IL 60690

Consolidated Edison Co. of
New York, Inc.
W. A. Messner
4 Irving Place
New York, NY 10003

No. of
Copies

Consolidated Edison Co. of New
York, Inc.
C. L. Newman
4 Irving Place
New York, NY 10003

Cooling System, Inc.
C. Mitchel
8490 Avenue 296
Visalia, CA 93877

Cornell University
F. K. Moore
Ithaca, NY 14850

Curtiss-Wright Corporation
R. J. Haberski
One Passaic Street
Wood Ridge, NJ 07075

Dames & Moore
L. Craton
Suite 1000
1100 Glendon Avenue
Los Angeles, CA 90024

Delmarva Power & Light
F. Cook
800 King Street
Wilmington, DE 19801

Dow Chemical Company
E. Wagener
2800 Mitchell Drive
Walnut Creek, CA 94598

Duke Power Company
S. K. Blackley
P.O. Box 2178
Charlotte, NC 28201

Duquesne Light Co.
J. Latshaw
435 6th Avenue
Pittsburgh, PA 15219

No. of Copies

Dynatech Company
E. Guyer
99 Erie Street
Cambridge, MA 02139

Ecodyne
J. Slotnik
607 First Street, S.W.
Massillon, OH 44646

Ecodyne Cooling Products
K. D. Whitehead
P.O. Box 1267
Santa Rosa, CA 95403

Electric Power Research Institute
J. Maulbetsch
3412 Hilview Avenue
P.O. Box 10412
Palo Alto, CA 94304

Electric Power Research Institute
J. A. Bartz
3412 Hilview Avenue
P.O. Box 10412
Palo Alto, CA 94304

Empire State Electric Energy Research Corp.
L. Geller
1271 Avenue of the Americas
New York, NY 10020

Environmental Protection Agency
T. G. Brna (MD-61)
IERL/RTP
Research Triangle Park, NC 27711

Environmental Protection Agency
A. Galley (WH-552)
401 M. Street SW
Washington, DC 20460

El Paso Electric Co.
D. G. Isbell
P.O. Box 982
El Paso, TX 79999

No. of Copies

Environmental Protection Agency
M. Maxwell (MD-61)
IERL/RTP
Research Triangle Park, NC 27711

Environmental Protection Agency
F. H. Rainwater
Pacific Northwest Water Laboratory
200 S.W. 35th Street
Corvallis, OR 97330

Environmental Sciences and Services
W. G. Hoydysh
150 East 73rd Street
New York, NY 10021

Environmental Systems Corporation
K. Wilber
P.O. Box 2525
Knoxville, TN 37901

ERG Incorporated
G. M. Benson
Lowell 57th Street
Oakland, CA 94608

Exxon Research Center
J. G. Stevens
Bldg. 1, Rm. 2048
P.O. Box 8
Linden, NJ 07036

Federal Power Commission
E. Sligh
825 N. Capitol Street
Washington, DC 20426

Florida Power & Light Co.
C. Henderson
9250 W. Flagler Street
Miami, FL 33174

No. of Copies

Foster Wheeler Development Corporation
R. J. Zoschak
Technical Director, Applied Thermodynamics Research
12 Peak Tree Hill Road
Livingston, NJ 07039

Foster Wheeler Energy Corporation
E. L. Damon
110 S. Orange Avenue
Livingston, NJ 07039

Foster Wheeler Energy Corporation
W. H. Fisher, Jr.
Project manager
110 S. Orange Avenue
Livingston, NJ 07039

Foundation Sciences, Inc.
L. E. Wilkinson
Cascade Building
Portland, OR 97204

Franklin Institute Research Laboratories
G. P. Wachtell
Twentieth & Parkway
Philadelphia, PA 19103

Frick Company
J. Bibroff
15302 El Mar Lane
Kerman, CA 93630

GEA Airexchangers, Inc.
B. Davis
P.O. Box 1377
Thomasville, GA 31792

GEA Power Cooling Systems, Inc.
G. Hesse
P.O. Box 81608
San Diego, CA 92138

No. of Copies

General Atomic Company
H. P. Fay
P.O. Box 81608
San Diego, CA 92138

General Electric Co.
E. H. Miller
Large Steam Turbine Division
300 Nott Street
Schenectady, NY 12301

General Motors Corp.
R. K. Shah
Harrison Radiator Division
Lockport, NY 14094

Georgia Power Co.
T. E. Byerley
P.O. Box 4545
Atlanta, GA 30302

Gilbert Associates, Inc.
J. F. Sebald
525 Lancaster Avenue
Reading, PA 19603

Heat Transfer Research Inc.
J. E. Taborek
1000 S. Fremont Avenue
Alhambra, CA 91802

Hudson Products
M. W. Larinoff
6855 Horwin Drive
Houston, TX 77036

Hudson Products
E. C. Smith
6855 Horwin Drive
P.O. Box 36100
Houston, TX 77036

H2M Corporation
H. D. Freudenthal
500 Broad Hollow Road
Melville, NY 11746

No. of Copies

Ingersoll-Rand
W. R. Scott, Jr.
Phillipsburg, NJ 08865

Italimpianti-Societa Italiana Impianti p.a.
C. Rocco
Piazza, Piccapietra 9
18121 Genoe, ITALY

Los Alamos Scientific Laboratory
D. Abbey
S-2, MS 606
Los Alamos, NM 87545

Los Angeles Department of Water and Power
Peter Lowery
111 N. Hope Street
Los Angeles, CA 90012

Louisiana Power & Light Co.
D. L. Aswell
142 Delaronde Street
New Orleans, LA 70174

The Charles T. Main Co.
E. S. Miliaras
Southeast Tower
Prudential Center
Boston, MA 02199

The Marley Company
C. A. Baird
12 S. 12th Street
Philadelphia, PA 19107

The Marley Company
J. D. Holmberg
5800 Fox Ridge Drive
Mission, KS 66202

The Marley Company
R. Landon
5800 Fox Ridge Drive
Mission, KS 66202

No. of Copies

Martin Marietta Laboratories
L. Bongers
1450 South Rolling Road
Baltimore, MD 21227

Massachusetts Institute of Technology
L. R. Glicksman
77 Massachusetts Avenue
Cambridge, MA 02139

Massachusetts Institute of Technology
M. W. Golay
77 Massachusetts Avenue
Cambridge, MA 02139

Massachusetts Institute of Technology
R. Harleman
Department of Civil Engineering
77 Massachusetts Avenue
Cambridge, MA 02139

McDonnell Douglas Astronautics Company
W. H. P. Drummond
5301 Balsa Avenue
Huntington Beach, CA 92647

Minnesota Power Cooperative, Inc.
L. A. Hillier
Box 1318
Grand Forks, ND 58201

R. D. Mitchell
Consulting Engineer
4531 East Best Road, SEDC
Larkspur, CO 80118

Montana Power Co.
R. Hofacher
40 E. Broadway
Butte, MT 59701

No. of
Copies

Niagara Blower
W. Kals
405 Lexington Avenue
New York, NY 10017

Northeast Utilities
R. H. Meyer
P.O. Box 270
Hartford, CT 06101

Northern States Power Co.
R. Stansfield
414 Nicollet Mall
Minneapolis, MN 55401

N.U.S. Corporation
S. Lefton
2 Palo Alto Square (Suite 624)
Palo Alto, CA 94304

Oak Ridge National Laboratory
J. W. Michel
OTEC Heat Exchange Project
Box Y
Oak Ridge, TN 37830

Oak Ridge National Laboratory
Roy C. Robertson
Engineering Technical Division
Bldg 9204-1, Y-12
Oak Ridge, TN 37830

Orange & Rockland Utilities, Inc.
R. H. Metzger
75 West Route 59
Spring Valley, NJ 10977

Oregon State University
L. P. Davis
Department of Mechanical
Engineering
Corvallis, OR 97330

Oregon State University
C. E. Wicks
Department of Chemical Engineering
Corvallis, OR 97330

No. of
Copies

Oregon State University
J. G. Knudson
Engineering Experiment Station
Corvallis, OR 97330

Pacific Gas & Electric
A. A. Ariey
77 Beale Street
San Francisco, CA 94106

Pacific Gas & Electric
R. E. Price
77 Beale Street
San Francisco, CA 94106

Pacific Power & Light Co.
W. C. Bruaer
Public Service Bldg.
Portland, OR 97204

Pennsylvania Power & Light
W. Dussinger
2 North Ninth Street
Allentown, PA 18101

Pennsylvania Power & Light
H. G. Pfeiffer
2 North Ninth Street
Allentown, PA 18101

PFR Engineering Systems, Inc.
T. Rozenmann, President
Suite 832
4676 Admiralty Way
Marina del Rey, CA 90291

Philadelphia Electric Co.
J. Allen
2301 Market Street
Philadelphia, PA 19101

Prof. Ing. Carlo Roma
Piazza delle Muse 8
Rome, ITALY

No. of Copies

Pickard Low & Garrick
L. Rust
1200 18th St. NW
Suite 612
Washington, DC 20036

Power Generation Cooling Systems
G. L. Henderson
4714-52nd Street S.
Seattle, WA 98118

Public Service of Colorado
R. F. Walker
5900 E. 39th Avenue
Denver, CO 80207

Public Service Company of Indiana
S. W. Shields
100 East Main Street
Plainfield, IN 46168

Public Service Company of New Mexico
C. D. Bedford
P.O. Box 2267
Albuquerque, NM 87103

Public Service Company of New Mexico
D. J. Jroves
P.O. Box 2267
Albuquerque, NM 87103

Quirk, Lawler and Mattusky, Eng.
J. Lawler
505 5th Avenue
New York, NY 10017

Radian Corporation
F. B. Mesich
P.O. Box 9948
Austin, TX 78766

No. of Copies

Research Cottrell
G. E. Collins
Hamon Cooling Tower Division
Box 750
Bound Brook, NJ 08805

Resources Conservation Company
H. Herrigel
P.O. Box 936
Renton, WA 98055

Reynolds Aluminum Co.
R. Lindberg
Reynolds Metallurgical Research Laboratory
Richmond, VA 23261

Richmond Field Station
H. H. Sephton
47th and Hoffman Blvd.
Richmond, CA 94804

San Diego Gas & Electric
R. G. Lacy
101 Ash Street
San Diego, CA 92107

Seattle City Light
R. G. Sheehan
1015 Third Avenue
Seattle, WA 98104

Southern California Edison
D. M. Burkhart
2244 Walnut Grove Avenue
Rosemead, CA 91770

Southern California Edison
F. A. McCracken
2244 Walnut Grove Avenue
Rosemead, CA 91770

Southern Services, Inc.
C. H. Goodman
P.O. Box 2625
Birmingham, AL 35202

No. of
Copies

Stanford University
A. L. London
Department of Mechanical
Engineering
Stanford, CA 94305

Stearns-Rogers, Inc.
J. Y. Parce
Box 5888
Denver, CO 80217

Stewart-Warner Corporation
South Wind Division
V. N. Tramontini
1514 Dover Street
Indianapolis, IN 46221

Stone & Webster Engineering Corp.
D. H. Guild
225 Franklin Street
Boston, MA 02107

Tampa Electric Co.
H. I. Wilson
P.O. Box 111
Tampa, FL 33601

Tennessee Valley Authority
Energy Research
R. D. Boroughs
1345 Commerce Union Bank Building
Chattanooga, TN 37401

Tennesse Valley Authority
H. B. Flora, III
1320 Commerce Union Bank Building
Chattanooga, TN 37401

Texas Electric Service Co.
W. Keel
115 W. Seventh Street
Fort Worth, TX 76102

No. of
Copies

Tucson Gas & Electric
A. A. Ward
220 W. 6th Street
Tucson, AZ 85701

Union Carbide Corp.
H. D. Fricke
Linde Division
61 East Park Drive
Tonawanda, NY 14150

Union Carbide Corp.
L. R. Niendorf
Linde Division
61 East Park Drive
Tonawanda, NY 14150

Union Carbide Corp.
J. M. Vance
ORGDP - K-25
P.O. Box P, Mail Stop 387
Oak Ridge, TN 37803

United Engineers & Constructors
G. A. Englesson
30 S. 17th Street
Philadelphia, PA 19103

United Engineers & Constructors
M. Hu
30 S. 17th Street
Philadelphia, PA 19103

University of Bremen
K. Simhan
Bremen, WEST GERMANY

University of Iowa
J. F. Kennedy
Hydraulic Research Institute
Iowa City, IA 52240

University of Kentucky
T. E. Eaton
Mechanical Engineering Department
Lexington, KY 40506

No. of Copies

University of South Florida
A. D. Craus
College of Engineering
Tampa, FL 33620

U.S. Congress
G. Haimes
214 Massachusetts Avenue NE
Washington, DC 20510

U.S. Fish and Wildlife Service
B. L. Foder
Information Transfer Specialist
National Power Plant Team
1451 Green Road
Ann Arbor, MI 48105

United States Steel Corp.
T. L. Myron
Research Laboratory
Monroeville, PA 15146

Utah Power & Light
M. W. Russon
1407 W. N. Temple
Salt Lake City, UT 84110

Utah Power & Light
Frank M. Davis
1407 W. N. Temple
Salt Lake City, UT 84110

Utah Power & Light
V. A. Finlayson
1407 W. N. Temple
Salt Lake City, UT 84110

Vermont Yankee Nuclear Power
E. Gaines, Jr.
77 Grove Street
Rutland, VT 05701

Virginia Electric & Power Co.
S. Ragone
700 E. Franklin Street
Richmond, VA 23261

No. of Copies

Washington Public Power Supply System
J. Chasse
P.O. Box 968
300 George Washington Way
Richland, WA 99352

Washington State University
R. W. Crain, Jr.
Department of Mechanical Engineering
Pullman, WA 99164

Washington Water Power Co.
D. L. Olson
E. 1411 Mission Avenue
Spokane, WA 99202

Water Purification Associates
H. Gold
238 Main Street
Cambridge, MA 02142

Western States Water Council
J. A. Barnett
Executive Director
220 South 2nd East
Suite 200
Salt Lake City, UT 84111

Westinghouse Electric Corp.
R. F. Boyle
Power Generation Systems Engineering
700 Braddock Avenue Room 9L51
East Pittsburgh, PA 15112

Westinghouse Electric Corp.
G. J. Silvestri
Steam Turbines Division - G108
Lester Branch
Box 9175
Philadelphia, PA 19113

No. of
Copies

Westinghouse Electric Corp.
K. A. Oleson
Steam Turbines Division - G108
Lester Branch
Box 9175
Philadelphia, PA 19113

William M. Rice University
W. G. Characklis
Environmental Science and
Engineering
Houston, TX 77001

ONSITE

DOE Richland Operations Office
Energy Programs Division

H. E. Ransom

Westinghouse Hanford Company
Hanford Engineering Development
Laboratory

J. Fletcher

Pacific Northwest Laboratory

R. T. Allemann

No. of
Copies

Pacific Northwest Laboratory (contd)

R. L. Dillon
K. M. Drost
D. W. Faletti
J. D. Goodenough
J. J. Hauth
S. G. Hauser
A. J. Haverfield
C. H. Henager
P. L. Hendrickson
A. B. Johnson
W. S. Kelly
R. S. Kemper
D. K. Kreid
W. V. Loscutoff
R. P. Marshall
S. W. Matsumoto
M. S. Olsen
Y. Onishi
L. T. Pederson
A. M. Sutey
D. S. Trent
E. V. Werry
K. R. Wheeler
F. R. Zaloudek
File - B. M. Johnson (30)
Technical Information (5)
Publishing Coordination (2)
PA